

Université Libre de Bruxelles  
Faculty of Applied Sciences



Royal Military Academy  
Polytechnical Faculty



---

Progressive Collapse Simulation of  
Reinforced Concrete Structures:  
Influence of Design and Material Parameters  
and Investigation of the Strain Rate Effects

---

Berta Santafé Iribarren

Supervisors: Prof. Thierry J. Massart (ULB)  
Prof. John Vantomme (RMA)  
Co-supervisor: Prof. Philippe Bouillard (ULB)

A dissertation submitted for the degree of Doctor in Engineering Sciences

Academic year 2010-2011

Thesis carried out under the joint supervision of the *Université Libre de Bruxelles* (Faculty of Applied Sciences) and the *Royal Military Academy* (Polytechnical Faculty).

This research was supported by the Belgian Ministry of Defence, under project DY-03.

# Summary

This doctoral research work focuses on the simulation of progressive collapse of reinforced concrete structures. It aims at contributing to the ‘alternate load path’ design approach suggested by the General Services Administration (GSA) and the Department of Defense (DoD) of the United States, by providing a detailed yet flexible numerical modelling tool.

The finite element formulation adopted here is based on a multilevel approach where the response at the structural level is naturally deduced from the behaviour of the constituents (concrete and steel) at the material level. One-dimensional nonlinear constitutive laws are used to model the material response of concrete and steel. These constitutive equations are introduced in a layered beam approach, where the cross-sections of the structural members are discretised through a finite number of layers. This modelling strategy allows deriving physically motivated relationships between generalised stresses and strains at the sectional level. Additionally, a gradual sectional strength degradation can be obtained as a consequence of the progressive failure of the constitutive layers. This means that complex nonlinear sectional responses exhibiting softening can be obtained even for simplified one-dimensional constitutive laws for the constituents.

This numerical formulation is used in dynamic progressive collapse simulations to study the structural response of a multi-storey planar frame subject to a sudden column loss. The versatility of the proposed methodology allows assessing the influence of the main material and design parameters in the structural failure. Furthermore, the effect of particular modelling options of the progressive collapse simulation technique, such as the column removal time or the strategy adopted for the structural verification, can be evaluated.

The potential strain rate effects on the structural response of reinforced concrete frames are also investigated. To this end, a strain rate dependent material formulation is developed, where the rate effects are introduced in both the concrete and steel constitutive response. These effects are incor-

porated at the structural level through the multilayered beam approach. In order to assess the degree of rate dependence in progressive collapse, the results of rate dependent simulations are presented and compared to those obtained via the rate independent approach. The influence of certain parameters on the rate dependent structural failure is also studied.

The differences obtained in terms of progressive failure degree for the considered parametric variations and modelling options are analysed and discussed. The parameters observed to have a major influence on the structural response in a progressive collapse scenario are the ductility of the steel bars, the degree of symmetry and/or continuity of the reinforcement and the column removal time. The results also depend on the strategy considered (GSA vs DoD). The strain rate effects are confirmed to play a significant role in the failure pattern. Based on these observations, general recommendations for the design of progressive collapse resisting structures are finally derived.

# Résumé

L'effondrement progressif est un sujet de recherche qui a connu un grand développement suite aux événements désastreux qui se sont produits au cours des dernières décennies. Ce phénomène est déclenché par la défaillance soudaine d'un nombre réduit d'éléments porteurs de la structure, qui provoque une propagation en cascade de l'endommagement d'élément en élément jusqu'à affecter une partie importante, voire la totalité de l'ouvrage. Le résultat est donc disproportionné par rapport à la cause. La plupart des codes de construction ont inclus des prescriptions pour le dimensionnement des structures face aux actions accidentelles. Malheureusement, ces procédures se limitent à fournir des 'règles de bonne pratique', ou proposent des calculs simplifiés se caractérisant par un manque de détail pour permettre leur mise en œuvre.

Cette thèse de doctorat intitulée *Simulation de l'Effondrement Progressif des Structures en Béton Armé: Influence des Paramètres Matériaux et de Dimensionnement et Investigation des Effets de Vitesse* a pour but de contribuer à la simulation numérique de l'effondrement progressif des structures en béton armé. Une formulation aux éléments finis basée sur une approche multi-échelles a été développée, où la réponse à l'échelle structurale est déduite à partir de la réponse au niveau matériel des constituants (le béton et l'acier). Les sections des éléments structuraux sont divisées en un nombre fini de couches pour lesquelles des lois constitutives unidimensionnelles sont postulées. Cet outil permet une dégradation graduelle de la résistance des sections en béton armé suite à la rupture progressive des couches. Des comportements complexes au niveau des points de Gauss peuvent être ainsi obtenus, et cela même à partir de lois unidimensionnelles pour les constituants.

Cette formulation est utilisée pour la simulation de l'effondrement progressif d'ossatures 2D, avec prise en compte des effets dynamiques. La versatilité de la présente stratégie numérique permet d'analyser l'influence de différents paramètres matériaux et de dimensionnement, ainsi que d'autres

paramètres de modélisation, sur la réponse structurale face à la disparition soudaine d'une colonne.

Les effets de la vitesse de déformation sur le comportement des matériaux constitutifs est aussi un sujet d'attention dans ce travail de recherche. Des lois constitutives prenant en compte ces effets sont postulées et incorporées au niveau structural grâce à l'approche multi-couches. Le but est d'étudier l'influence des effets de la vitesse de chargement sur la réponse structurale face à la disparition d'un élément porteur. Les résultats obtenus à l'aide de cette approche avec effets de vitesse sont comparés à ceux obtenus avec des lois indépendantes de la vitesse.

Les différences dans la réponse à la disparition d'une colonne sont analysées pour les variations paramétriques étudiées. Les paramètres ayant une influence importante sont notamment: la ductilité des matériaux constitutifs et la disposition et/ou la symétrie des armatures. Les effets de vitesse sont également significatifs. Sur base de ces résultats, des recommandations sont proposées pour le dimensionnement et/ou l'analyse des structures face à l'effondrement progressif.

# Contents

Summary	i
Résumé	iii
List of Figures	xii
List of Tables	xiii
Symbols and Abbreviations	xv
<b>1 Introduction</b>	<b>1</b>
1.1 General introduction . . . . .	1
1.2 Motivation and methodology . . . . .	4
1.3 Structure of the manuscript . . . . .	6
<b>2 Progressive collapse analysis procedures</b>	<b>7</b>
2.1 State-of-the-art . . . . .	7
2.1.1 Indirect design . . . . .	8
2.1.2 Direct design: ‘Alternate load path’ . . . . .	10
2.2 Scope and objectives . . . . .	16
<b>3 Rate Independent Modelling of RC Structures</b>	<b>19</b>
3.1 Material behaviour . . . . .	19
3.1.1 Concrete in compression . . . . .	19
3.1.2 Concrete in tension . . . . .	22
3.1.3 Reinforcing steel . . . . .	25
3.2 Constitutive equations . . . . .	26
3.3 Modelling of RC members . . . . .	28
3.3.1 Kinematics description . . . . .	28
3.3.2 Layered beam formulation . . . . .	30
3.3.3 Experimental illustration . . . . .	37
3.4 Time integration scheme for the dynamic problem . . . . .	42

3.5	Strain localisation and size effects . . . . .	45
3.5.1	Mesh-sensitivity in RC beams . . . . .	45
3.5.2	Characteristic length . . . . .	49
<b>4</b>	<b>Numerical Simulations of Progressive Collapse</b>	<b>51</b>
4.1	The ‘sudden column loss’ approach . . . . .	51
4.2	Reference case of study . . . . .	53
4.2.1	Description . . . . .	53
4.2.2	Simulation results . . . . .	56
4.3	Influence of the material parameters of concrete and steel re- inforcement . . . . .	63
4.3.1	Tensile strength of concrete . . . . .	63
4.3.2	Ultimate strain of concrete and steel . . . . .	65
4.4	Influence of the reinforcement scheme . . . . .	68
4.5	Influence of the column removal duration . . . . .	78
4.6	Influence of the design code for progressive collapse verification	81
4.7	Discussion . . . . .	84
<b>5</b>	<b>Investigation of the Strain Rate Effects</b>	<b>89</b>
5.1	Strain rate effects in RC . . . . .	89
5.2	Rate dependent response of concrete and steel . . . . .	92
5.3	Rate dependent constitutive model . . . . .	97
5.3.1	Particularities of the rate dependent model parameters	98
5.4	Rate dependent multilayered approach . . . . .	103
5.4.1	Application: rate dependent moment-curvature rela- tionships for a given RC section . . . . .	104
5.5	Time integration scheme for the strain rate dependent approach	110
5.6	Rate dependent simulations of progressive collapse . . . . .	112
5.6.1	Reference case of study . . . . .	113
5.6.2	Analysis of the individual contribution of the material features to the global rate effects . . . . .	120
5.6.3	Influence of the tensile strength of concrete . . . . .	123
5.6.4	Influence of the ultimate strain of concrete . . . . .	124
5.6.5	Influence of the reinforcement scheme . . . . .	126
5.6.6	Influence of the column removal duration . . . . .	128
5.6.7	Influence of the design code . . . . .	130
5.7	Discussion . . . . .	133
<b>6</b>	<b>Concluding Remarks and Recommendations</b>	<b>137</b>
6.1	Challenges of the research . . . . .	137
6.2	Main contributions . . . . .	138

6.2.1	Rate independent non-linear constitutive models . . . .	139
6.2.2	Multilayered beam approach . . . . .	139
6.2.3	Numerical simulations . . . . .	140
6.2.4	Investigation of the strain rate effects . . . . .	140
6.3	Overview of the results . . . . .	141
6.3.1	Influence of the material parameters . . . . .	141
6.3.2	Influence of the reinforcement scheme . . . . .	142
6.3.3	Influence of the simulation options . . . . .	143
6.3.4	Influence of the strain rate effects . . . . .	144
6.4	General recommendations . . . . .	145
6.4.1	Material properties . . . . .	145
6.4.2	Reinforcement scheme . . . . .	146
6.4.3	Load combination . . . . .	146
6.4.4	Modelling of the triggering event . . . . .	146
6.4.5	Strain rate effects . . . . .	147
6.4.6	Other numerical aspects . . . . .	147
6.5	Future prospects . . . . .	147
<b>References</b>		<b>151</b>
<b>Appendix</b>		<b>161</b>
<b>List of Publications</b>		<b>165</b>
<b>Acknowledgements</b>		<b>167</b>



# List of Figures

1.1	Ronan Point building after collapse, London 1968. Source: [6].	2
1.2	A.P. Murrah Federal Building before and after collapse, Oklahoma City 1995. Sources: [8, 9].	3
1.3	Progressive collapse mechanism of the WTC towers according to Bažant et al. Reproduced from [12].	4
2.1	Moment-rotation relationship of a typical flexural plastic hinge [24, 76].	14
3.1	Stress-strain diagram of the proposed model for concrete in compression [52].	20
3.2	Effect of lateral reinforcement ratio on the behavior of steel confined concrete. Reproduced from [54].	21
3.3	Compressive stress-strain relation for confined concrete [53, 74].	22
3.4	Tensile stress-crack opening relation [52, 62].	23
3.5	Stress-strain diagram of the proposed model for concrete in tension.	24
3.6	Typical stress-strain curve for hot-rolled steel bars [51].	25
3.7	Stress-strain curve of the proposed model for steel.	26
3.8	Typical stress-strain relationship of an elasto-plastic model.	27
3.9	Beam element: nodal degrees of freedom.	28
3.10	Illustration of a multilayered beam section.	31
3.11	Multilayered beam: generalised stresses evaluation.	32
3.12	Uniform bending test description.	33
3.13	Bending moment–curvature diagrams for different bottom reinforcement amounts.	34
3.14	Final sectional state for different bottom reinforcement amounts.	35
3.15	Representation of the sectional response.	35
3.16	Bending moment–curvature diagrams for different axial loads.	36
3.17	Final sectional state for different axial loads.	37
3.18	Four-point bending experimental test.	38
3.19	Stress-strain diagram for steel: experimental vs. numerical.	39

List of Figures

---

3.20	Moment-curvature diagrams: experimental vs. numerical response. . . . .	40
3.21	Dynamic integration scheme [67]. . . . .	44
3.22	Mesh-sensitivity test: beam dimensions and different discretisations employed. . . . .	45
3.23	Load-deflection diagram as a function of the mesh-refinement. . . . .	46
3.24	Curvature distribution along $x$ as a function of the mesh-refinement. . . . .	47
3.25	Final deformed shape of the beam and detailed sectional response for the different discretisations. . . . .	48
4.1	Sudden column loss approach: loading history. . . . .	52
4.2	Structure under study. . . . .	53
4.3	Beams dimensions and reinforcing details. . . . .	55
4.4	Finite element discretisation. . . . .	56
4.5	Reference case of study: response of the structure to a sudden column removal. . . . .	56
4.6	Evolution of $N$ for an exterior column removal. . . . .	58
4.7	Evolution of $M$ for an exterior column removal. . . . .	58
4.8	Evolution of $N$ and $M$ in the beam directly associated with the removed column. . . . .	59
4.9	Reference case of study: response to the sudden removal of an interior column. . . . .	60
4.10	Evolution of $N$ for an interior column removal. . . . .	61
4.11	Evolution of $M$ for an interior column removal. . . . .	61
4.12	Evolution of $N$ and $M$ in the right-hand beam directly associated with the removed interior column. . . . .	62
4.13	Vertical displacement of the node on top of the removed column. . . . .	62
4.14	<b>MO1</b> : response upon consideration of the tensile strength of concrete. . . . .	64
4.15	<b>MO1</b> : vertical displacement history. . . . .	65
4.16	<b>MO2</b> : response for $\epsilon_{c,lim} = -0.5\%$ . . . . .	66
4.17	<b>MO3</b> : response for $\epsilon_{s,lim} = 10\%$ . . . . .	66
4.18	<b>MO4</b> : response for $\epsilon_{c,lim} = -0.5\%$ and $\epsilon_{s,lim} = 10\%$ . . . . .	67
4.19	<b>MO2</b> to <b>MO4</b> : vertical displacement history. . . . .	68
4.20	Additional higher-rise structure used for the present analysis. . . . .	71
4.21	<b>REF</b> : response of both structures. . . . .	72
4.22	<b>REF</b> : response to an interior column removal. . . . .	72
4.23	<b>RS1</b> : response of both structures. . . . .	74
4.24	<b>RS1</b> : response to an interior column removal. . . . .	74
4.25	<b>RS2</b> : response of both structures. . . . .	75

4.26	<b>RS2</b> : response to an interior column removal. . . . .	75
4.27	<b>RS3</b> : response of both structures. . . . .	76
4.28	<b>RS3</b> : response to an interior column removal. . . . .	76
4.29	<b>RS</b> : vertical displacement history as a function of the reinforcement scheme. . . . .	77
4.30	<b>TED</b> : vertical displacement history as a function of the triggering event duration. . . . .	79
4.31	<b>TED</b> : response as a function of the triggering event duration. . . . .	80
4.32	<b>DoD</b> vs <b>GSA</b> : response for an exterior column removal. . . . .	82
4.33	<b>DoD</b> vs <b>GSA</b> : response for an interior column removal. . . . .	83
4.34	<b>DoD</b> vs <b>GSA</b> : vertical displacement history. . . . .	83
5.1	Strain rate effects on the compressive strength of concrete. Reproduced from [81]. . . . .	90
5.2	<b>REF</b> : evolution of the strain rate in the external layers of sections S1, S2 and S3. . . . .	91
5.3	Strain rate dependent model for concrete in compression. . . . .	93
5.4	Strain rate dependent model for concrete in tension. . . . .	95
5.5	Strain rate dependent model for steel. . . . .	96
5.6	Typical stress-strain relationship of an elasto-viscoplastic model. . . . .	98
5.7	Model parameters for concrete in compression. . . . .	100
5.8	Rate-dependent tensile response of the model for concrete as a function of the choice for $\eta_t$ . . . . .	101
5.9	DIFs of the fracture energy $G_f$ as a function of $\dot{\epsilon}$ . . . . .	101
5.10	Model parameters for concrete in tension. . . . .	102
5.11	Parameter $\eta_s(\dot{\epsilon})$ in steel. . . . .	103
5.12	Rate dependent multilayered approach. . . . .	104
5.13	Evolution of the curvature rates in the reference case of study. . . . .	104
5.14	Rate dependent uniform bending test description. . . . .	105
5.15	Scheme A: Bending moment–curvature diagrams as a function of the curvature rate. . . . .	106
5.16	SchemeA: sectional final state as a function of the curvature rate. . . . .	107
5.17	Scheme B: Bending moment–curvature diagrams as a function of the curvature rate. . . . .	108
5.18	Scheme B: sectional final state as a function of the curvature rate. . . . .	109
5.19	Dynamic Increase Factors for the maximum bending moment. . . . .	110
5.20	Dynamic integration scheme for the rate dependent approach [67]. . . . .	112
5.21	<b>REF</b> : response to the sudden column removal. . . . .	113

List of Figures

---

5.22	<b>REF</b> : response to an interior column removal. . . . .	113
5.23	<b>REF</b> : vertical displacement history for the rate dependent approach. . . . .	114
5.24	Evolution of $N$ for an exterior column removal. . . . .	115
5.25	Evolution of $M$ for an exterior column removal. . . . .	115
5.26	Evolution of $N$ for an interior column removal. . . . .	116
5.27	Evolution of $M$ for an interior column removal. . . . .	116
5.28	<b>REF</b> : evolution of the strain rate in the extreme layers of section S3. . . . .	117
5.29	Maximum values of $N$ (kN) obtained for an exterior removal. . . . .	118
5.30	Maximum values of $M$ (kNm) obtained for an exterior removal. . . . .	118
5.31	<b>REF</b> : response of the 8-storey frame. . . . .	119
5.32	<b>REF</b> : response of the 8-storey frame to an interior column removal. . . . .	119
5.33	<b>REF</b> : rate dependent vertical displacement of the 8-storey frame. . . . .	120
5.34	Individual material contributions to the global rate effects. . . . .	121
5.35	Vertical displacement history as a function of the individual material contributions to the global rate effects. . . . .	122
5.36	<b>MO1</b> : Response upon consideration of the tensile strength of concrete. . . . .	123
5.37	<b>MO1</b> : Vertical displacement history upon consideration of the tensile strength of concrete. . . . .	124
5.38	Influence of the ultimate strain of concrete. . . . .	125
5.39	<b>MO2</b> : Vertical displacement history. . . . .	125
5.40	<b>RS1</b> : response to an exterior column removal. . . . .	127
5.41	<b>RS1</b> : response to an interior column removal. . . . .	127
5.42	<b>RS1</b> : Vertical displacement history. . . . .	127
5.43	<b>TED1</b> : removal time $t_r = 50$ ms. . . . .	129
5.44	<b>TED3</b> : removal time $t_r = 250$ ms. . . . .	129
5.45	<b>TED4</b> : removal time $t_r = 300$ ms. . . . .	129
5.46	<b>TED</b> : Vertical displacement history as a function of the removal time. . . . .	130
5.47	<b>DoD</b> vs <b>GSA</b> : Rate dependent response for an exterior column removal. . . . .	132
5.48	<b>DoD</b> vs <b>GSA</b> : Rate dependent response for an interior column removal. . . . .	132
5.49	<b>DoD</b> vs <b>GSA</b> : Vertical displacement history. . . . .	132
A.1	Maximum compressive strain rate $\dot{\epsilon}$ . . . . .	161

# List of Tables

3.1	Values of the fracture energy ( $G_f$ ) found in the literature. . . .	23
3.2	Material parameters of the constitutive models: in accordance with [51, 52] . . . . .	28
3.3	Material parameters for the experimental comparison. . . . .	39
3.4	Some empirical expressions of the characteristic length ( $L_{ch}$ ). . .	50
4.1	Design loads. . . . .	54
4.2	Loads applied to the beams for the simulations (excluding self-weight). . . . .	55
4.3	Interpretation of the structural failure symbols. . . . .	57
4.4	Material options (MO) tested. . . . .	64
4.5	Reinforcement schemes (RS) tested. . . . .	70
4.6	Triggering event durations (TED) tested. . . . .	79
4.7	Study cases depending on the design code (GSA vs DoD). . . .	81
5.1	Material parameters of the rate dependent constitutive models for steel and concrete . . . . .	99
A.1	Young's modulus of concrete in tension $E_t$ . . . . .	162
A.2	Viscoplastic parameter of concrete in tension $\eta_t$ . . . . .	162
A.3	Young's modulus of concrete in compression $E_c$ . . . . .	162
A.4	Viscoplastic parameter of concrete in compression $\eta_c$ . . . . .	163
A.5	Viscoplastic parameter of steel $\eta_s$ . . . . .	164



# Symbols and Abbreviations

## Symbols

- $A$ : cross-sectional area
- $\alpha$ : numerical damping ratio
- $\beta$ : Newmark's parameter
- $[B]$ : interpolation matrix derivatives
- $c$ : nodal torque
- $\chi$ : curvature
- $\dot{\chi}$ : curvature rate
- $\Delta$ : increment
- $\epsilon$ : strain
- $\dot{\epsilon}$ : strain rate
- $\epsilon_c$ : compressive strain
- $\epsilon_{c,lim}$ : ultimate compressive strain of concrete
- $\epsilon_{s,lim}$ : ultimate strain of steel
- $\epsilon^p$ : plastic strain
- $\epsilon^{vp}$ : viscoplastic strain
- $\dot{\epsilon}^{vp}$ : viscoplastic strain rate
- $\bar{\epsilon}$ : axial strain
- $\dot{\bar{\epsilon}}$ : axial strain rate

## Symbols and Abbreviations

---

$E^{gen}$ :	generalised strains vector
$\dot{E}^{gen}$ :	generalised strain rates vector
$E$ :	Young's modulus
$E_c$ :	compressive Young's modulus of concrete
$E_t$ :	tensile Young's modulus of concrete
$f_c$ :	compressive strength of concrete
$f_t$ :	tensile strength of concrete
$f_y$ :	yield stress of steel
$f_u$ :	ultimate stress of steel
$\{f^{int}\}$ :	internal forces vector
$\{f^{ext}\}$ :	external forces vector
$f^x$ :	nodal horizontal force
$f^y$ :	nodal vertical force
$f$ :	yield function
$\phi$ :	steel reinforcement diameter
$G_c$ :	crushing energy of concrete
$G_f$ :	fracture energy of concrete
$\gamma$ :	Newmark's parameter
$H$ :	constitutive tangent operator
$[H_t]$ :	cross-sectional tangent operator
$\eta$ :	Perzyna's viscoplastic parameter
$[J_p]$ :	constitutive Jacobian matrix
$[J]$ :	structural Jacobian matrix
$\kappa$ :	cumulated (visco)plastic strain
$\kappa^t$ :	cumulated tensile (visco)plastic strain

$\kappa^c$ :	cumulated compressive (visco)plastic strain
$\dot{\kappa}$ :	cumulated (visco)plastic strain rate
$[K_t]$ :	structural tangent operator
$L_{el}$ :	element size
$L_{ch}$ :	characteristic length
$M$ :	bending moment
$[M]$ :	mass matrix
$N$ :	axial stress
$N$ :	Perzyna's viscoplastic parameter
$[N]$ :	interpolation matrix
$\{q\}$ :	nodal displacements vector
$\{\dot{q}\}$ :	nodal velocities vector
$\{\ddot{q}\}$ :	nodal accelerations vector
$R$ :	vector of residuals
$\rho_w$ :	volumetric ratio of shear reinforcement
$\rho_T$ :	top steel reinforcement ratio
$\rho_B$ :	bottom steel reinforcement ratio
$\rho_t$ :	tensile steel reinforcement ratio
$\rho_c$ :	compressive steel reinforcement ratio
$\rho$ :	density
$\sigma$ :	stress
$\sigma_c$ :	compressive stress
$\bar{\sigma}$ :	yield stress
$\bar{\sigma}_0$ :	initial yield stress
$\Sigma^{gen}$ :	generalised stresses vector

## Symbols and Abbreviations

---

$t$ :	time
$\Delta t$ :	time step
$t_r$ :	column removal time
$\theta$ :	nodal rotation
$u$ :	axial nodal displacement
$v$ :	vertical nodal displacement
$w$ :	crack width
$\Omega$ :	layerwise area

## Abbreviations

ALP:	Alternate Load Path
DIF:	Dynamic Increase Factor
DL:	Dead Loads
DoD:	Department of Defense
FEM:	Finite Element Method
<i>fib</i> :	International Federation for Structural Concrete
GSA:	General Services Administration
LL:	Live Loads
MO:	Material Option
RC:	Reinforced Concrete
RD:	Rate Dependent
REF:	Reference case of study
RI:	Rate Independent
RS:	Reinforcement Scheme
SL:	Snow Loads
TED:	Triggering Event Duration

# 1

## Introduction

A general introduction to the framework of progressive collapse is given in the present chapter. The motivation of this research and the adopted methodology are also presented, followed by the outline of the manuscript.

### 1.1 General introduction

Progressive collapse may be described as a situation originated by the failure of one or more structural members following an abnormal loading event. This local failure leads to a load redistribution in the structure, which results in an overall damage to an extent disproportionate to the initial triggering event. This occurs on account of the residual structure not being able to find an alternative equilibrium state by redistributing loads in the surrounding elements. The General Services Administration of the United States defines this phenomenon as ‘a situation where local failure of a primary structural component leads to the collapse of adjoining members which, in turn, leads to additional collapse. Hence, the total damage is disproportionate to the original cause’ [1]. Other definitions found in the progressive collapse related literature are: ‘collapse of all or a large part of a structure precipitated by failure or damage of a relatively small part of it’ [2]; ‘a catastrophic partial or total structural failure that ensues from an event that causes local structural damage that cannot be absorbed by the inherent continuity and ductility of the structural system’ [3]... While a number of different definitions of progressive collapse coexist, the notion of disproportionality is common to all of them [5]. The best-known progressive collapse scenarios in recent history have often been a result of terrorist attacks. Nevertheless, other scenarios such as natural hazards or accidental actions (gas explosions, earthquakes...) may also be the triggering event leading to a disproportionate structural failure.

## 1.1 General introduction

---

The partial collapse of the 22-storey Ronan Point apartment tower in Newham (east London) in 1968, drew the interest of the research community towards this phenomenon for the first time. A gas explosion in a corner of the 18th floor blew out a load-bearing wall, which in turn caused the collapse of the upper floors due to the loss of support. The impact of the upper floors on the lower ones led to a sequential failure all the way down to the ground level [2]. As a result, the entire corner of the building collapsed, as can be observed in Figure 1.1. This partial collapse was attributed to the inability of the structure to redirect loads after the loss of a load-carrying member. It is a particularly representative example since the magnitude of the collapse was completely out of proportion with respect to the triggering event.

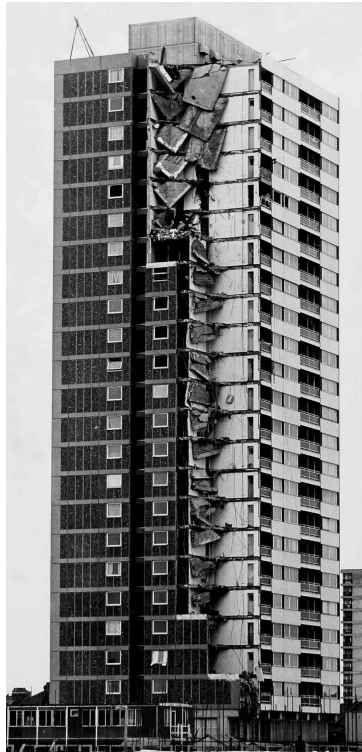


**Figure 1.1:** Ronan Point building after collapse, London 1968.  
Source: [6].

Another famous example of disproportionate collapse occurred in Oklahoma City in 1995. The Alfred P. Murrah Federal Building collapsed following the explosion of a bomb truck, which initially damaged between one and four

ground columns [7]. This partial loss of support resulted in the failure of the transfer girder located right above the failing columns and led to the consequent collapse of the upper floors. The final result was the collapse of about half of the total floor area of the building. Figure 1.2 shows the building before and after the partial collapse. The Oklahoma City bombing pushed the American institutions to investigate the mechanism that led to such a catastrophic failure. One year later, in 1996, the Federal Emergency Management Agency (FEMA) via the Building Performance Investigation Team (BPAT) released the report entitled *The Oklahoma City Bombing: Improving Building Performance Through Multi-Hazard Mitigation* [10]. The final conclusion was that ‘Many of the techniques used to upgrade the seismic resistance of buildings also improve a building’s ability to resist the extreme loads of a blast and reduce the likelihood of progressive collapse following an explosion’ [10]. Later works confirmed that the collapse could have been reduced by about 50% if seismic detailing had been provided to this reinforced concrete structure. Fully continuous reinforcement could have reduced both the structural damage and the casualties by 80% [11]. According to [7], it was the combined effects of the direct blast damage and the structural configuration that led to the progressive collapse that occurred.



**Figure 1.2:** A.P. Murrah Federal Building before and after collapse, Oklahoma City 1995. Sources: [8,9].

The issue of progressive collapse was brought to the forefront again after the attacks against the World Trade Center towers in New York City in September 11, 2001 (illustration in Figure 1.3). The large number of casualties and the economic loss that accompanied this multiple collapse brought a

renewed interest in the subject among other federal institutions of the United States, such as the General Services Administration (GSA) and the Department of Defence (DoD), which released their *Progressive collapse analysis and design guidelines for new federal office buildings and major modernization projects* [1] and *Unified Facilities Criteria (UFC): Design of buildings to resist progressive collapse* [15] respectively.

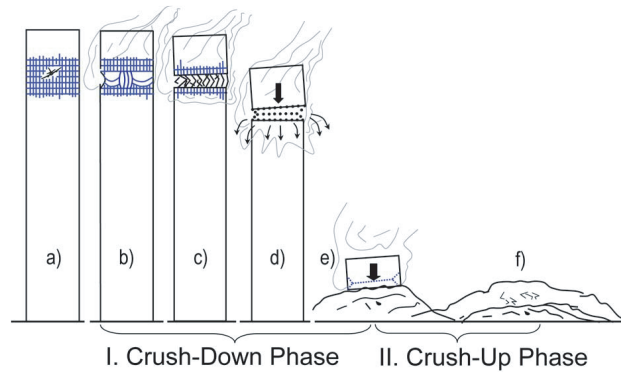


**Figure 1.3:** Progressive collapse mechanism of the WTC towers according to Bažant et al. Reproduced from [12].

In short, the fact that the most representative examples of progressive collapse have occurred in the last decades has led to both American and European general building codes to include guidelines for the evaluation of the potential for progressive collapse [1, 15, 16]. However, most of these documents are based on simplified analysis approaches or they merely give general recommendations for the mitigation of the consequences of a structural local failure. Hence, increasing interest is being drawn in the civil engineering research community to derive new specific design rules against progressive collapse. Nevertheless, it appears to be a very ambitious task to propose a general analysis procedure applicable to every loading scenario and building type.

## 1.2 Motivation and methodology

The present doctoral work deals with the modelling of reinforced concrete (RC) frames in the framework of progressive collapse analyses. The methodology developed here uses a direct transition from the behaviour of concrete and steel at the constituent level to the response of the structural members

at the global scale. A multilayered beam formulation is adopted, where the structural members are discretised through a finite number of layers for which one-dimensional constitutive relations are described.

The complexity of quantifying the rotational capacity of RC members has been demonstrated in the literature dealing with the behavioural characterisation of RC structures [48]. This complexity stems from the heterogeneous nature of the beams cross-sections, which are constituted of various materials (concrete and steel) with different constitutive behaviour. In particular, the numerical representation of the material response of concrete constitutes the major difficulty of the present modelling problem. It is a non-trivial task due to the multiple particularities of concrete behaviour: the different response in tension and in compression, the discrete character of the tensile failure, the softening nature of the compressive behaviour which involves a strain localisation at the structural level, the confining effect of the transversal reinforcement in compressive concrete, the characterisation of the strain rate effects, etc.

The global response of a RC member depends on the design options, such as the amount and position of the steel reinforcing bars, as well as on the material properties of their constituents, in both the elastic and plastic range, such as the strength, ductility, etc. Hence the interest of a multilevel approach where the response at the structural scale is directly and naturally derived from the response at the constituents level: it avoids the need for postulating closed-form relationships between generalised stresses and strains at the sectional level, preventing the related identification problem whenever the design and/or material parameters need to be modified or when a rate dependent approach is considered. Furthermore, it allows for a gradual sectional strength degradation, as a consequence of the progressive failure of the constitutive layers, as it will be explained later. This also means that rather complex nonlinear sectional responses exhibiting softening can be obtained even with simplified 1D constitutive laws for the constituents. Conversely, the advantages offered by the present formulation are counterbalanced by the higher computational cost required by a multiscale approach.

The sudden column loss technique will be used for simulating the abnormal loading event that causes localised structural failure, and which could give rise to progressive collapse. This technique assumes the instantaneous removal of a load-bearing member, to study the ability of the structure to redistribute loads among the remaining elements. It is considered as a useful tool for the assessment of structural robustness.

### 1.3 Structure of the manuscript

This dissertation is organised as follows. **Chapter 2** provides the state-of-the-art in the progressive collapse analysis techniques and presents the scope and objectives of the present contribution. In **Chapter 3** the rate independent material behaviour of concrete and steel is described and corresponding 1D constitutive models are proposed. The multilayered beam description used for the modelling of the reinforced beam elements is detailed, followed by the time integration scheme used for the dynamic computations. An experimental illustration of the model is performed for a single simply-supported RC beam. Other numerical issues related to the present computational analysis such as the problem of strain localization are also presented.

The application of the proposed methodology in the simulation of progressive collapse of RC structures is presented in **Chapter 4**, where a planar frame representing a building front section is subjected to a sudden column loss. A reference solution is obtained for a structure designed according to the Eurocodes. This section also presents the results for varying material constitutive parameters of concrete and steel, which are varied in a realistic range of values obtained from the literature. The influence of other design parameters, such as the reinforcement rate and/or detailing, are analysed. As far as the technique of the sudden column loss simulation is concerned, the effect of the column removal time in the structural failure pattern is also assessed. The influence of the location of the removed column is studied, as well as the procedure (in terms of load combination) adopted for the progressive collapse analysis.

**Chapter 5** focuses on the investigation of the strain rate effects on structural progressive collapse. A material strain rate dependent formulation is described here and the related results are compared to those obtained via the rate independent approach. The influence of certain design and material parameters in the rate dependent response is likewise assessed.

A discussion of the overall findings is given in **Chapter 6**, along with some concluding remarks and recommendations. Finally, the future prospects are discussed.

## 2

# Progressive collapse analysis procedures

The state-of-the-art in the field of progressive collapse retrofitting and analysis techniques is presented in this chapter and the most popular current approaches are reviewed and discussed. The contribution of the present thesis to the field of progressive collapse simulations is finally introduced.

### 2.1 State-of-the-art

Various approaches for progressive collapse mitigation can be found in the literature. Different classifications of such design strategies exist as well [1–4, 13–15, 17]. The first contributions to the subject [3, 4] identified three basic design methods for progressive collapse prevention:

- Event control: protection against incidents that might cause progressive collapse.
- Indirect design: preventing progressive collapse by specifying minimum requirements with respect to strength and continuity.
- Direct design: considering resistance against progressive collapse and the ability to absorb damage as a part of the design process. The ‘specific local’ resistance method and the ‘alternate path method’ have been identified as the two basic approaches to direct design.

Slightly different categorisations have been proposed since. According to [13, 14], the following design strategies are the most often mentioned in the literature and have made their way into the design codes:

- High safety against local failure

- Specific local resistance of key elements (direct design)
- Non-structural protective measures (event control)
- Design for load case ‘local failure’ (direct design)
  - Alternate load paths
  - Isolation by compartmentalization
- Prescriptive design rules (indirect design)

Leaving aside the subtle differences between the existing classifications, and discarding the ‘event control’ as a structural design approach, the two main types of (strictly speaking) design strategies that can be discerned are:

- **Indirect design:** based on common ‘good practice’ rules
- **Direct design:** requiring specific analytical or numerical computations

### 2.1.1 Indirect design

The ‘indirect design’ approach is included by many international standards such as the GSA [1], the DoD [15] and the Eurocodes [16]. However, it fails to give specific guidance for the collapse-resistant design of structures. For instance, the **GSA** recommends the following list of general features, as a ‘supplementary guidance’ that must be considered in the initial phases of structural design, prior to the structural analysis, in order to ‘provide for a much more robust structure and increase the probability of achieving a low potential for progressive collapse’ for reinforced concrete structures [1]:

- **Redundancy:** Redundancy tends to promote an overall more robust structure and helps to ensure that alternate load paths are available in the case of a structural element(s) failure. Additionally, it generally provides multiple locations for yielding to occur, which increases the probability that damage may be constrained.
- **The use of detailing to provide structural continuity and ductility:** It is critical that the primary structural elements (i.e., girders and beams) be capable of spanning two full spans. This requires both beam-to-beam structural continuity across the removed column, as well as the ability of both primary and secondary elements to deform flexurally well beyond the elastic limit without experiencing structural collapse. In this document, primary structural elements are defined as the essential parts of the building’s resistance to abnormal loads and

progressive collapse (thus columns, girders, roof beams, and the main lateral resistance system). The secondary structural elements are all other load bearing members (floor beams, slabs, etc.).

- **Capacity for resisting load reversals:** It is recommended that both the primary and secondary structural elements be designed such that these components are capable of resisting load reversals in the case of a structural element(s) failure.
- **Capacity for resisting shear failure:** It is essential that the primary structural elements maintain sufficient strength and ductility under an abnormal loading event to preclude a shear failure such as in the case of a structural element(s) failure. When the shear capacity is reached before the flexural capacity, the possibility of a sudden, non-ductile failure of the element exists which could potentially lead to a progressive collapse of the structure.

The **DoD**, in turn, presents the ‘Tie Forces’ method as indirect approach: it prescribes a tensile force capacity of the floor or roof system, to allow the transfer of load from the damaged portion of the structure to the undamaged portion [15]. The ability of developing catenary effects is thus considered an essential characteristic to be fulfilled by the residual structure. A similar approach was employed by the British standards after the Ronan Point collapse [15] and is currently used in the Eurocodes [16].

The pertaining document EN 1991-1-7 [16] issued by the **European standards** provides strategies for safeguarding civil engineering works against accidental actions. These strategies are classified in two main groups depending on the identified or unidentified character of the accidental action:

- Strategies based on identified accidental actions:
  - Designing the structure to have sufficient minimum robustness
  - Preventing or reducing the action (protective measures)
  - Designing the structure to sustain the action
- Strategies based on limiting the extent of localised failure
  - Enhanced redundancy (alternate load paths)
  - Key element designed to sustain notional accidental action
  - Prescriptive rules (integrity and ductility)

At a glance, the delimitation between the above-mentioned measures may appear vague. They are sometimes subject to the designer’s interpretation, since no quantification is given for most of such concepts. The definition of robustness itself remains unquantified; it is described here as ‘the ability of a structure to withstand events like fire, explosions, impact or the consequences of human error, without being damaged to an extent disproportionate to the original cause’.

Although this document specifies the design actions for which the structures should be resistance checked as a function of their ‘consequence class’, no details are given concerning the type of analysis that should be considered. For instance, the recommended strategies for a consequence class of ‘upper risk’ (comprising structures greater than 3-4 storeys but not exceeding 15) would consist of a provision for horizontal and vertical ties. Alternatively, the building should be checked to ensure that upon the notional removal of each supporting member (one at a time in each storey of the building) the building remains stable and that any local damage does not exceed a certain limit. The recommended value for this limit is 15% of the floor area, or 100 m<sup>2</sup>, whichever is smaller, in each of two adjacent storeys. Whenever the notional removal of such elements results in an extent of damage in excess of the agreed limit, they must be designed as ‘key elements’. A ‘key element’ should be capable of sustaining an accidental design action of 43 kN/m applied in horizontal and vertical directions (in one direction at a time) to the member and any attached components. In spite of the descriptive nature of such design measures, no additional specification is provided for their practical accomplishment in what refers to analysis techniques or element-removal conditions.

### 2.1.2 Direct design: ‘Alternate load path’

#### Standards and Guidelines

In contrast to the measures pertaining to the ‘indirect design’, which are characterised by an absence of detailed procedures, the ‘direct design’ presents itself as a practical alternative for the progressive collapse mitigation. It constitutes the main design strategy in the GSA [1] and DoD [15] guidelines. More specifically, the ‘alternate load path’ (ALP) method is adopted. Most of the current literature on progressive collapse is based on this technique. The present research work also aims at contributing to this approach.

The ALP method consists in considering stress redistributions through-

out the structure following the loss of a vertical support element [1,4,15]. The structure is bound to find alternative paths for the forces initially carried by the failing elements. It is thus a threat-independent approach to progressive collapse: the main purpose is to analyse the progressive spread of damage after localised failure has occurred. The objective is to prevent or mitigate the potential for progressive collapse, not necessarily to prevent collapse initiation from a specific cause, since ‘it is not feasible to rationally examine all potential sources of collapse initiation’ [1].

The GSA and DoD requirements for the ALP application include the analysis of the structural response to a key structural element removal, in order to simulate a local damage comparable to the one produced in a blast or impact load scenario. If the structure is able to find alternative paths for redistributing the loads, the building is then considered to exhibit a low potential for progressive collapse. Although these guidelines provide detailed step-by-step procedures for the ALP analysis in terms of element(s) removal locations, load combinations to be applied and structural acceptance criteria, they do not give specific directions in what refers to the computational modelling aspects (i.e. constitutive models, simulation procedures, etc.). Different strategies are suggested for linear static, non-linear static and non-linear dynamic analyses. The vertical load combinations to be applied to the structure under study are:

$$\begin{aligned} \text{GSA} &\Rightarrow \text{DL} + 0.25 \text{ LL} \\ \text{DoD} &\Rightarrow (0.9 \text{ or } 1.2) \text{ DL} + (0.5 \text{ LL or } 0.2 \text{ SL}) \end{aligned}$$

where DL = Dead loads (i.e. permanent loads); LL = Live loads (variable loads); SL = Snow loads. These loads are multiplied by a ‘dynamic factor’ of 2 in the static analyses in order to implicitly and crudely take into account the dynamic effects.

A characteristic feature of the linear static approach in both guidelines is that the real loading sequence is inverted, in the sense that the step-by-step analyses are performed on the residual structure, where the failed members are consecutively removed from the topology as they reach the damage criteria. The element removal is thus performed prior to the application of the gravity loads at each step.

Apart from these guidelines, issued by official institutions, most of the ‘individual’ contributions to the subject are based on the ALP approach. Among these, a large number of numerical formulations with various extents of sophistication are presented. Moreover, the simulation techniques are found to

differ depending on the type of structure under study, i.e. steel structures vs. reinforced concrete structures, due to the significant differences in terms of global response and member modelling aspects. A review of these scientific contributions is given next.

### **Current simulation approaches**

As a complement to the recommendations provided by the design codes, more detailed computational procedures based on the ALP approach made their way into the literature related to progressive collapse simulations. Some authors proposed static non-linear calculations accounting for dynamic inertial effects via load amplification factors, specifically for steel structures [18–22]. The DoD and GSA dynamic load amplification factor of 2 (applicable for both reinforced concrete and steel structures) was considered to be highly conservative by some authors working on steel structures [19, 20, 22, 23, 27] and on reinforced concrete frames [24]; while insufficient for others whose research is focused on steel frames [25, 26, 28]. Equivalent static pushover procedures have also been identified for steel structures, based on energetic considerations [19–22], in order to obtain a systematic estimate of the dynamic load factors. In [22], an optimisation approach based on nonlinear dynamic analyses was adopted to determine the most appropriate values for these factors, by performing a parametric study on topological variables for regular steel frames.

Besides these equivalent quasi-static approaches, which constitute a major part of the related literature, non-linear dynamic procedures were recently conducted for both reinforced concrete and steel structures, to a variable extent of complexity [23–26, 28–36]. While in most of the recent works the structures are still modelled using 2D frames [23, 25, 26, 28, 33, 34], full non-linear 3D dynamic computations with geometrically nonlinear formulations are sometimes found in the literature related to steel structures [32, 36]. Nevertheless, such detailed approaches are scarce for reinforced concrete structures, partially due to the high complexity involved in the modelling of the sectional response of heterogeneous RC beams, which depends on their design and on the material properties of their constituents in the non-linear range. Hence, most of the progressive collapse related references are focused on steel structures [18–23, 25–28, 32, 34–37]. Fewer contributions tackle the dynamic analysis of progressive collapse of reinforced concrete structures, among which [24, 29–31, 33, 38, 40]. Recent works as [29–31] use explicit finite element formulations based on hydrocodes, which are mainly adopted in the simulation of blast-induced progressive collapse analyses. In [29], an

initial computation is performed where the effects of the blast on the structure are quantified. The initial velocity, displacement and the initial damage of the structural members that are not completely damaged by direct blast loading are calculated, in order to be applied in a subsequent progressive collapse analysis, where the completely damaged members are instantaneously removed from the topology, while the previously calculated non-zero initial conditions (thus displacements and velocities) are introduced. The commercial software LS-DYNA employed in [29] allows for a number of material modelling simplifications: the modelling of the reinforced concrete response can be based on a priori homogenized cross-sectional properties of beams and may thus not incorporate all aspects of the real response of RC members. For instance, in [29] a simplified material model for reinforced concrete sections is adopted, where the steel reinforcement ratio is chosen without taking into account explicitly either the location or the geometry of the reinforcing steel bars. In [30], the software LS-DYNA is employed as well. The blast load is modelled as a pressure-time distribution on the failing element(s). Other works such as [31] use the commercial software AUTODYN, which also allows for the detailed modelling of the collapse initiating event. The material models are often based on simplifying assumptions: in this case the model used is a homogenised elastoplastic material similar to concrete but with higher tensile strength to take into account the collaboration of the reinforcement to resist tensile stresses. A finer discretisation with the reinforcements explicitly represented would require extremely reduced time steps, since this parameter in explicit dynamic programs is directly related to the size of the elements. As a consequence, this threat-dependent approach, which may become prohibited for large and/or finely discretised structures due to its computational cost, is mainly used to study the direct effects of an explosion or impact on the structure rather than the long terms effects of such failure. It is thus out of the scope of the present work.

A considerable number of contributions to the progressive collapse simulations of RC structures are based on implicit finite element codes. Nevertheless, due to the aforementioned complexities in the dynamic characterisation of the RC structures, the related material modelling is repeatedly based on simplified approaches. The modelling of the reinforced concrete response is in most of the cases based on a priori postulated cross-sectional properties of beams requiring an identification of such generalised constitutive laws, as in [28, 33, 38, 40, 76]. In this type of analyses, a lumped plasticity idealization is adopted, and potential plastic hinges are assigned a priori to the beam locations where localisation is most likely to occur. In such lumped plasticity approaches, the rest of the elements are considered to have an elastic

response. A plastic hinge is hence defined as the region of the beam where most of the permanent rotation is concentrated [50]. The behaviour of a plastic hinge is defined by a priori postulated moment-rotation curves, as shown in Figure 2.1.

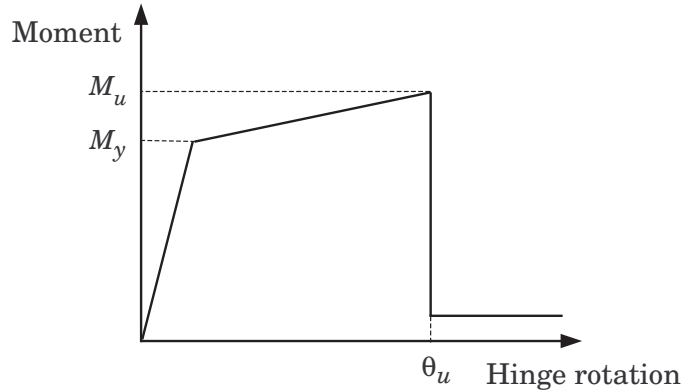


**Figure 2.1:** Moment-rotation relationship of a typical flexural plastic hinge [24, 76].

The values that define this curve (i.e. the yield moment  $M_y$ , the ultimate moment  $M_u$  and the ultimate rotation  $\theta_u$ ) vary depending on the type of element, material properties, reinforcement ratio, and the axial load level on the element [76]. This means that closed-form relations for the moment–rotation diagrams must be obtained prior to the structural analysis for varying material and/or design parameters, and this accounting for complex phenomena such as the evolving interactions between flexural loading and axial loading. The complexity of the identification of such closed-form laws is reflected in [48], where closed-form relationships to estimate the moment–curvature response are proposed for varying reinforcement arrangements and axial loads, by means of a ductility analysis according to the Eurocodes prescriptions. The corresponding analytical predictions of the curvature ductility are presented as an input for pushover analysis for seismic design purposes.

The lumped closed-form plasticity approach introduces a number of simplifications, since all the possible parametric variabilities cannot be considered. Namely, the interactions between axial force and bending moment practically need to be ignored or, at best, simplified. It is the case in [76], where a plastic hinge formulation is adopted in the frame of seismic analysis of RC frames: the axial loads are considered constant on columns and non-existent on beams. This hypothesis may not be valid in particular for progressive collapse analysis, where the loss of load-carrying members results in important

variations of the axial load distributions. In [40], simplified plastic flexural hinges are also employed, where a constant value for the resisting moment of the sections is assigned, calculated as a function of their dimensions and reinforcement ratio. In [38] only steel yielding is considered as sectional failure, and corresponding plastic hinges are assigned to possible locations where yielding may occur. Yet, it is well known that compressive crushing of concrete may also lead to a high reduction of the sectional load-bearing capacity [49]. A later work from the same author includes the steel bar fracture on a single beam test [39] using more detailed material modelling.

On top of the approximate hypotheses related to the plastic hinge approach, there is a limit to the accuracy in using a combination of moment–curvature with hinge lengths to determine a beam rotation, since the moment–curvature relationship is a measure of the sectional ductility of the beam cross-section and not of the member ductility [50]. Indeed, the ductility of RC members (as their rotational capacity) is a very important parameter for the safe design of RC structures, since it determines the ability of the structure to redistribute moment and fail gradually [49]. Its study is essential since it provides a reliable estimate of the rotational capacity of buildings [48]. In particular, the concrete softening behaviour is considered as an important component of the rotational capacity, which needs to be taken into account in order to ensure the ductility of RC structures. One main component of this rotational capacity is due to the softening branch of the moment–curvature response [49]. Generally speaking, this characteristic is most often not accommodated in conventional plastic hinge approaches in which a sudden drop of the sectional strength is often considered after the ultimate moment is reached, failing in providing a gradual sectional strength degradation.

Most of the aforementioned drawbacks are avoided with the layered approach, since all the particular modelling parameters are naturally taken into account in the beam response, as well as the axial force–bending moment interactions. Moreover, there is no need for a prediction of the possible locations where rotations might be concentrated and the sectional failure takes place in a progressive manner. As will be explained in Chapter 3, the element size will be chosen according to the characteristic length where strain localisation is observed to take place. Conversely, a higher computational cost is required for this type of formulation, although it is justified by its enhanced simulation possibilities.

## 2.2 Scope and objectives

As previously mentioned, the present contribution falls within the multi-level modelling of RC frames and uses a direct transition from the behaviour of concrete and steel at the constituent level to the response of the structural members at the global scale. The multilayered beam approach [43, 46] was used in the context of earthquake engineering for cyclic loading calculations [44, 45] or for the characterisation of a beam-column connection macromodel for progressive collapse simulations [33]. In [47] a layered model is developed to characterise the response of a simply supported RC slab to blast loadings.

However, a fully multilevel approach has not yet been applied for the detailed modelling of reinforced concrete structures subjected to progressive collapse and hence constitutes a contribution to the study of this phenomenon. A geometrically linear formulation will be used. In recent works dealing with steel and concrete structures, such as [32, 36, 40], this geometrical linearity assumption is also considered. Nevertheless, its validity will be discussed in light of the results obtained. The complexity and computational cost of the methodology adopted here should be balanced with the objectives of the study. It aims at a realistic representation of the cross-sectional behaviour of reinforced concrete members where axial load-bending moment interactions are considered in combination with material nonlinearities, potentially including material rate effects. It offers a more accurate characterisation of the sectional response with respect to other simplified techniques based on closed-form relationships between generalised stresses and strains at the sectional level. The complexity of characterising the response of RC members was introduced previously. The ductility as the ability of the structure to redistribute moments and fail gradually is addressed in the literature [49, 50]. In particular, the concrete softening behaviour is considered as an important component of the rotational capacity, which needs to be taken into account in order to ensure the ductility of RC structures. The multilayered approach adopted here allows for a gradual strength degradation as a consequence of the progressive failure of the constitutive layers, ensuring a proper account for the potential ductility of the RC members.

The purpose here is to analyse the structural response of RC frames subjected to a ‘sudden column loss’: the vertical bearing member is removed instantaneously. This event-independent approach is widely used in the context of progressive collapse simulation techniques [1, 15, 18–26, 28, 32–36, 41, 42], in contrast to the event-dependent approaches [29–31] where the collapse

triggering event is also modelled. According to [41], the sudden column loss approach constitutes a useful design scenario for the assessment of structural robustness, since it offers an upper bound on the deformations obtained with respect to an event-dependent simulation approach.

Dynamic simulations are carried out on a two-dimensional representation of RC frames designed in accordance with Eurocode 2 requirements [51] in terms of reinforcement amounts, contrarily to other works where the simplifications introduced in the RC members modelling may result in unrealistic or overreinforced designs. It is the case of [29, 31] where a unique steel reinforcement ratio of 4% and 2%, respectively, is adopted for all elements of the structure. In order to assess the flexibility of this multiscale formulation, the influence of particular structural design and material modelling options on the structural response will be analysed. Certain analysis features, such as the load combinations to be applied to the structure, are often discussed in the context of progressive collapse simulations. The issue of reinforcement detailing is also addressed in the framework of progressive collapse mitigation techniques: seismic detailing as a means to reduce or even prevent collapse is debated [1, 3, 10, 11, 15, 26, 33]. However, the importance in the choice of other parameters has not yet been addressed in the literature, even if their influence in the results might be significant. It is the case of the material parameters, for which the values are conventionally considered as fixed quantities and thus are not subjected to further investigations. The multilevel nature of the approach considered here allows for an investigation of the influence of both design and material variables on the structural response. This sensitivity analysis constitutes thus another objective of the present research work, since it arises naturally from the possibilities offered by the present formulation.

Furthermore, the strain rate effects on the progressive collapse of RC structures are investigated. For a wide range of triggering events (impact, blast...), progressive collapse is a dynamic process involving rather high deformation rates. The strongly rate dependent behaviour of concrete and steel suggests that RC structures subjected to high loading rates might have a different response than when loaded statically [83, 84]. Since progressive collapse is a dynamic phenomenon which depends strongly on stress redistribution, these effects might be expected to play a significant role in the overall structural response to progressive collapse. Other contributions include these effects in the modelling of RC structures in an analytical phenomenological manner, by applying strength increase factors in the concrete and steel response [29, 30] as a function of the strain rate. Nevertheless, the degree of

## 2.2 Scope and objectives

---

influence of such effects at the global scale has not yet been investigated in contributions related to structural progressive collapse. Here, a strain rate dependent material approach is developed as well, to assess the level of dependence of the structural failure process on the material strain rate effects. The introduction of such constitutive laws in the multilayered beam model allows for naturally taking into account the strain rate effects at the structural scale.

In summary, the following objectives are pursued in the present research work:

- Modelling of the non-linear material behaviour of concrete and steel.
- Development of a layered beam approach for the modelling of RC frames.
- Investigation of the influence of design and material parameters in the progressive collapse analysis
- Development of a strain rate dependent material model for concrete and steel
- Study of the strain rate effects in the response of a RC structure undergoing progressive collapse

# 3

## Rate Independent Modelling of RC Structures

In this chapter, the computational approach for the modelling of reinforced concrete members is detailed, starting from the constitutive laws at the material scale for concrete and steel. The finite element formulation is described next, where the kinematic relationships of the beam element adopted here are given. The multilayered approach employed to link the material constitutive equations to the response at the cross-sectional scale is described, and its response is compared to the results of an experimental test. The algorithm for the time integration of the structural equations in dynamics is also presented. Finally, localisation issues arising from the softening nature of the sectional response are discussed and illustrated.

### 3.1 Material behaviour

#### 3.1.1 Concrete in compression

The International Federation for Structural Concrete (*fib*) in its *Bulletin 42* [52] describes the behaviour of concrete in compression as a stress-strain curve which depends on the concrete grade. The static compression curve is approximated by:

$$\frac{\sigma_{c,st}}{f_{c,st}} = -\frac{k\eta - \eta^2}{1 + (k-2)\eta} \quad \text{for } |\epsilon_c| < |\epsilon_{c,lim}| \quad (3.1)$$

in which  $\sigma_{c,st}$  is the static compressive stress and  $\epsilon_c$  the compressive strain. A C30 concrete type will be considered in the sequel with  $f_{c,st} = 37.9$  MPa the static compressive strength;  $k = 1.882$  the plasticity number and  $\eta = \epsilon_c/\epsilon_{c1}$ , with  $\epsilon_{c1} = -2.230/00$  the strain at maximum stress. The parameters  $k$  and  $\epsilon_{c1}$

### 3.1 Material behaviour

---

are calculated as follows [52]:

$$k = \frac{E_c}{f_{c,st}/|\epsilon_{c1}|} \quad (3.2)$$

$$\epsilon_{c1} = -1.60 \left( \frac{f_{c,st}}{10^7} \right)^{0.25} \frac{1}{1000} \quad (3.3)$$

with  $E_c$  the Young's modulus.

In the present work, a bilinear stress-strain relationship is adopted for the sake of simplicity, analogously to the simplified model suggested in Eurocode 2 (EN 1992-1-1) [51] for the design of RC cross-sections. In Figure 3.1 this simplified model is compared to the prescriptions of the *fib*, where the compressive stress-strain static curve is depicted. The assumed ultimate compressive strain is set to  $\epsilon_{c,lim} = -0.35\%$ , which is the value most commonly assumed for this parameter [51, 52]. Once this limit strain is reached, the stress vanishes in order to represent the failure of concrete in compression. It must be noted that, although this simplified model provides a less stiffer response in the elastic phase, due to its reduced modulus of elasticity, the total crushing energy  $G_c$  (i.e. the area under the compressive stress-strain curve) is preserved.

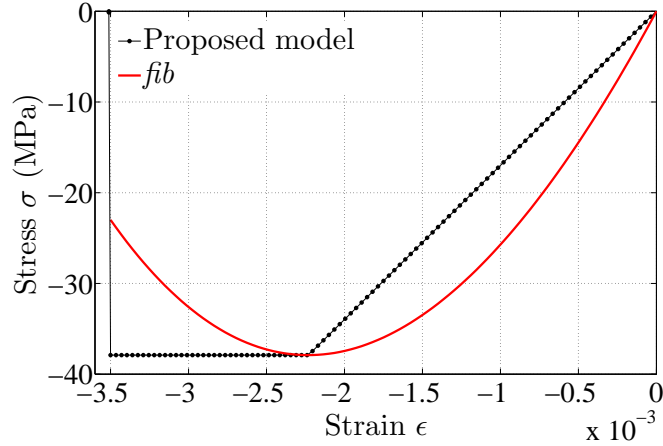


**Figure 3.1:** Stress-strain diagram of the proposed model for concrete in compression [52].

#### Confined concrete

Shear reinforcement has a confining effect on concrete. The compressive strength and ductility of concrete are highly dependent on the level of con-

finement provided by the lateral reinforcement, as seen in Figure 3.2, where this effect is shown for several shear reinforcement ratios [54].

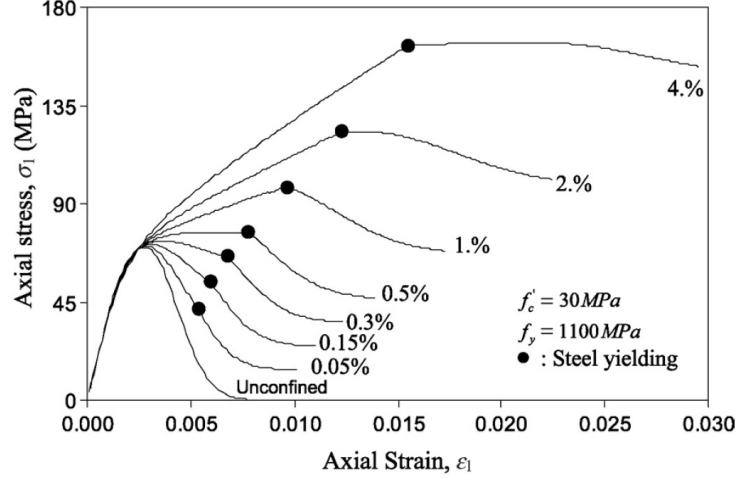


**Figure 3.2:** Effect of lateral reinforcement ratio on the behavior of steel confined concrete. Reproduced from [54].

The amount and the constitutive behaviour of the confining steel thus determine the level of confinement, which results in an increase of the compressive ultimate strain of concrete  $\epsilon_{c,lim}$  and/or the compressive strength  $f_{c,st}$  [51, 54, 74, 76, 79]. The Eurocode 2 [51] provides an expression for calculating the compressive strength and ultimate strain of confined concrete as a function of the lateral confining stress. However, from a practical point of view, these expressions are not of much use since no information is given for the estimation of this confining stress.

For moderate amounts of shear reinforcement, the compressive strength is assumed to remain unchanged and the simplified stress-strain relation shown in Figure 3.3 can be adopted [53, 74]. In practice, the increase of the ultimate strain in concrete  $\Delta\epsilon_{c,lim}$  is often calculated as a function of the volumetric ratio of shear reinforcement  $\rho_w$  by using empirically-based expressions [76, 79]. One of these expressions frequently adopted in the literature (and mostly used for columns, where the compressive load is high and constant over the section) is the following [76]:

$$\Delta\epsilon_{c,lim} = 1.4 \frac{\rho_w f_y \epsilon_{s,lim}}{f_{c,st}} \quad (3.4)$$

where  $f_y$  is the yield strength of the stirrups (i.e. the shear reinforcement

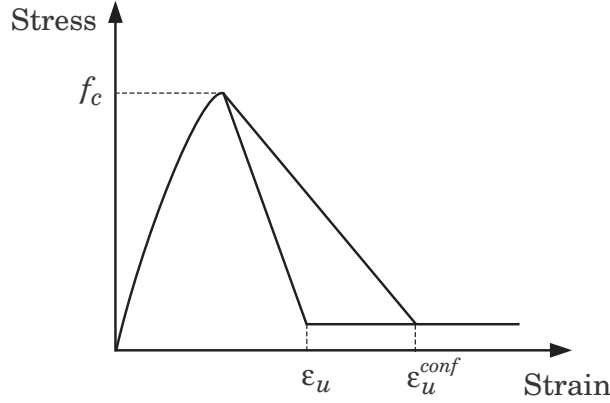


**Figure 3.3:** Compressive stress-strain relation for confined concrete [53, 74].

steel bars);  $\epsilon_{s,lim}$  is the ultimate strain of the stirrups; and  $\rho_w$  is defined as [51]:

$$\rho_w = \frac{A_{sw}}{s b \sin\alpha} \quad (3.5)$$

with  $A_{sw}$  the area of shear reinforcement within length  $s$ ;  $s$  the spacing of the shear reinforcement;  $b$  the section breadth; and  $\alpha$  the angle between shear reinforcement and the longitudinal axis (usually  $90^\circ$ ). The recommended minimum amount of shear reinforcement is, according to Eurocode 2 [51]:

$$\rho_{w,min} = \frac{0.08\sqrt{f_{c,st}}}{f_y} \quad (3.6)$$

where  $f_{c,st}$  and  $f_y$  are expressed in MPa. To give an idea of the order of magnitude of this value, the minimum stirrup ratio for a C30 concrete and S500 steel stirrups would be  $\rho_{w,min} = 0.1\%$ .

#### 3.1.2 Concrete in tension

In tension, a stress-crack opening relation (Figure 3.4) is often used to describe the material response [52, 62], due to the fact that the tensile fracture of concrete is a discrete phenomenon. The area under this diagram, which is called the specific fracture energy  $G_f$  (expressed in  $[\text{Nm}/\text{m}^2]$ ), is therefore used as a characteristic property that represents the energy dissipated in the tensile failure process. It is defined as the energy required to propagate a tensile crack of unit area [52]. The value for this parameter depends on material characteristics such as the aggregate type and size, the water-to-cement ratio or the curing conditions. Various empirical expressions can be

found for this parameter, as a function of the compressive strength, maximum aggregate size, etc. Furthermore, structural parameters such as the beam dimensions appear to have an influence [52]. For a C30 concrete type, the values for the fracture energy are usually comprised between 100 and 160 Nm/m<sup>2</sup>. Table 3.1 gives the numerical values according to the various references consulted, where the corresponding empirical formulae are also indicated.

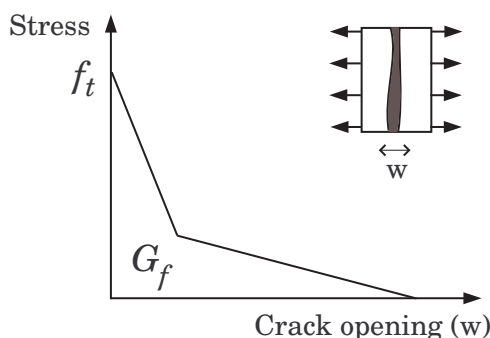


**Figure 3.4:** Tensile stress-crack opening relation [52, 62].

**Table 3.1:** Values of the fracture energy ( $G_f$ ) found in the literature.

Reference	$G_f$ [Nm/m <sup>2</sup> ]
He 2006 [63]	120
Weerheijm 2007 [56]	100
$fib(1): G_f = G_{F0} \left( \frac{f_{c,st}}{10^7} \right)^{0.7}$ [52]	64–147
$fib(2): G_f = G_{F0} \ln \left( 1 + \frac{f_{c,st}}{10^7} \right)$ [52]	102–166
$fib(3): G_f = 180 \left( 1 - 0.77 \frac{10^7}{f_{c,st}} \right)$ [52]	144
$fib(4): G_f = 110 \left( \frac{f_{c,st}}{10^7} \right)^{0.18}$ [52]	140
Schuler 2006 [57]	125
Krauthammer 2009 [72]	133
Mechtcherine 2009 [73]	130–140

$G_{F0}$  depends on the aggregate size and/or type;  $f_{c,st} = 37.9$  MPa

In the present work, a local stress-strain relation is proposed in tension,

### 3.1 Material behaviour

---

bearing in mind that such a relation must always be related to a characteristic length where cracking occurs, so that the the proper fracture energy is dissipated [60]. Unless a gradient enhancement is considered in the FEM (finite element method) approach, the element sizes will have to be chosen in such a way that the tensile strain energy over an element is equivalent to the fracture energy  $G_f$  of the discrete crack. The next expression should thus be satisfied:

$$G_f = \int \sigma dw = L_{el} \int_{\epsilon_{max}}^{\epsilon_{ult}} \sigma d\epsilon \quad (3.7)$$

with  $w$  the crack width,  $L_{el}$  the element size,  $\epsilon_{max}$  the strain at maximum stress and  $\epsilon_{ult}$  the ultimate tensile strain. The static tensile strength is taken equal to  $f_{t,st} = 3.25$  MPa, as indicated in the *fib* bulletin [52] for a C30 concrete. It is calculated from the value of the compressive strength by applying the following formula [52]:

$$f_{t,st} = 2.64 \left( \ln \left( \frac{f_{c,st}}{10} \right) - 0.1 \right) \quad (3.8)$$

where  $f_{t,st}$  and  $f_{c,st}$  are expressed in MPa. The Young's modulus in tension corresponds to the value of the tangent elastic modulus given in [52]. An exponential yield stress evolution is adopted in order to represent the stress reduction due to concrete cracking. The choice of the model parameters for a C30 concrete type results in a specific fracture energy of  $G_f = 135$  Nm/m<sup>2</sup> for quasi-static conditions, thus matching the empirical previsions found in the literature [52, 57, 72, 73]. Figure 3.5 depicts the tensile response of the proposed model.

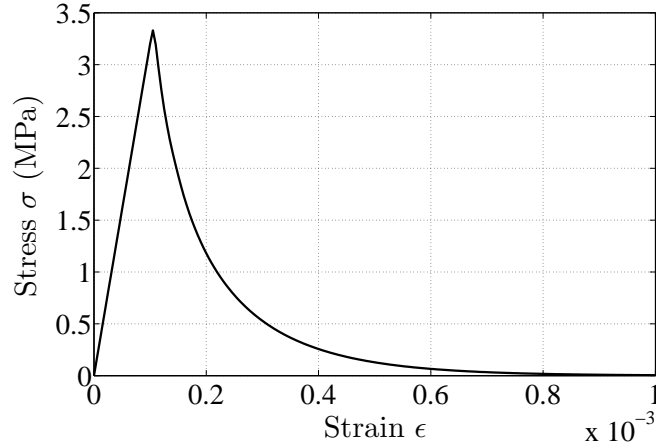


**Figure 3.5:** Stress-strain diagram of the proposed model for concrete in tension.

### 3.1.3 Reinforcing steel

For the reinforcement, hot rolled S500 steel class is assumed. The typical stress-strain curve for this type of steel [51] is represented in Figure 3.6.

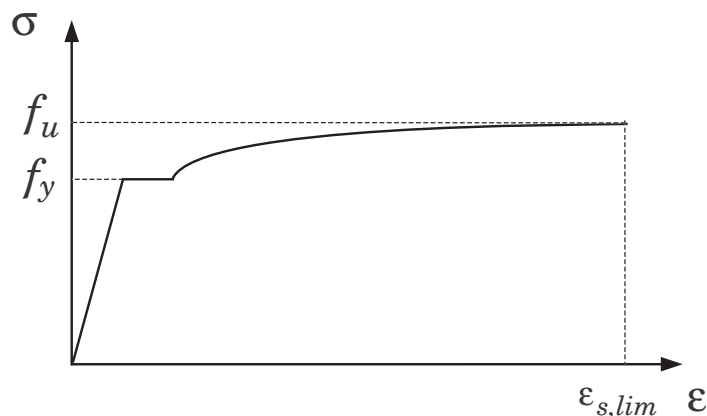


**Figure 3.6:** Typical stress-strain curve for hot-rolled steel bars [51].

The yield strength is set  $f_y = 500$  MPa. The value for the Young's modulus is the most commonly adopted for steel:  $E = 200$  GPa. Regarding the value of the ultimate strain  $\epsilon_{s,lim}$ , a large variability is found in the literature. According to [85], it may take values ranging from 7 to 18% for Grade 60 steel bars, which have equivalent properties to the S500 steel ones. In [55],  $\epsilon_{s,lim} = 7\%$  is adopted. In [33], 20% is used, while the value for this parameter is 1% in [42]. Eurocode 2 [51] considers three different steel classes, depending on their ductility properties, namely their ultimate strain  $\epsilon_{s,lim}$  and the ultimate-to-yield stress ratio  $f_u/f_y$  (see Figure 3.6). The values for  $\epsilon_{s,lim}$  are comprised between 2.5% (class A) and 7.5% (class C); the ratio  $f_u/f_y$  takes values between 1.05 (class A) and 1.35 (class C).

Here,  $\epsilon_{s,lim}$  is taken equal to 4%, which in practice would correspond to a ductility class close to B. The design stress-strain diagram proposed in Eurocode 2 [51], consisting of a bilinear approximation, is adopted. To this end, the evolution of the yield stress is modelled through a linear hardening approximation. The resulting ultimate-to-yield stress ratio for the present model is  $f_u/f_y = 1.06$ , thus falling within the interval observed by Eurocode 2. In order to represent the failure of steel, the stress is set to zero for strains exceeding this value. Figure 3.7 depicts the corresponding stress-strain curve.

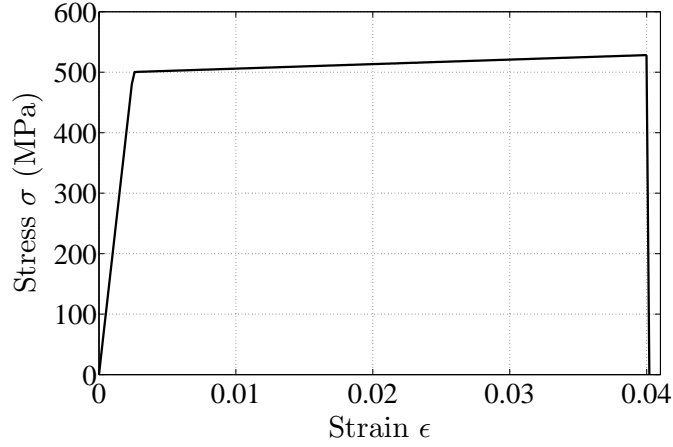


**Figure 3.7:** Stress-strain curve of the proposed model for steel.

### 3.2 Constitutive equations

Based on the information reported in Section 3.1, a 1D elasto-plastic model is adopted for the behavioural characterisation of concrete and steel. In a general way, the plastic domain is defined by an evolution law which depends on the plastic strain history parameter  $\kappa$ . The latter is defined in a one-dimensional approach as

$$\kappa = \int \dot{\kappa} dt \quad \text{with} \quad \dot{\kappa} = |\dot{\epsilon}^p| \quad (3.9)$$

with  $\dot{\epsilon}^p$  the plastic strain rate. This parameter  $\kappa$  consists here of two terms,  $\kappa^t$  and  $\kappa^c$  controlling respectively the plastic flow in tension and in compression. The evolution law  $f$  is defined as:

$$f(\sigma, \kappa) = \begin{cases} \sigma - \bar{\sigma}_t(\kappa^t) \leq 0 & \text{for } \sigma \geq 0 \\ \sigma - \bar{\sigma}_c(\kappa^c) \geq 0 & \text{for } \sigma < 0 \end{cases} \quad (3.10)$$

where  $\sigma$  is the stress (MPa) and  $\bar{\sigma}_t$  and  $\bar{\sigma}_c$  the tensile and compressive yield stresses, which depend on  $\kappa^t$  and  $\kappa^c$  respectively. The previously defined evolution law  $f$  (also called the yield function) implies that, in a classical elasto-plastic approach, the current stress  $\sigma$  cannot exceed the value of the yield stress  $\bar{\sigma}$ . This phenomenon is illustrated in Figure 3.8. If this dependence is nonlinear, a local Newton-Raphson scheme is used to determine the plastic state and the stress update. The stress update corresponding to an increment from state  $n$  to state  $n+1$  can be written as:

$$\sigma_{n+1} = \sigma_n + E(\Delta\epsilon_{n+1} - \Delta\epsilon_{n+1}^p) \quad (3.11)$$

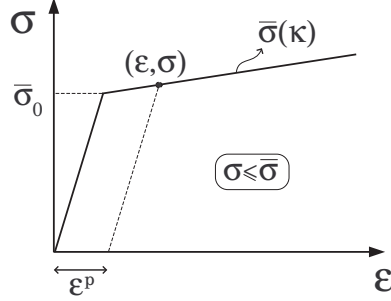


**Figure 3.8:** Typical stress-strain relationship of an elasto-plastic model.

with  $E$  the elastic modulus (GPa),  $\Delta\epsilon_{n+1}$  the strain increment and  $\Delta\epsilon_{n+1}^p$  the plastic strain increment.

Eqs. (3.10) and (3.11) provide the set of constitutive expressions to be linearised at each iteration in a return-mapping algorithm in a general fashion:

$$\sigma_{n+1} - \sigma_{n+1}^{trial} + E\Delta\epsilon_{n+1}^p = 0 \quad (3.12)$$

$$f(\sigma_{n+1}, \kappa_{n+1}) = 0 \quad (3.13)$$

with  $\sigma_{n+1}^{trial} = \sigma_n + E\Delta\epsilon_{n+1}$  the trial stress. By using (3.9),  $\Delta\epsilon^p$  can be substituted in Eq. (3.12) and the constitutive problem can be expressed in a residual form as a function of two variables ( $\sigma$  and  $\kappa$ ):

$$\{R(\sigma_{n+1}, \kappa_{n+1})\} = \left\{ \begin{array}{l} \sigma_{n+1} - \sigma_{n+1}^{trial} + E\Delta\kappa_{n+1} \\ f(\sigma_{n+1}, \kappa_{n+1}) \end{array} \right\} = 0 \quad (3.14)$$

This system of equations is solved using a Newton-Raphson iterative scheme. Based on the linearised form of Eq. (3.14), the correction at local iteration ( $j+1$ ) is computed as:

$$\left\{ \begin{array}{l} \delta\sigma_{n+1} \\ \delta\kappa_{n+1} \end{array} \right\}_{j+1} = -[J_p]_j^{-1} \{R_j\} \quad (3.15)$$

where the Jacobian  $[J_p]$  is defined as:

$$[J_p] = \frac{\partial \{R\}}{\partial \{\sigma, \kappa\}} \quad (3.16)$$

which can be used to evaluate the material tangent operator  $H$  consistent with the return-mapping algorithm:

$$H = \frac{\partial \sigma}{\partial \epsilon} \quad (3.17)$$

### 3.3 Modelling of RC members

The constitutive parameters values used are shown in Table 3.2.

**Table 3.2:** Material parameters of the constitutive models: in accordance with [51, 52]

steel					
$\bar{\sigma}_0$ [MPa]	$E$ [GPa]	$\epsilon_{s,lim}$	$\bar{\sigma}(\kappa)$ [MPa]		
500	200	4%	$\bar{\sigma}_0(1 + 1.5\kappa)$		

concrete			concrete		
compression			tension		
$\bar{\sigma}^c$ [MPa]	$E_c$ [GPa]	$\epsilon_{c,lim}$	$\bar{\sigma}_0^t$ [MPa]	$E_t$ [GPa]	$\bar{\sigma}^t(\kappa)$ [MPa]
37.9	17	0.35%	3.25	32	$\bar{\sigma}_0^t \exp(-6700\kappa)$

## 3.3 Modelling of RC members

### 3.3.1 Kinematics description

Two-noded Bernoulli beam elements are employed in the present FEM formulation. The elemental displacement vector  $\{q_e\}$  constitutes the spacial discretisation of the continuous displacement field:

$$\{q_e\} = \{u_1, v_1, \theta_1, u_2, v_2, \theta_2\}^t \quad (3.18)$$

It includes six degrees of freedom per element, where  $u_1, u_2$  stand for the nodal axial displacements;  $v_1, v_2$  the nodal deflections and  $\theta_1, \theta_2$  the nodal rotations of nodes 1 and 2 respectively, as shown in Figure 3.9.

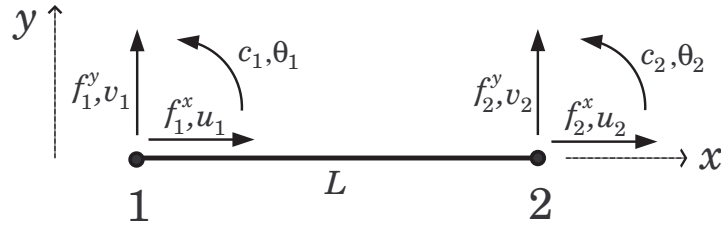


**Figure 3.9:** Beam element: nodal degrees of freedom.

In the Bernoulli beam approximation, the cross-sections remain plane and perpendicular to the longitudinal axis of the beam (i.e. axis  $x$ ), which means that no shear deformation is considered. This choice may be justified

### 3. Rate Independent Modelling of RC Structures

---

by the fact that the structures under study will be considered to be properly designed against shear failure, as prescribed by the GSA [1], so that flexural effects are predominant in the beam response. The generalised strains vector, consisting hence of the mean axial strain  $\bar{\epsilon}$  and the curvature  $\chi$ , can be calculated at a given axial coordinate  $x$  from the nodal displacements as follows:

$$\{E^{gen}\} = \begin{Bmatrix} \bar{\epsilon} \\ \chi \end{Bmatrix} = \begin{Bmatrix} \frac{du}{dx}, \frac{d^2v}{dx^2} \end{Bmatrix}^t = [B] \{q_e\} \quad (3.19)$$

where  $u$  and  $v$  are respectively the continuous horizontal and vertical displacements at  $x$ . The matrix  $[B]$  relates to the interpolation adopted in the discretisation. It is composed of the derivatives of the shape functions with respect to the axial coordinate. Here, a linear interpolation is used for the axial displacement  $u$ , while a Hermite polynomial interpolation is employed for the deflection  $v$ :

$$\{u, v\}^t = [N] \{q_e\} \quad (3.20)$$

where

$$[N] = \begin{bmatrix} 1 - \frac{x}{L} & 0 & 0 & \frac{x}{L} & 0 & 0 \\ 0 & 1 - 3\left(\frac{x}{L}\right)^2 + 2\left(\frac{x}{L}\right)^3 & x\left(1 - \frac{x}{L}\right)^2 & 0 & 3\left(\frac{x}{L}\right)^2 - 2\left(\frac{x}{L}\right)^3 & -x\left(\frac{x}{L}\right) + x\left(\frac{x}{L}\right)^2 \end{bmatrix} \quad (3.21)$$

is the interpolation matrix, with  $L$  the element length. Considering this expression for matrix  $[N]$ , and substituting Eq.(3.20) in Eq. (3.19), the matrix  $[B]$  results:

$$[B] = \begin{bmatrix} \frac{d}{dx} & 0 \\ 0 & \frac{d^2}{dx^2} \end{bmatrix} [N] = \begin{bmatrix} -1/L & 0 & 0 & 1/L & 0 & 0 \\ 0 & -\frac{6}{L^2} + \frac{12x}{L^3} & -\frac{4}{L} + \frac{6x}{L^2} & 0 & \frac{6}{L^2} - \frac{12x}{L^3} & -\frac{2}{L} + \frac{6x}{L^2} \end{bmatrix} \quad (3.22)$$

The corresponding generalised stresses are:

$$\{\Sigma^{gen}\} = \{N, M\}^t \quad (3.23)$$

with  $N$  the axial force and  $M$  the bending moment. They are evaluated at the Gauss points locations by using the multilayered approach explained next in Section 3.3.2. Finally, the elemental internal forces  $\{f_e^{int}\}$  are calculated by integrating the generalised stresses  $\{\Sigma^{gen}\}$  over the element:

$$\{f_e^{int}\} = \{f_1^x, f_1^y, c_1, f_2^x, f_2^y, c_2\}^t = \int_{V_e} [B]^t \{\Sigma^{gen}\} dV \quad (3.24)$$

This vector contains the horizontal nodal forces  $f_1^x$  and  $f_2^x$ , the vertical nodal forces  $f_1^y$  and  $f_2^y$ , and the nodal torques  $c_1$  and  $c_2$ . Three Gauss points are used for the numerical integration.

#### 3.3.2 Layered beam formulation

A multilayered beam approach [43–47] is used for the evaluation of the generalised stresses  $\{\Sigma^{gen}\}$  from the generalised strains  $\{E^{gen}\}$ . Each cross-section where the beam response has to be computed – i.e. the Gauss points of a finite element – is discretised into a finite number of longitudinal layers where the one-dimensional constitutive equations for concrete and steel are applied. The cross-sectional behaviour of the element is thus directly derived by integration of the stress-strain response of the layers.

This numerical procedure is carried out in the following manner. First, the axial strains in each layer ( $\epsilon_i$ ) are computed from the generalised strains  $\{E^{gen}\} = \{\bar{\epsilon}, \chi\}^t$ :

$$\epsilon_i = \bar{\epsilon} - \bar{y}_i \chi \quad (3.25)$$

where  $\bar{y}_i$  is the cross-sectional average vertical coordinate of layer  $i$  computed from the sectional center of gravity. Then the layer-wise stresses (i.e. the axial stresses  $\sigma_i$ ) are obtained by applying the 1D constitutive equations on each layer. Since a perfect adherence is assumed between the steel bars and concrete, for the layers containing the steel reinforcements, the stresses in concrete and steel are computed separately and the layer average stress is obtained depending on the steel volume fraction of the considered layer. The stress is computed at the mid-height of the layer, and assumed to be constant over its thickness. Finally the cross-section generalised stresses  $\{\Sigma^{gen}\}$  are evaluated by integrating the layer-wise one-dimensional stresses  $\sigma_i$  through the cross-sectional area of the beam:

$$\begin{aligned} N &= \sum \sigma_i \Omega_i \\ M &= - \sum \sigma_i \bar{y}_i \Omega_i \end{aligned} \quad (3.26)$$

with  $\Omega_i$  the cross-sectional area of the layer. Figure 3.10 gives a schematic representation of the cross-sectional parameters.

Note that such averaged relations can only be applied in a point-wise manner in classical structural computations provided they do not exhibit overall softening, in order to keep a well-posed description. If softening is obtained in the beam response and unless a nonlocal or gradient type beam formulation is used, the corresponding dissipation at the structural scale is

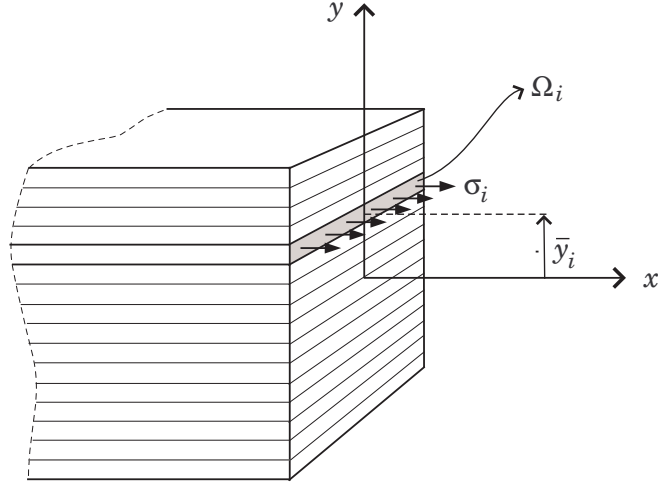


**Figure 3.10:** Illustration of a multilayered beam section.

computationally determined by the element size [64, 65]. As a result, the structural discretisation will be chosen subsequently to provide localisation on a physically motivated beam length (size of the plastic hinges).

The related cross-sectional consistent tangent operator  $[H_t]$  can be derived from the layer-wise consistent tangent operators  $H_i$  from Eq. (3.17) as follows:

$$[H_t] = \frac{\partial\{\Sigma^{gen}\}}{\partial\{E^{gen}\}} = \begin{bmatrix} \sum H_i \Omega_i & -\sum H_i \bar{y}_i \Omega_i \\ -\sum H_i \bar{y}_i \Omega_i & \sum H_i \bar{y}_i^2 \Omega_i \end{bmatrix} \quad (3.27)$$

This layered approach is summarised in Figure 3.11, which also shows that only the longitudinal reinforcements are taken into account. As previously mentioned, the structures under study will be considered to be properly designed so that flexural failure is more likely to occur than shear failure in a progressive collapse scenario. As an additional simplifying assumption, a perfect bond is assumed between the layers. The structural scale assumption (Bernoulli) remains consistent with this approach at the fine scale. Moreover, this approach allows for a gradual element-wise strength degradation as a consequence of the progressive failure of the constitutive layers, for which the stress is set to zero when the failure criteria are fulfilled. It allows for a ductile sectional response, which is proven to be an important factor for the moment redistribution in the structure [49, 50]. This also means that rather complex nonlinear sectional responses exhibiting softening can be obtained even with simplified 1D constitutive laws for the constituents (such as linear

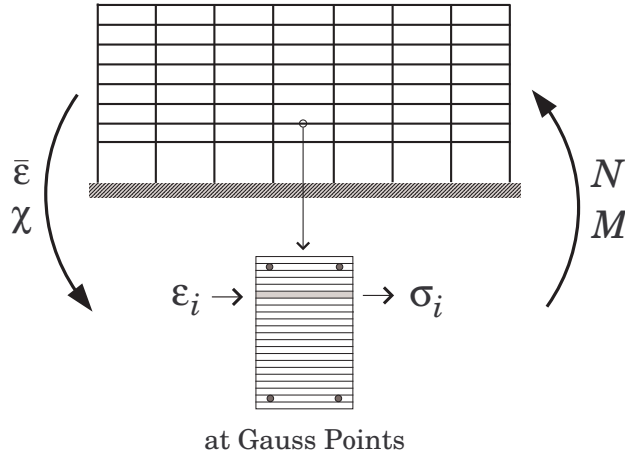


**Figure 3.11:** Multilayered beam: generalised stresses evaluation.

hardening) provided they are followed by a sudden drop of the stress at the ultimate strain. The evolving interactions between  $N$  and  $M$  are also naturally considered. The straightforwardness of the present formulation to describe the RC sectional behaviour with respect to the closed-form approaches is pointed out.

**Application: response of the multilayered model for different reinforcement schemes and axial loads**

In order to illustrate the response of the multilayered beam model developed for RC beams, and to show the advantages of such a multilevel approach with respect to a priori identified analytical closed-forms for the moment–curvature relationships, a uniform bending test is performed on a single beam.

The test description is depicted in Figure 3.12: a uniform bending is created on a simply supported beam by applying an angular displacement  $\theta$  at both ends. The uniform curvature  $\chi$  is calculated as:

$$\chi = \frac{\delta\theta}{\delta x} = \frac{2\theta}{L} \quad (3.28)$$

with  $L$  the beam length. Since the cross-sectional response of a beam depends on the design parameters, the test is carried out for three different reinforcement arrangements (Schemes A, B and C). In particular, the bottom reinforcement is varied so that the top-to-bottom reinforcement ratio takes three different values:  $(\rho_T/\rho_B)_A = 1.5$ ;  $(\rho_T/\rho_B)_B = 1$  and  $(\rho_T/\rho_B)_C = 3.84$ .

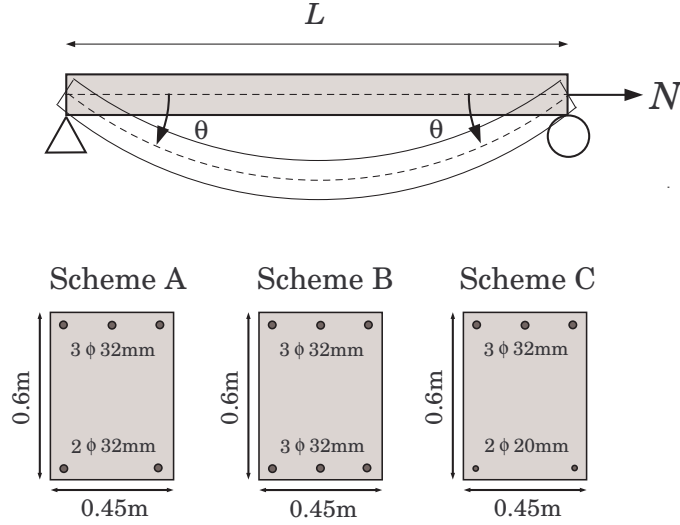


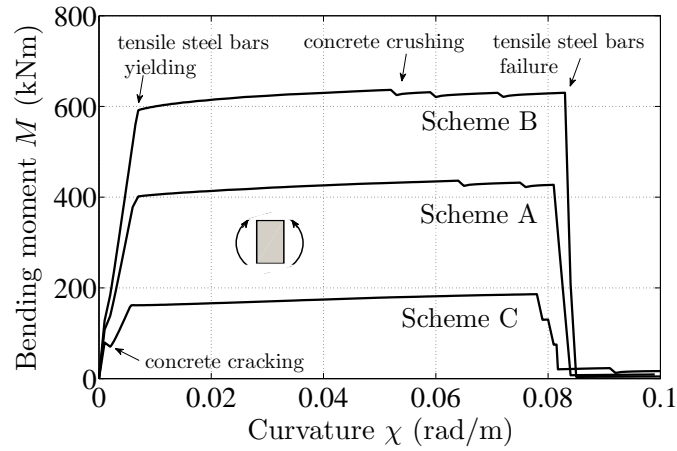
**Figure 3.12:** Uniform bending test description.

The overlap (vertical distance between the steel bars and the nearest section edge) is set to 5 cm for the three schemes.

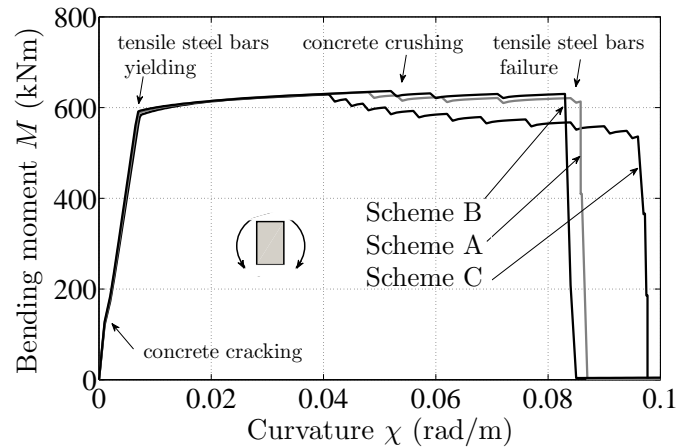
The first set of computations is performed for an axial load  $N = 0$ . The resulting bending moment–curvature diagrams for positive and negative bending are depicted in Figure 3.13, where the description of the sectional failure progression is indicated next to the curves.

First, cracking of tensile concrete takes place. Then yielding of the tensile steel bars occurs, followed by the crushing of compressive concrete and the fracture of the tensile reinforcements. It can be observed that the response of the multilayered beam model corresponds to the actual behaviour of a RC beam. As expected, the bending moment obtained for Schemes A and C is higher for negative bending since the upper reinforcement ratio is larger than the lower one, while the same resistance level for positive and negative bending is obtained for the symmetrical Scheme B. For positive bending ( $M > 0$ ), the sectional resistance increases as a function of the bottom steel ratio, which in this case acts as the tensile steel ( $\rho_t = \rho_B$ ). The fracture of the tensile steel bars logically occurs earlier for lower tensile steel amounts: for Scheme C, the tensile steel failure takes place before the crushing of compressive concrete. In the case of negative bending ( $M < 0$ ), the same level of resistance is obtained for the three reinforcement schemes since the amount of tensile steel (i.e. top bars) is identical ( $\rho_t = \rho_T$ ). The concrete

### 3.3 Modelling of RC members



(a) Positive bending



(b) Negative bending

**Figure 3.13:** Bending moment–curvature diagrams for different bottom reinforcement amounts.

crushing initiates earlier for lower bottom reinforcement amounts, in order to compensate the higher tensile (i.e. top steel) amount. The tensile steel bars failure occurs later for lower bottom reinforcement amounts, contrarily to the case of positive bending. The final ductility of the section is thus linked to the tensile-to-compressive reinforcement ratio ( $\rho_t/\rho_c$ ). Note that this result is made possible by the gradual failure of the concrete layers under compression after the onset of crushing in the section. If this softening character of the sectional response was not taken into account, the related increase in the ductility would not be obtained (the section would be considered as ‘failed’ on the onset of crushing).

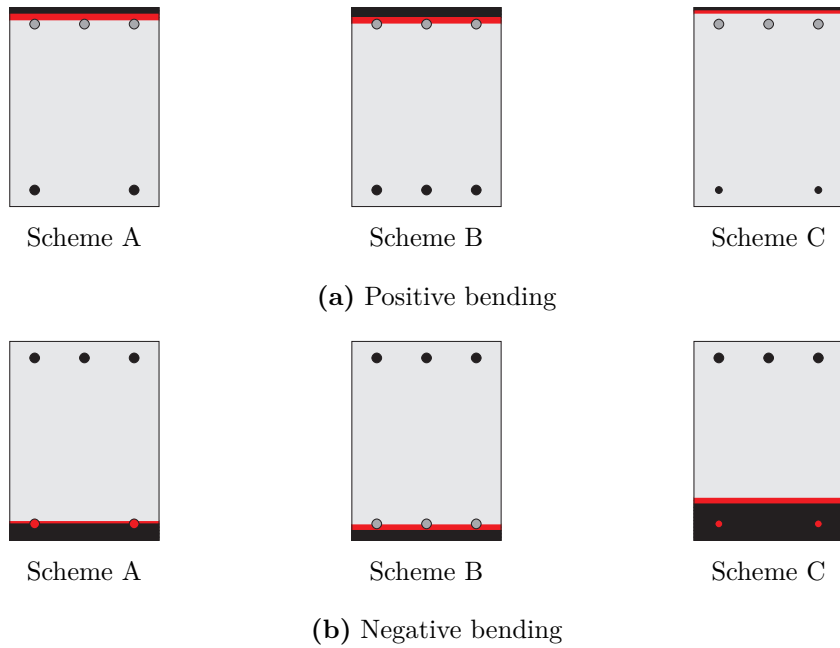


**Figure 3.14:** Final sectional state for different bottom reinforcement amounts.

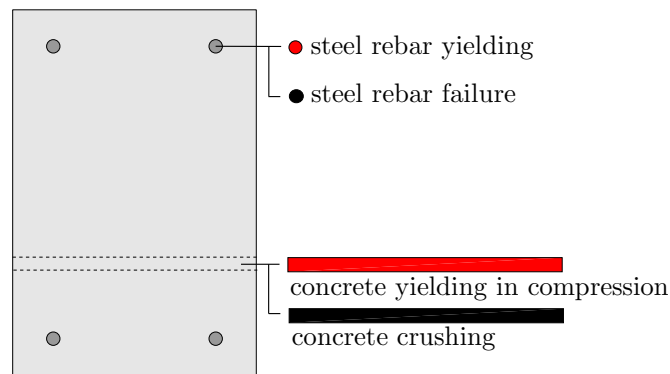
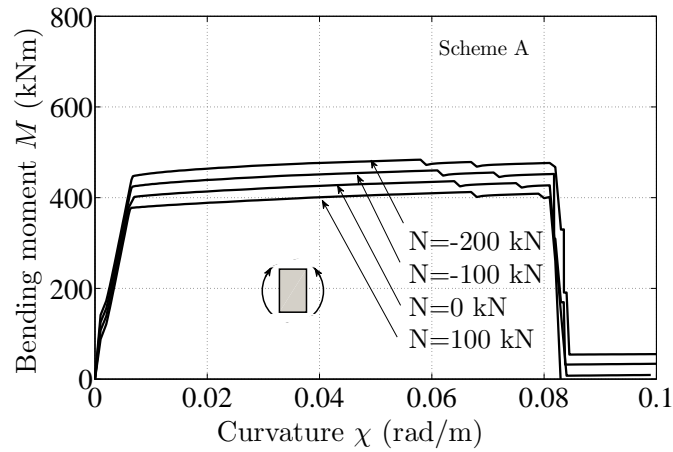


**Figure 3.15:** Representation of the sectional response.

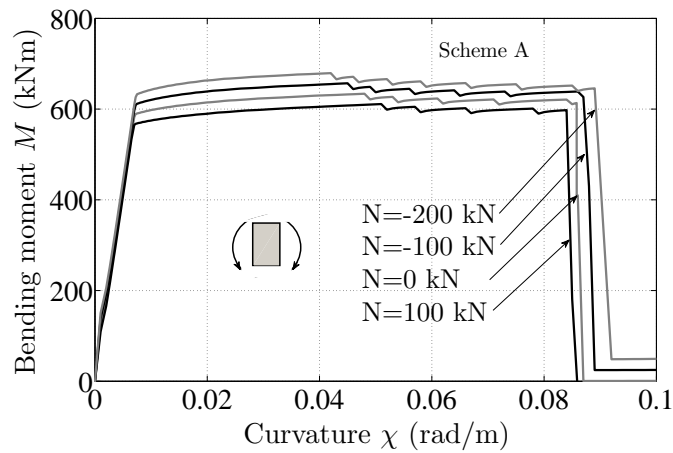
The final state of the beams is detailed in Figure 3.14: red areas correspond to the material regions having exceeded the yield stress (i.e. the plastic region is reached in concrete or steel), while black ones correspond to those regions where the ultimate strain is surpassed (crushing of concrete or steel bars failure). Tensile cracking is not represented for the sake of clarity. The interpretation of the colours used for the sectional response representation is summarised in Figure 3.15. Note that, for both positive and negative bending,

### 3.3 Modelling of RC members

the crushed concrete area (thus the black zone) increases as a function of the tensile reinforcement amount and decreases with the compressive reinforcement amount. The progressive degradation and ductility of the section appears to be related to the amount of crushed concrete. These results confirm that the crushing of concrete may lead to a reduction of the sectional load-bearing capacity depending on the reinforcement scheme, and must therefore be taken into account together with the tensile steel bars yielding in order to properly characterise the rotational capacity of the beams. In this study, Schemes A and B under negative bending result in a better exploitation of the materials: at the moment of the tensile reinforcement failure not only the compressive concrete area is higher, but also the compressive steel bars reach



(a) Positive bending



(b) Negative bending

**Figure 3.16:** Bending moment–curvature diagrams for different axial loads.

the plastic region (in red). In order to show the interactions that exist between the axial and the flexural response of the beam, the test is reproduced for various values of the axial load  $N$ , exclusively for Scheme A. The results are shown in Figure 3.16, again under positive and negative bending.

An increase of the sectional resistance is observed for higher values of the compressive axial load, together with a higher ductility (the fracture of the tensile steel bars occurs later for increasing compressive axial loads). The sectional response depicted in Figure 3.17 shows that the increase of the compressive axial load leads to a better exploitation of concrete due to the growth of the compressive region in the section.

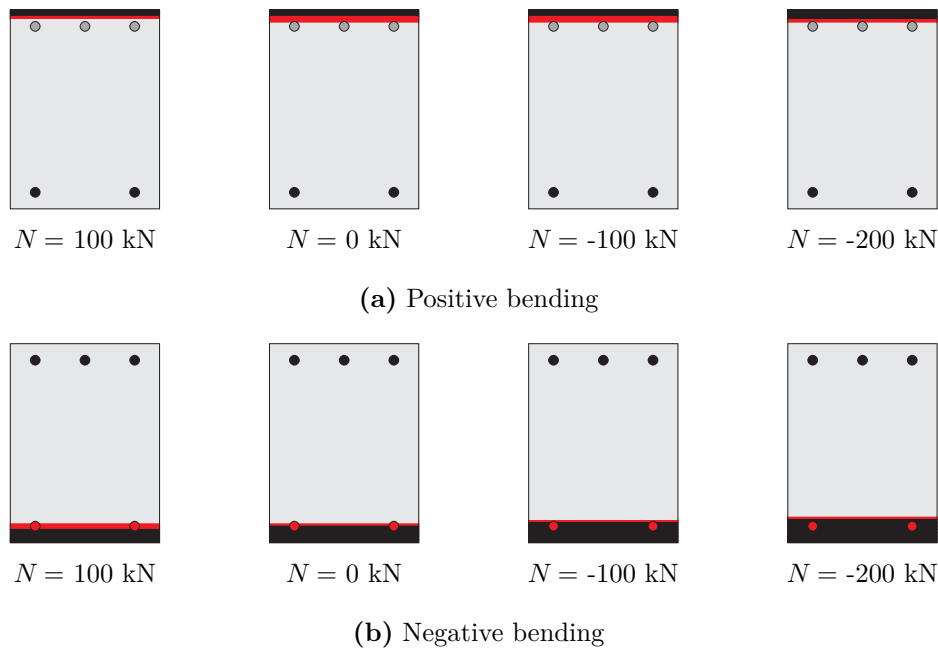
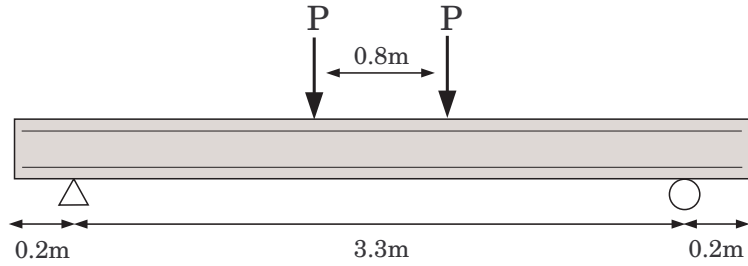


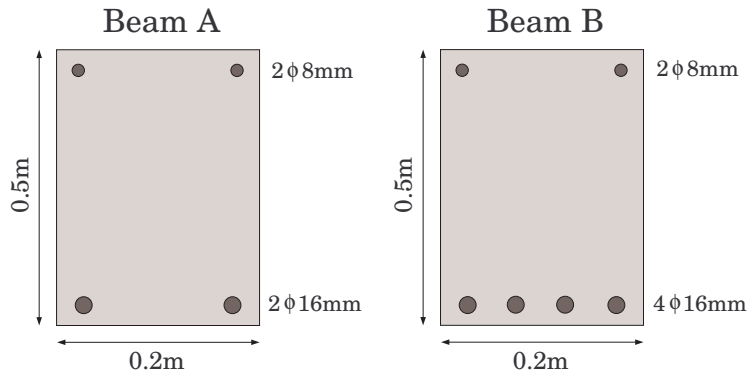
**Figure 3.17:** Final sectional state for different axial loads.

### 3.3.3 Experimental illustration

An illustrative manner of assessing the response of the multilayered approach is presented here by means of an experimental comparison. A four-point bending test on a simply supported beam was conducted in the context of a Master's thesis at the Vrije Universiteit van Brussel (VUB) [66].



(a) Test configuration.



(b) Beams cross-sectional description.

**Figure 3.18:** Four-point bending experimental test.

The experimental set-up is sketched in Figure 3.18a. This test was carried out on two RC beams (A and B) with different reinforcement arrangement. Their cross-sections are described in Figure 3.18b. The overlap is 5 cm. The concrete class for both tests was C60. As for steel, S550 type rebars were used. The values of the parameters adopted to fit such material characteristics are shown in Table 3.3. For concrete in compression, they are obtained according to the EN 1992-1-1 [51] prescriptions for a C60 concrete: the bilinear approximation proposed for the stress-strain curve is adopted again. In tension, the softening evolution law adopted here results in a specific fracture energy of  $G_f = 180 \text{ Nm/m}^2$ . According to the prescriptions of the *fib* (equations *fib*(1) to *fib*(4) in Table 3.1) this parameter takes values between 135 and  $220 \text{ Nm/m}^2$  for a C60 concrete class, depending on the aggregate characteristics. The value of the tensile strength is obtained through expression (3.8).

For the steel reinforcement, the ultimate strain is chosen accordingly to the results obtained from a tension test on a 11.98 mm diameter bar with the same properties as those used in the test [66]. Figure 3.19 shows the experimental strain-stress curve for steel and its corresponding numerical

### 3. Rate Independent Modelling of RC Structures

approximation. The observed limited ductility of the steel is accounted for the fact that it has been pre-tensioned in the past. Note that the studied beams were constructed specifically for academic purposes and hence the steel properties do not correspond to the traditional criteria for ductility.

**Table 3.3:** Material parameters for the experimental comparison.

steel					
$\bar{\sigma}_0$ [MPa]	$E$ [GPa]	$\epsilon_{s,lim}$	$\bar{\sigma}(\kappa)$ [MPa]		
550	200	0.85%	$\bar{\sigma}_0(1 + 1.5\kappa)$		

concrete					
compression			tension		
$\bar{\sigma}^c$ [MPa]	$E_c$ [GPa]	$\epsilon_{c,lim}$	$\bar{\sigma}_0^t$ [MPa]	$E_t$ [GPa]	$\bar{\sigma}^t(\kappa)$ [MPa]
68	31	0.35%	4.8	38.8	$\bar{\sigma}_0^t \exp(-5830\kappa)$

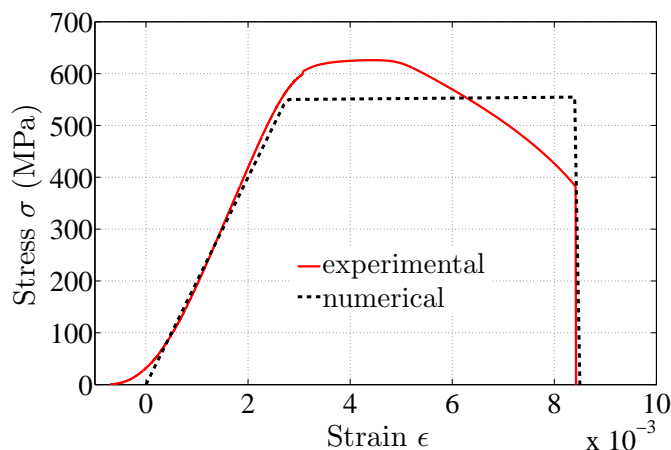
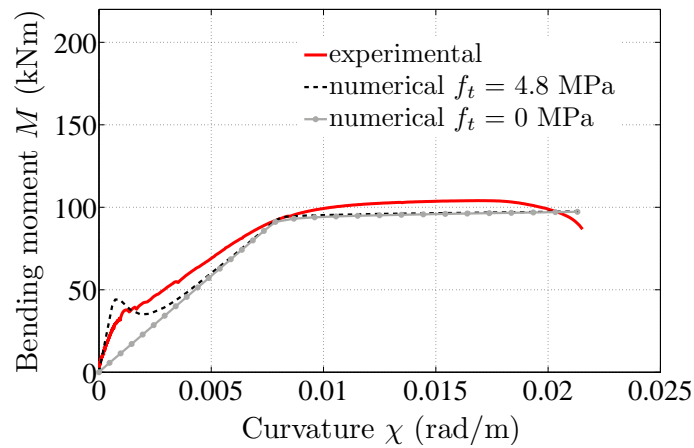


**Figure 3.19:** Stress-strain diagram for steel: experimental vs. numerical.

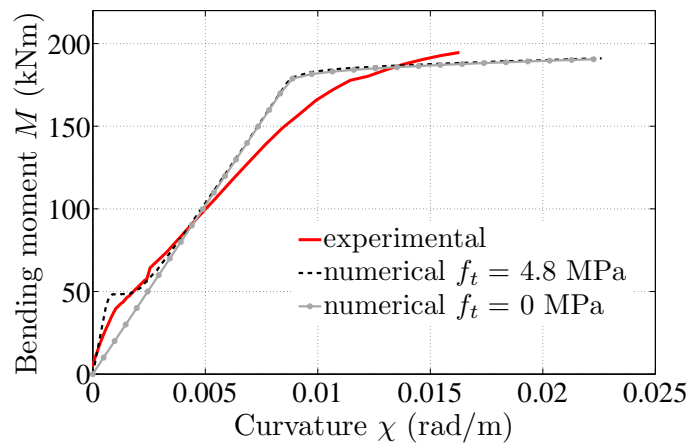
The element size is taken approximately equal to the cross-sectional depth ( $L_{el} = 200$ - $250$  mm), except for the element located at the mid-span, for which the length is  $L_{el} = 400$  mm. This size corresponds to the order of magnitude of the physical length where the localisation takes place. The reason for this choice will be given in Section 3.5, where the issues of mesh-sensitivity and strain localisation in reinforced concrete are discussed. A total number of 50 layers are used for the cross-sectional discretisation, thus 10 mm thick each, which gives a good approximation of the continuous cross-sectional

### 3.3 Modelling of RC members

behaviour. Stirrups are not taken into account in the analysis. The displacement control method is used, since the softening nature of the layered beam model prevents the load control method from being applied in a static analysis. Since failure occurs at the mid-point of the beam due to the fracture of the tensile steel, the numerical simulation is stopped when the ultimate strain of  $\epsilon_{s,lim} = 0.85\%$  is reached in the steel bars. The bending moment vs. curvature curves obtained at the mid-span for Beams A and B are shown in Figure 3.20. For each experimental test, two slightly different computations have been conducted: in one the tensile strength of concrete is considered, while in the other it is not ( $f_t = 0$ ).



(a) Beam A



(b) Beam B

**Figure 3.20:** Moment-curvature diagrams: experimental vs. numerical response.

For Beam A, the model matches the experimental results quite accurately for both values of the concrete tensile strength, as seen in Figure 3.20a. The initiation of cracking in concrete occurs at the same point for both the test and the computation in which the tensile resistance of concrete is considered (at approx. 0.001 rad/m). The curve obtained for a  $f_t > 0$  would suggest that the tensile strength of  $f_t = 4.8$  MPa obtained following the *fib* predictions (Eq. (3.8)) overestimates the real value for this parameter. However, it must be noted that this disagreement might stem from the fact that a displacement control technique is adopted for the numerical simulation, whereas a force control technique is used in the experimental test. The steel bars yielding in tension would also take place at approximately the same moment (at 0.008 rad/m approx.). The maximum bending moment is however lower in the simulations, due to the choice of the numerical stress-strain curve, which underestimates the peak stress with the aim of preserving the total failure energy with respect to the experimental stress-strain curve for steel (Figure 3.19).

For Beam B (Figure 3.20b), the agreement is not so good in the final ascending branch of the moment-curvature diagram, where the elastic modulus of steel appears to be overestimated in the numerical simulations. This discrepancy could be also due to the bilinear approach adopted for modelling both the concrete in compression and the steel. In reality, the stress-strain evolutions for both materials are much more curved. It must be pointed out that unfortunately the experimental test for Beam B had to be stopped before the actual failure of the steel bars took place, due to a technical problem. It is thus impossible to know whether the numerical results adjust the experimental ones beyond this point. However, the same trend is observed in terms of bending moment capacity of the section with respect to Beam A. For both Beams A and B, no crushing of the compressive concrete is obtained in the numerical simulation, as it was the case in the experimental results. This means that the ultimate compressive strain  $\epsilon_{c,lim}$  is not reached at any point of the beam.

Although some approximate hypotheses have been assumed for the numerical simulation, i.e. no modelling of the stirrups, a perfect bond layered model, a simplified stress-strain relationship for concrete [51], Bernoulli's hypothesis and a small displacements approach, a reasonable agreement can be perceived between the experimental and numerical results in terms of sectional resistance and ductility. It should be emphasized, however, that relevant conclusions can by no means be drawn out of this single test. The aim of this experimental comparison was merely to provide an insight on the

degree of adequacy of the multilayered beam approach.

### 3.4 Time integration scheme for the dynamic problem

An implicit Newmark scheme is adopted for the integration of the equations of motion in the simulations [67]. The discretised equations describing the equilibrium in dynamics read

$$\{f^{int}(\{q\})\} + [M]\{\ddot{q}\} = \{f^{ext}\} \quad (3.29)$$

with  $\{f^{int}\}$  the internal nodal forces,  $\{f^{ext}\}$  the external forces and  $[M]$  the mass matrix.  $[M]$  is defined as follows:

$$[M] = \sum_e \int_{V_e} [N]^t \rho [N] dV \quad (3.30)$$

Substituting the value of matrix  $[N]$  from expression (3.21) in Eq. (3.30) and performing the numerical integration, the mass matrix yields the following constant value:

$$[M] = \begin{bmatrix} \frac{\rho AL}{3} & 0 & 0 & \frac{\rho AL}{6} & 0 & 0 \\ 0 & \frac{156\rho AL}{420} & \frac{22\rho AL^2}{420} & 0 & \frac{54\rho AL}{420} & \frac{-13\rho AL^2}{420} \\ 0 & \frac{22\rho AL^2}{420} & \frac{4\rho AL^3}{420} & 0 & \frac{13\rho AL^2}{420} & \frac{-3\rho AL^3}{420} \\ \frac{\rho AL}{6} & 0 & 0 & \frac{\rho AL}{3} & 0 & 0 \\ 0 & \frac{54\rho AL}{420} & \frac{13\rho AL^2}{420} & 0 & \frac{156\rho AL}{420} & \frac{-22\rho AL^2}{420} \\ 0 & \frac{-13\rho AL^2}{420} & \frac{-3\rho AL^3}{420} & 0 & \frac{-22\rho AL^2}{420} & \frac{4\rho AL^3}{420} \end{bmatrix} \quad (3.31)$$

where  $A$  is the total cross-sectional area of the beam and  $\rho$  is the sectional density. Note that this density includes the contribution of the distributed loads applied to the beam (i.e. the live loads and the weight of the slab and additional concrete layer), so that their inertia is taken into account in the dynamic computations. It is calculated as:

$$\rho = \rho_{\text{section}} + \frac{\text{Loads}}{gA} \quad (3.32)$$

with  $g = 9.81 \text{ m/s}^2$  the gravity constant.  $\rho_{\text{section}}$  is the averaged density calculated from the densities of concrete and steel,  $\rho_c = 2400 \text{ kg/m}^3$  and  $\rho_s = 7800 \text{ kg/m}^3$ , respectively. The internal forces  $\{f^{int}\}$  are a nonlinear function of the displacements  $\{q\}$ . To solve Eq. (3.29) within an incremental-iterative scheme, a linearisation of the equations must be performed. Writing

### 3. Rate Independent Modelling of RC Structures

---

equilibrium as a residual form, the related structural Jacobian matrix  $[J]$  is computed as the derivative of the residual with respect to the displacements:

$$[J] = \frac{\partial(\{f^{int}(\{q\})\} + [M]\{\ddot{q}\} - \{f^{ext}\})}{\partial\{q\}} \quad (3.33)$$

Using the notion of structural tangent operator  $[K_t]$ , which denotes the variation of the internal forces with respect to the displacements, the expression of the iteration matrix  $[J]$  is given by:

$$[J] = [K_t] + [M] \frac{\partial\{\ddot{q}\}}{\partial\{q\}} \quad (3.34)$$

where  $[K_t]$  is computed by applying the cross-sectional consistent tangent operator  $[H_t]$  calculated in Eq. (3.27):

$$[K_t] = \sum_e \int_{V_e} [B]^t [H_t] [B] dV \quad (3.35)$$

where  $[B]$  relates the generalised strains to the nodal displacements (Eq. (3.22)). Finally, the Newmark formulae allow for computing the remaining term  $\frac{\partial\{\ddot{q}\}}{\partial\{q\}}$  in Eq. (3.34), by defining relationships between the nodal displacements, velocities and accelerations. These formulae are expressed for a given time  $t_{n+1}$  as [67]:

$$\begin{aligned} \{\dot{q}_{n+1}\} &= \{\dot{q}_n\} + (1 - \gamma)\Delta t \{\ddot{q}_n\} + \gamma\Delta t \{\ddot{q}_{n+1}\} \\ \{q_{n+1}\} &= \{q_n\} + \Delta t \{\dot{q}_n\} + \Delta t^2 \left(\frac{1}{2} - \beta\right) \{\ddot{q}_n\} + \Delta t^2 \beta \{\ddot{q}_{n+1}\} \end{aligned} \quad (3.36)$$

with  $\Delta t$  the time step; and  $\gamma$  and  $\beta$  the Newmark parameters associated with the quadrature scheme, which determine the stability of the method [67].

Considering these equations, the iteration matrix results in:

$$[J] = [K_t] + [M] \frac{1}{\beta\Delta t^2} \quad (3.37)$$

A numerical damping of 5% is introduced in order to reduce the spurious high frequency vibrations in the structural response, which significantly increase the computational time in large-scale calculations. The value of the Newmark's algorithm parameters  $\gamma$  and  $\beta$  are chosen such that this damping (affecting mainly the high frequency range) is provided in the simulation, while ensuring unconditional stability [67]:

$$\gamma = \frac{1}{2} + \alpha; \quad \beta = \frac{1}{4} \left(\gamma + \frac{1}{2}\right)^2 \quad (3.38)$$

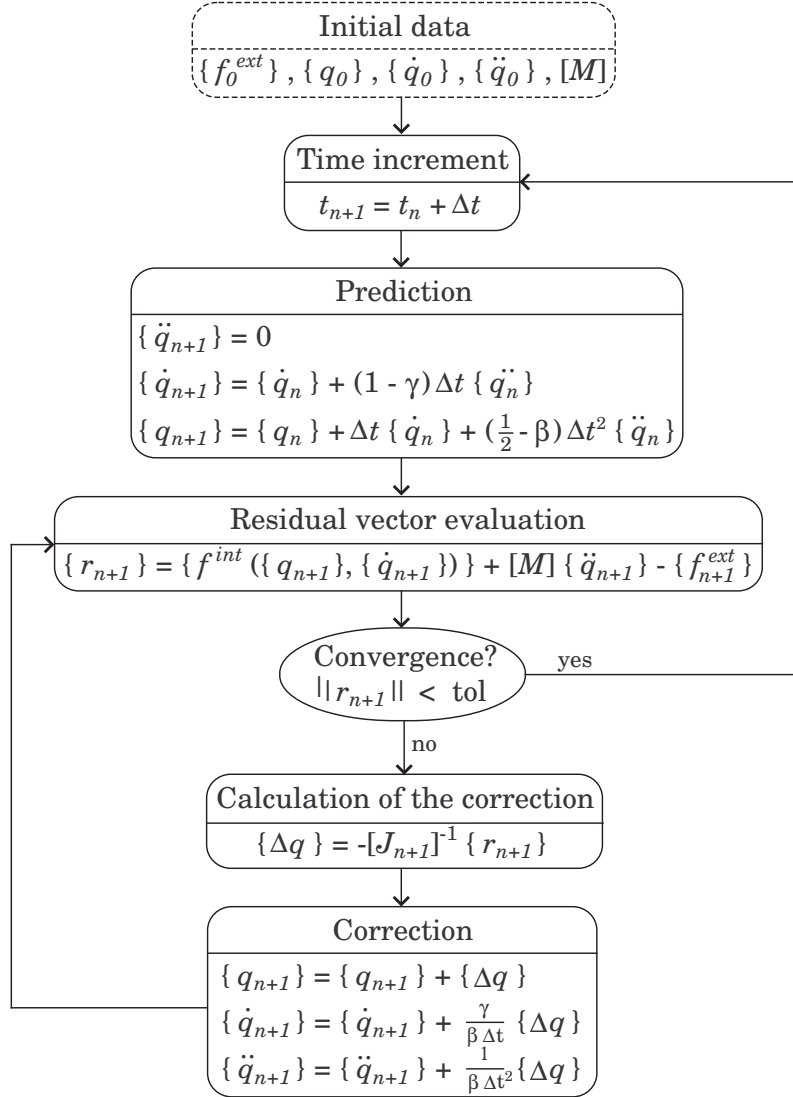


**Figure 3.21:** Dynamic integration scheme [67].

with  $\alpha = 0.05$  the numerical damping ratio. This value for the numerical damping is often used in the simulations of progressive collapse of RC structures [24,33,35]. Figure 3.21 gives a flowchart of the time integration scheme. It can be observed that at each time step  $n+1$ , the iteration starts from a prediction of the displacements, velocities and accelerations by setting  $\ddot{q}_{n+1} = 0$ . The residuals are then evaluated: if the accuracy threshold is exceeded the correction terms need to be calculated by computing the iteration matrix  $J$ .

### 3.5 Strain localisation and size effects

#### 3.5.1 Mesh-sensitivity in RC beams

As already mentioned in the multilayered beam description (Section 3.3.2), the multilevel formulation adopted here allows for a gradual cross-sectional strength degradation as a consequence of the layerwise failure. For advanced states of resistance degradation, a strain-softening behaviour may be exhibited at the sectional level, with the consequent ill-posedness of the structural boundary value problem. This implies a loss of objectivity in the formulation, which is manifested by a pathological sensitivity of the results to the size of the finite elements [64, 65]. The global solution depends on the mesh refinement: the softening region where the deformation is localised is directly determined by the element size. Therefore, the related dissipated energy will also decrease upon mesh-refinement. Hence the need to adopt a structural discretisation which provides a physically motivated amount of energy release.

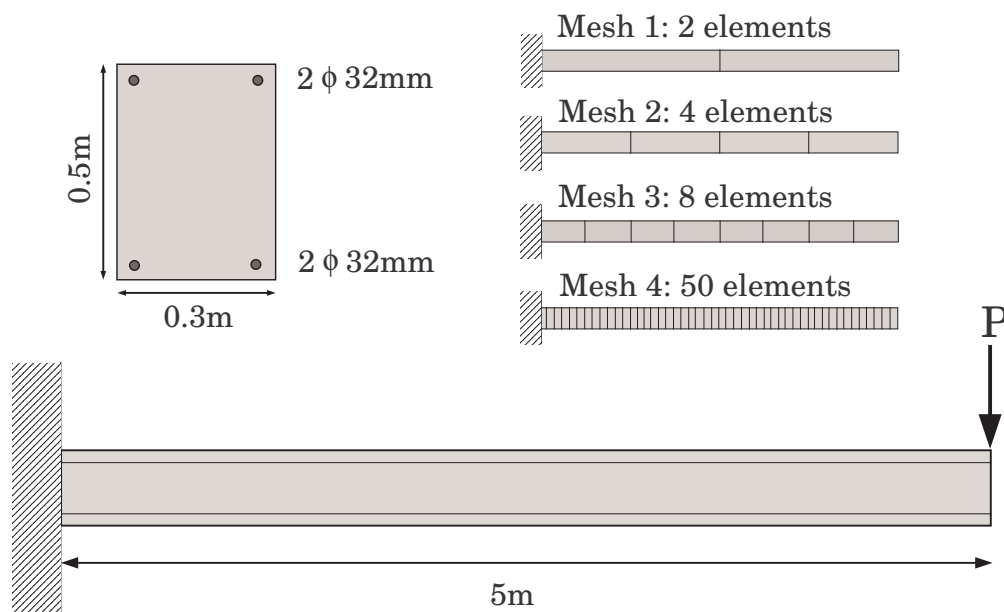


**Figure 3.22:** Mesh-sensitivity test: beam dimensions and different discretisations employed.

This numerical phenomenon can be easily illustrated by a mesh-sensitivity test on a single cantilever beam subjected to a point force on its free end. The

### 3.5 Strain localisation and size effects

---

test is described in Figure 3.22, where the different meshes adopted for the finite element discretisation are also illustrated. The material parameters are those presented in Table 3.2. The displacement control method is adopted here as well. Since the maximum value of the bending moment is obtained at the clamped end of the beam, the plastic deformation is always localised on the leftmost element of the mesh. The energy dissipated in the failure process depends thus on the size of this element. Figure 3.23 shows the load-deflection curve at the loaded point for the four different meshes adopted.

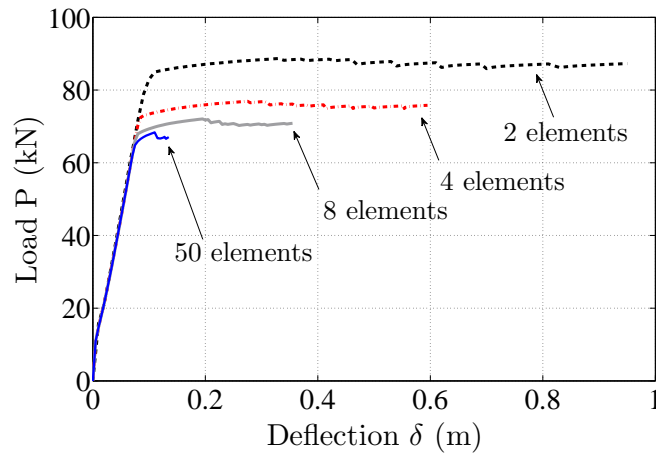


**Figure 3.23:** Load-deflection diagram as a function of the mesh-refinement.

As expected, the energy release decreases with the number of elements used in the discretisation, and consequently so does the global ductility of the structure: the final deflection decreases inversely to the element number in a significant manner. The curvature distribution along the axial coordinate of the beam is also depicted in Figure 3.24. It can be seen that the rotational deformation is concentrated at the two leftmost elements, whatever the element size.

The beam failure process is the following: first, yielding of the tensile steel bars takes place, followed by the crushing of compressive concrete. Finally, the ultimate strain of steel is reached leading to the fracture of the tensile rebars. Figure 3.25 provides the final deformed shape of the beam, as well as the sectional response of the most representative elements: the elements where the steel yielding has occurred are depicted in red, while those having reached failure are depicted in black. The same representation criteria is adopted here for the illustration of the sectional response.

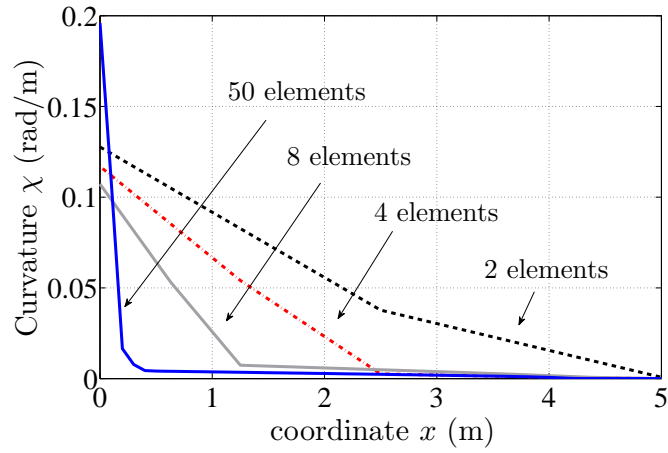


**Figure 3.24:** Curvature distribution along  $x$  as a function of the mesh-refinement.

As it will be explained next, a mesh consisting of approximately 12 elements would provide the best estimation for the failure energy since the corresponding element size ( $L_{el} \approx 0.4$  m) would fit the best the predictions of the characteristic length for a C30 concrete [52].

### 3.5 Strain localisation and size effects

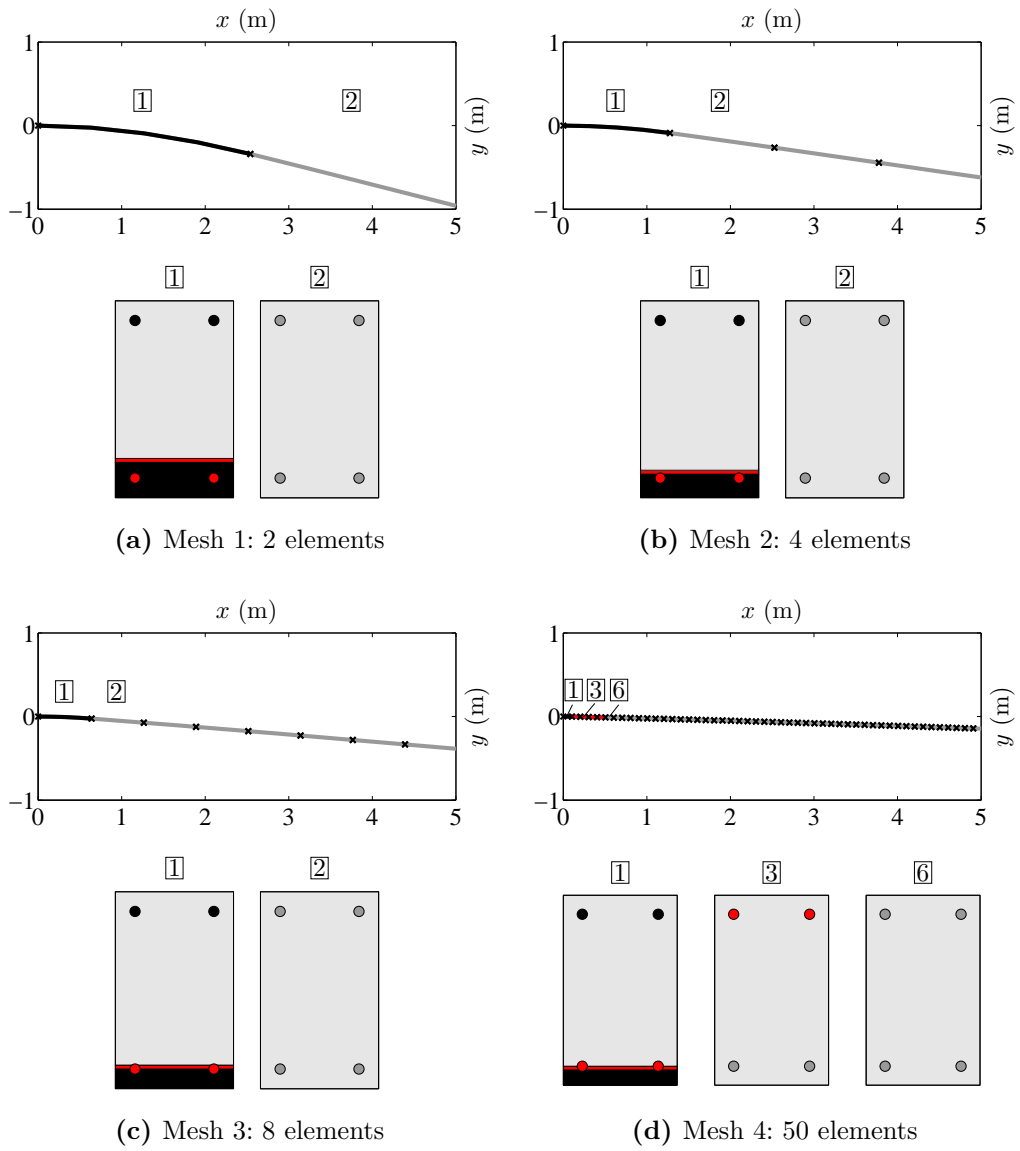


**Figure 3.25:** Final deformed shape of the beam and detailed sectional response for the different discretisations.

### 3.5.2 Characteristic length

There are several ways to overcome the present numerical issue: a material modelling depending on the element size [55], non-local plastic models [65,68], the introduction of viscous effects [69,89]... These formulations have in common the property of playing a regularizing effect by introducing an internal length. In [65] a non-local yield moment is introduced in order to preserve the well-posedness of the bending problem in softening RC beams.

Besides these numerical solutions that avoid mesh-sensitivity related problems, a straightforward manner to partly prevent this pathology in the case of concrete structures is the determination of the characteristic length where strain localisation actually takes place. The finite elements discretisation is then adapted accordingly to this physical parameter. This issue was already introduced in Section 3.1.2, where the tensile material behaviour of concrete is described. There, the discrete character of failure in concrete was addressed, and the consequent need of choosing an element size corresponding to the characteristic length where cracking occurs. The lumped plasticity approaches often employed in the context of flexural analyses of RC frames are also based in this concept of characteristic length [24, 28, 38, 74, 76].

The *fib* gives a mathematical formula for calculating the characteristic length of concrete, as a function of the material properties [52]:

$$L_{ch} = \frac{E_c G_f}{f_t^2} \quad (3.39)$$

with  $L_{ch}$  the characteristic length;  $E_c$  the Young's modulus;  $G_f$  the fracture energy; and  $f_t$  the tensile strength. This formula is mainly used in fracture mechanics, as in [73]. Numerous empirically-based expressions for this parameter can be found in the literature related to the nonlinear analysis of RC beams [74–76]. In most of them, the characteristic length appears as a function not of the material properties but rather of the beam dimensions. Eurocode 2 assumes that the plastic deformation takes place over a length of approximately 1.2 times the depth of section [51]. However, this estimation results in much higher values than those found in the literature [50, 74–76]. Table 3.4 summarises some of the expressions currently used.

Note that the expression provided by the *fib* results in a characteristic length equal to 0.41 m for the material parameters adopted in the present work (C30 concrete), regardless of the beam dimensions. Here, the finite element discretisation employed for the subsequent structural computations

### 3.5 Strain localisation and size effects

---

**Table 3.4:** Some empirical expressions of the characteristic length ( $L_{ch}$ ).

Characteristic length $L_{ch}$ [m]	
$L_{ch} = \sqrt{A}$	[75]
$L_{ch} = 0.25d + 0.075z$	[50, 74]
$L_{ch} = \frac{E_c G_f}{f_t^2} = 0.41$	[52, 73]
$L_{ch} = 0.5d$	[38, 76]
$L_{ch} = 0.08z + 0.022f_y d_b \geq 0.044f_y d_b$	[50, 76]
$L_{ch} \approx 1.2d$	[51]

$E_c = 32$  GPa;  $G_f = 140$  Nm/m<sup>2</sup>;  $f_t = 3.25$  MPa;  $f_y = 500$  MPa.

$A$ : section area;  $d$ : section depth;  $d_b$ : diameter of the longitudinal rebars;

$z$ : beam span or distance to the point of contraflexure.

will be adapted accordingly, in order to obtain element sizes falling within the previous range of values.

## 4

# Numerical Simulations of Progressive Collapse

A description of the technique adopted in the present work for the simulation of progressive collapse is presented. A reference RC structure is described, and its response to the sudden loss of a load-bearing member is studied. This computation is repeated for several parametric variations, to assess the influence of the main material and design parameters in the structural response.

### 4.1 The ‘sudden column loss’ approach

The ‘sudden column loss’ approach is the most widely used simulation technique for progressive collapse analyses [1, 15, 18–28, 32–36, 40–42]. It is an event-independent approach, meaning that the abnormal loading event causing localized damage that could trigger progressive collapse (impact, blast or other extreme loading situation) is not precisely simulated, but rather its direct effects on the structure. The resulting failing element(s) are removed from the initial topology and the reaction of the structure to this sudden member loss is then studied. The sudden column loss approach is considered a useful design scenario for the assessment of structural robustness. The GSA [1] and the DoD [15] include this technique in their respective guidelines via the ALP approach: one critical load-bearing member, typically a column, is damaged and thus unable to sustain load. The residual structure must be able to accommodate this loss by developing an alternate load path. According to [41], the sudden column loss offers an upper bound on the deformations obtained with respect to an event-dependent simulation approach. In the present chapter, the purpose is to analyse the structural response of a RC frame when subjected to the sudden loss of one of its ground columns. This initial failure would correspond to a blast or impact loading scenario

#### 4.1 The ‘sudden column loss’ approach

---

resulting in a full column removal.

In practical terms, the sudden column loss technique employed here consists in removing the column from the initial structural topology and replacing it by its resultant forces, simultaneously applied with the regular loads in a first static loading step. The column resultant forces are subsequently removed (in a given removal time, upon which the removal shall be either considered as ‘sudden’ or related to the nature of the initial event) while the regular loads are kept constant. This procedure preserves the real loading sequence, unlike in [1, 15, 18, 26], where the regular loads are applied on the remaining structure once the failing column(s) have been removed. The GSA approach is adopted here in terms of the combination of loads to be applied to the structure for the progressive collapse analysis. As previously mentioned, the GSA guidelines specify a loading combination of

$$\text{Total Loads} = \text{Dead Loads} + 0.25 \times \text{Live Loads}$$

to be applied for the dynamic simulation of progressive collapse. The loading history used for the simulation of the sudden column loss is shown in Figure 4.1: all the loads are applied to the structure in a sufficiently large time  $t_0 = 60$  s for this part of the loading to be considered static, preventing inertial effects from developing. Then the member forces  $\vec{R}$  which replace the failing column are decreased to zero in a given removal time  $t_r$  and the response of the structure is observed over a time span of 2 s. Unless specified otherwise, the time step employed is  $\Delta t = 5$  ms and the removal time  $t_r$  is also set to 5 ms to simulate the instantaneous column loss. Besides, this removal time typically corresponds to the impulsive phase duration of an explosion [78].

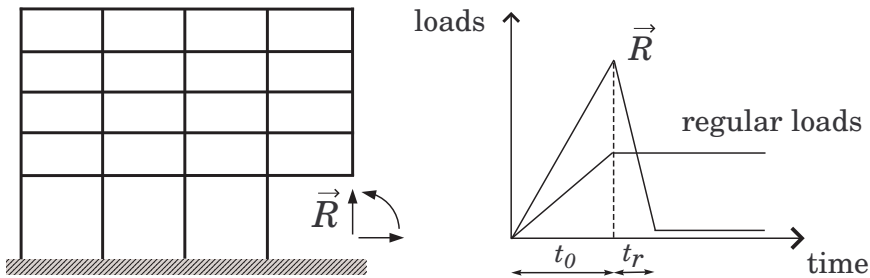


**Figure 4.1:** Sudden column loss approach: loading history.

## 4.2 Reference case of study

### 4.2.1 Description

Figure 4.2 shows the structure under study, consisting of a two-dimensional representation of a five-storey eight-bay RC frame. The sudden column loss of its rightmost ground column is simulated. The floor span and height are 6 m and 3 m respectively, except for the ground floor which is 6 m high. The span in the perpendicular direction is 6 m. The columns and beams sections are  $450 \times 450 \text{ mm}^2$  and  $600 \times 450 \text{ mm}^2$  respectively. The slab is 20 cm thick and an additional concrete layer of 10 cm is assumed.

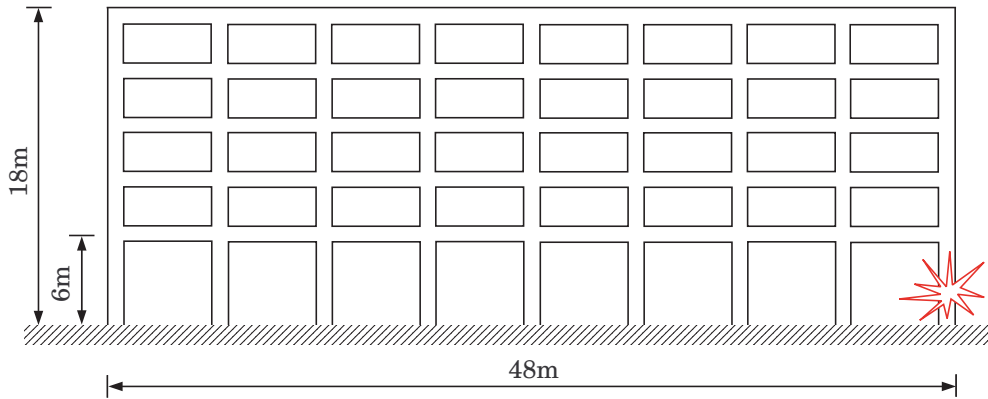


**Figure 4.2:** Structure under study.

The floor is assumed not to provide any resistance, however its weight and inertia are implicitly included in the simulations. Therefore, the loads applied to the beams are those corresponding to the slab and beam weights as well as the live loads. The columns are subjected to their gravitational load. On the basis of the previously pre-defined geometric dimensions, the minimal amount of reinforcement required for the beam sections has been obtained by means of the structural design analysis software Diamonds 2010 by Buildsoft [77], according to Eurocode 2 [51]. The live loads are calculated according to Eurocode 1 (document EN 1991-1-1) [70]: a distributed load of  $3 \text{ kN/m}^2$  is required for the floors, which are considered here to belong to category B (i.e. office areas) and a load of  $1 \text{ kN/m}^2$  is required for the roof, belonging to category H (roofs not accessible except for normal maintenance and repair). The out-of-plane span being of 6 m, the resulting live loads for the present two-dimensional approach are  $18 \text{ kN/m}$  ( $3 \text{ kN/m}^2 \times 6 \text{ m}$ ) on the floors and

## 4.2 Reference case of study

---

6 kN/m ( $1 \text{ kN/m}^2 \times 6 \text{ m}$ ) on the roof. The set of load combinations considered for the structural design in the software Diamonds 2010 are those prescribed by Eurocode 0 (document EN 1990: Basis of structural design) [71]. Table 4.1 provides the value of the loads and the corresponding multiplying factors for obtaining the set of loads combinations.

**Table 4.1:** Design loads.

	<b>Dead Loads</b>	<b>Live Loads</b>
Loads [kN/m]	43.2 <sup>(1)</sup>	3 kN/m <sup>2</sup> (roof 1 kN/m <sup>2</sup> ) <sup>(2)</sup> [70]
Combination factors	1.35/1 [71]	1.5/0 [71]

<sup>(1)</sup> excluding the beam self-weight

<sup>(2)</sup> to be multiplied by the perpendicular span: 6 m

For the sake of simplicity, only three different RC cross-sections have been considered based on the obtained minimum reinforcement amount: two for the beams and one for the columns, as indicated in Figure 4.3. It can be observed that fully continuous bottom reinforcement is provided in the beams and 66% of the top reinforcement is made continuous as well, in order to ensure beam-to-beam continuity across the columns, which according to the GSA is essential for resisting the load reversals that follow the loss of a primary support [1]. The sectional dimensions and the reinforcing details are indicated in Figure 4.3: 32 mm diameter bars have been used for the reference design, which results in a total reinforcement ratio of 1.6% for the columns, 0.6% to 0.9% for the beams in tension and 0.6% for the beams in compression. The overlap is 5 cm.

The resulting loads to be applied on the floors for a sudden column loss simulation according to the GSA approach are shown in Table 4.2 and compared with those corresponding to the DoD approach, which prescribes 50% of the live loads. Note that the inertia of the live loads and the dead loads (thus the slab and the additional concrete layer weights) are also taken into account in the dynamic computation, by adding their contribution to the mass matrix, as explained in Section 3.4.

Since the energy dissipated in the simulated progressive failure process depends on the discretisation adopted due to the softening nature of the problem, here the elements have been given a length between  $L_{el} = 0.4 \text{ m}$  and  $L_{el} = 0.45 \text{ m}$ , so that failure localisation occurs on a region comparable to the

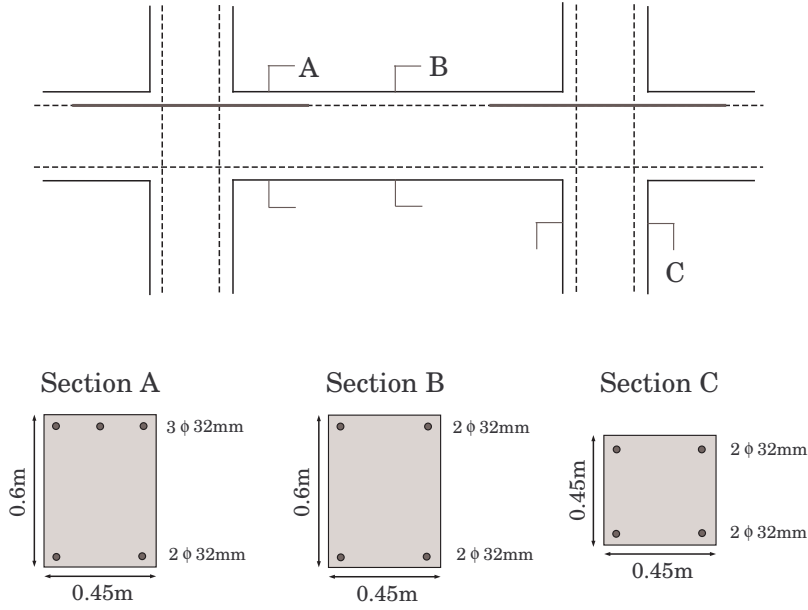


**Figure 4.3:** Beams dimensions and reinforcing details.

**Table 4.2:** Loads applied to the beams for the simulations (excluding self-weight).

Loads [kN/m]	Dead	Live	Total GSA	Total DoD
Floors	43.2	18	47.7	52.2
Roof	43.2	6	44.7	46.2

corresponding characteristic hinge length where most of the permanent beam rotation is known to be concentrated (as explained in Section 3.5.2). This value has been obtained from the expressions for the characteristic length provided in Table 3.4 ( $L_{ch} = 0.41$  m according to the *fib*). Furthermore, the discretisation is such that there is always an element placed exactly in the middle of the span, where strain localisation is likely to occur together with the beam ends. Figure 4.4 shows the finite element mesh used for the computations, where each of the three element types (sections A to C in Figure 4.3) is depicted in a different colour.

The cross-sectional discretisation – i.e. the thickness of the layers in the multilayered approach – is taken equal to 1cm. All computations are performed using a geometrically linear description. The material parameters



**Figure 4.4:** Finite element discretisation.

are those indicated in Table 3.2. The tensile strength of concrete is ignored here for simplicity, since its effects at the structural scale can be considered negligible (as will be demonstrated in Section 4.3).

#### 4.2.2 Simulation results

Figure 4.5 depicts the results of the reference case of study at different times, starting from the onset of the column removal. A close-up view of the right-most side of the structure is provided for the sake of clarity. The true-scale deformed shape of the structure is shown. The interpretation of the symbols employed to describe the failure pattern of the structure is summarised

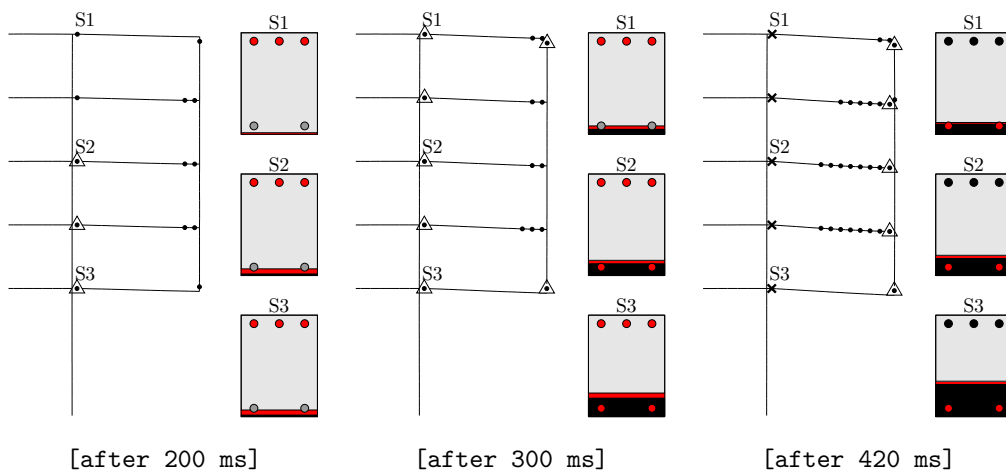


**Figure 4.5:** Reference case of study: response of the structure to a sudden column removal.

in Table 4.3: black dots ( $\bullet$ ) represent the plastification of the steel bars at the considered element; triangles ( $\triangle$ ) indicate that crushing of concrete in compression has occurred in less than one third of the element section (less than  $1/3$  of the concrete layers has reached the ultimate strain); squares ( $\square$ ) stand for concrete crushing in more than one third of the section; and crosses ( $\times$ ) represent the failure of the steel rebars and thus the final failure of the section.

**Table 4.3:** Interpretation of the structural failure symbols.

Symbol	Interpretation
$\bullet$	Yielding of the steel rebars
$\triangle$	Crushing of concrete in less than $1/3$ of the section
$\square$	Crushing of concrete in more than $1/3$ of the section
$\times$	Failure of the steel rebars

It is emphasized that all these symbols do NOT represent plastic hinges as such, but represent merely the state of a section. Note also that the failure of a layer (once the ultimate strain in concrete or steel is reached) does not stop curvature increment, but it eliminates the layer contribution to the cross-sectional strength. This allows for a gradual strength degradation through the section. However, the failed elements are not removed from the topology and thus remain attached to the structure after reaching complete failure, keeping transferring stresses to the intact elements in the vicinity. As a consequence, the impact of failing members on adjacent elements is not included. The progressive degradation process is also depicted for various sections of the structure, where colours have the same interpretation as given in Figure 3.15: both for steel and for concrete, white indicates the tensile region and the compressive areas where plasticity has not initiated (i.e. the elastic range); red represents the zones having reached the plastic domain; and black denotes material failure (the corresponding layer-wise stress has dropped to zero after the ultimate strain is reached).

From the structural results in Figure 4.5 it can be observed that failure progresses as follows: first the yielding of the tensile steel rebars occurs, followed by the crushing of concrete. Finally, the tensile rebars reach the ultimate strain causing the failure of the beam in the corresponding sections. Note the progressive increase of the black area representing the compressive failure of concrete. The progressive failure of the frame is limited to the ex-

## 4.2 Reference case of study

---

ternal bay initially supported by the removed column. Although failure does not spread beyond this region, the maximum allowable extent of collapse according to the GSA is exceeded since it should be '*confined to the structural bays directly associated with the instantaneously removed vertical member in the floor level directly above the instantaneously removed vertical member*' [1]. In the present case, all the floors above the failing column are included in the collapse region. As shown in Figure 4.5, the complete failure of the exterior bay occurs 420 ms after the onset of the column removal. The amount of continuous reinforcement provided here seems insufficient to prevent progressive collapse for instantaneous removal of an exterior column.

The axial force and bending moment diagrams at three different times

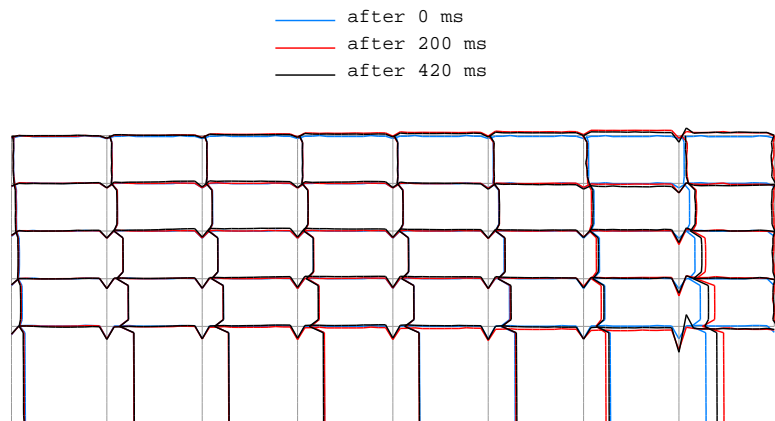


**Figure 4.6:** Evolution of  $N$  for an exterior column removal.

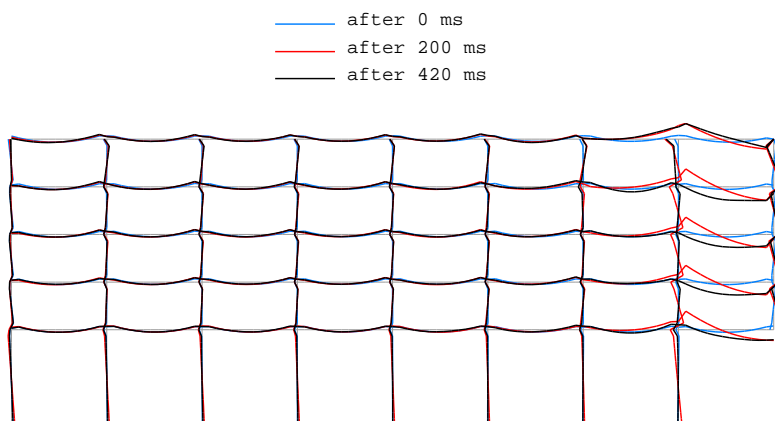


**Figure 4.7:** Evolution of  $M$  for an exterior column removal.

(between the onset of removal and final failure) are depicted in Figures 4.6 and 4.7. It can be observed that the removal of the rightmost column results in an increase of the compressive axial load in the adjacent column, as well as in a decrease of the compressive load in the columns situated right above the removed element. An important change in the bending moment diagram takes place as well: a considerable increase of the values can be noticed at the beam ends opposite to the failing column. A close-up view of the evolution of the axial force ( $N$ ) and bending moment ( $M$ ) in the beam directly associated with the removed column is also given in Figures 4.8a and 4.8b respectively.

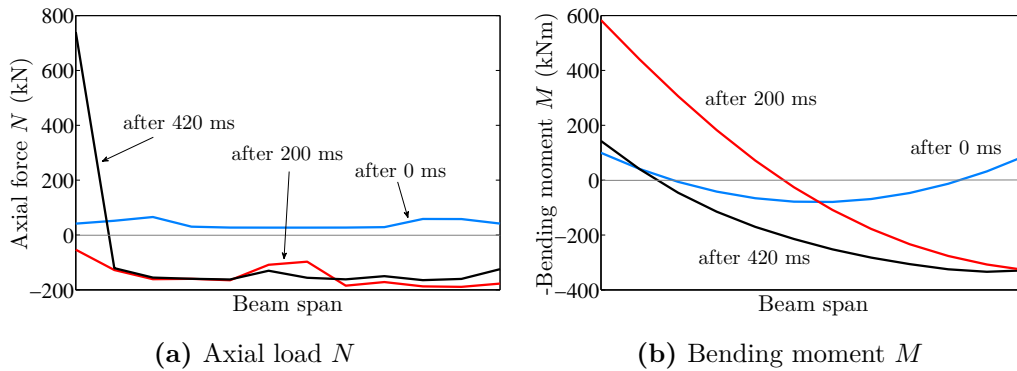


**Figure 4.8:** Evolution of  $N$  and  $M$  in the beam directly associated with the removed column.

Even though the description is geometrically linear,  $N$  increases significantly in the section where failure occurs; its value cannot be considered constant either in time or along the beam span, contrarily to the assumption made by many closed-form approaches. The variation of  $M$  along the beam span following the column removal is also significant: an important bending moment reversal takes place at the level of the connection with the removed column, as well as a considerable increase of  $M$  at the adjacent column. As the structural strength degradation develops and the steel failure occurs, this maximum bending moment decreases to reach its initial value. This demonstrates the advantages of using a multilevel approach where the interactions between flexural and axial force at the sectional level are directly derived from the constituents scale, in contrast to closed-form formulations which introduce significant simplifications with this respect.

To investigate the influence of the topological location of the failing member, the sudden column loss of an interior column is considered instead. Figure 4.9 summarises the frame response to the loss of the third ground column

## 4.2 Reference case of study

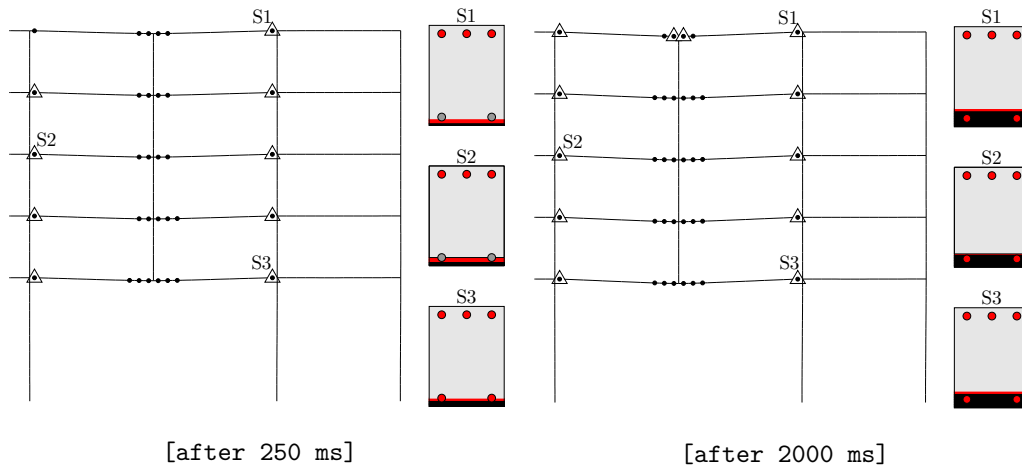


**Figure 4.9:** Reference case of study: response to the sudden removal of an interior column.

from the right. In this particular case, and contrarily to the previous computation, the frame resists to the sudden column loss: about 500 ms after the removal onset the response has stabilised and no further structural damage is observed.

Although yielding of the steel rebars or concrete crushing takes place in some sections, complete failure is not observed in any of the beams. The damaged area in this case is also restrained to both bays directly associated with the failing column. Regarding the allowable collapse region, the prescriptions of the GSA [1] are not exceeded in terms of structural integrity. From the point of view of the structural serviceability, the extent of damage would be considerable though. Nevertheless, the issue of serviceability is out of the scope of progressive collapse analysis, which are focused on the verification of the structural integrity. The fact that an interior support is now removed results in an increased ability of the frame to redistribute loads among the remaining elements at both sides. This is made possible by the continuous bottom reinforcement provided in the beams, which is able to accommodate the bending moment reversal caused by the column removal.

The evolution of the  $N$  and  $M$  diagrams in the structure is shown in Figures 4.10 and 4.11 respectively. Figures 4.12a and 4.12b give a close-up view of these generalised stresses distributions at the beam situated on the right of the removed column. As for an exterior column removal, a reversal of the bending moment is observed in the beam elements located next to the removed column, as well as an increase of the bending moment and the axial

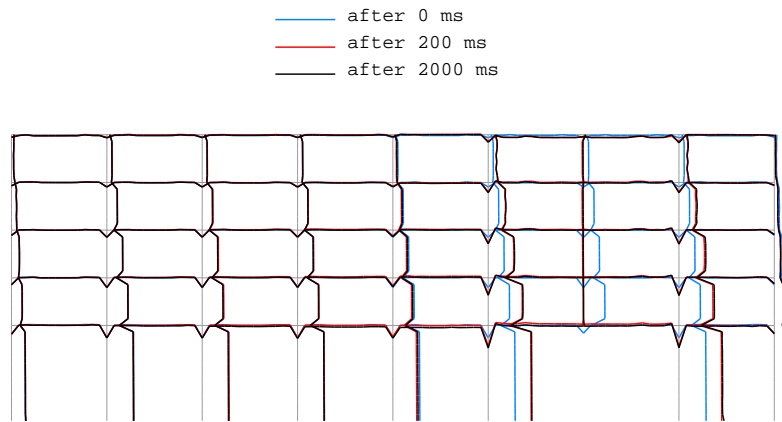


**Figure 4.10:** Evolution of  $N$  for an interior column removal.

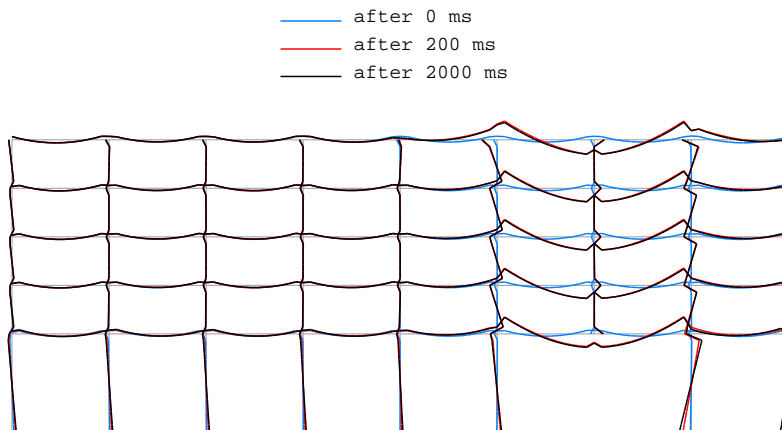


**Figure 4.11:** Evolution of  $M$  for an interior column removal.

force in the elements situated at the opposite end of the same beam. However, the moment diagram remains steady since the structural degradation does not progress.

The vertical displacement of the node located at the connection with the removed column as a function of time is shown in Figure 4.13, for both exterior and interior column removals. The cross indicates the moment of collapse of the bay(s) directly associated with the removed column, when it occurs.

## 4.2 Reference case of study

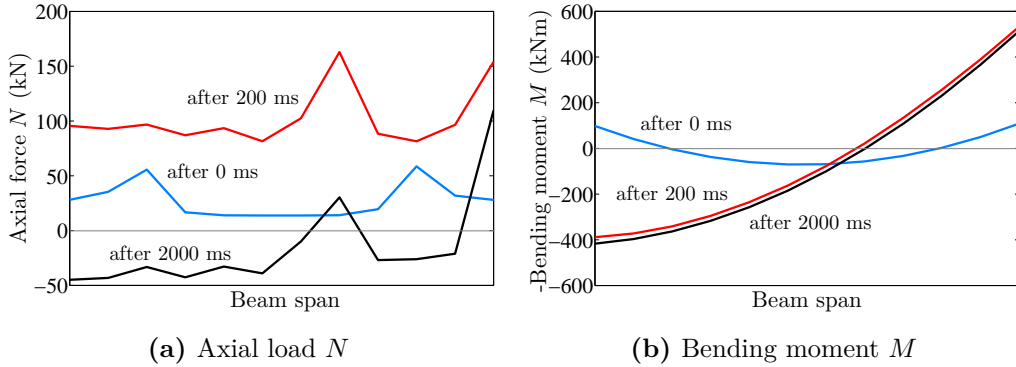


**Figure 4.12:** Evolution of  $N$  and  $M$  in the right-hand beam directly associated with the removed interior column.

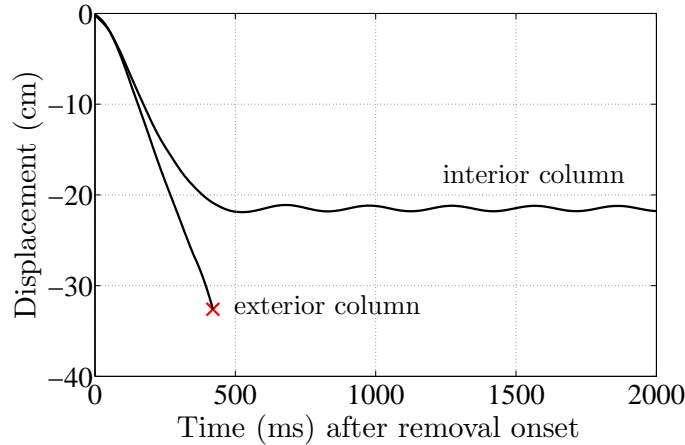


**Figure 4.13:** Vertical displacement of the node on top of the removed column.

To show the flexibility of the multilayered beam formulation to account for variations of the simulation parameters, the influence of design and material parameters that govern the rate independent structural response is analysed next. Note that most of the following parametric variations, which may have a direct effect on the cross-sectional response, are naturally incorporated at the structural level thanks to the multilayered approach. This is in contrast with other simplified approaches in which the derivation of closed-form relationships between generalised stresses and strains requires an offline identification process whenever certain material/design parameters are changed.

In the first set of numerical simulations, the effect of taking into account

the tensile strength of concrete, ignored up to now (and often neglected in the literature), will be analysed. The material parameters affecting the ultimate behaviour of concrete and steel are varied over the commonly used range found in the literature, to see their influence on the structural response as well. The second set of computations focuses on the variation of given design parameters, such as the reinforcement ratio and/or arrangement and the structural topology. Next, the influence of the loading scenario is assessed: the value of the column removal time  $t_r$  is varied, in order to relate it to the nature of the triggering event (explosion, impact...) and set a comparison with respect to the sudden column loss approach, which considers an instantaneous removal and is often used as a tool for the assessment of the structural robustness. Finally, the influence of the procedure for the evaluation of the potential for progressive collapse (GSA vs. DoD) in terms of loads combination is studied.

### 4.3 Influence of the material parameters of concrete and steel reinforcement

For a given, fixed design, it is important to assess the influence of material parameters for which varying values are found in the literature. The choice of such material parameters may indeed play an important role in the degree of structural failure. To this end, the contribution of the tensile strength of concrete to the structural response to progressive collapse is analysed here. The sudden column loss simulation (where ‘sudden’ stands for the minimum removal duration, thus the time step size 5 ms) is also performed for different values of the ultimate strains of steel and concrete respectively. The computations carried out in this section are summarised in Table 4.4, where the values that were employed in the reference test (**REF**) are also indicated for the sake of comparison.

#### 4.3.1 Tensile strength of concrete

The tensile resistance of concrete is often ignored in structural computations, since its contribution to the global resistance is considered negligible [22, 48]. To assess the effect of the tensile strength in the response of the structure to the sudden column loss, the previous reference test (in which this parameter was not taken into account) is performed again, now considering the tensile contribution (**MO1**). The material parameters are provided in Table 3.2.

### 4.3 Influence of the material parameters of concrete and steel reinforcement

**Table 4.4:** Material options (MO) tested.

	$f_{t,st}$ [MPa]	$\epsilon_{c,lim}$	$\epsilon_{s,lim}$
<b>REF</b>	0	-0.35%	4%
<b>MO1</b>	3.25	-0.35%	4%
<b>MO2</b>	0	-0.5%	4%
<b>MO3</b>	0	-0.35%	10%
<b>MO4</b>	0	-0.5%	10%

$f_{t,st}$ : tensile strength of concrete;

$\epsilon_{c,lim}$ : ultimate strain of concrete;

$\epsilon_{s,lim}$ : ultimate strain of steel

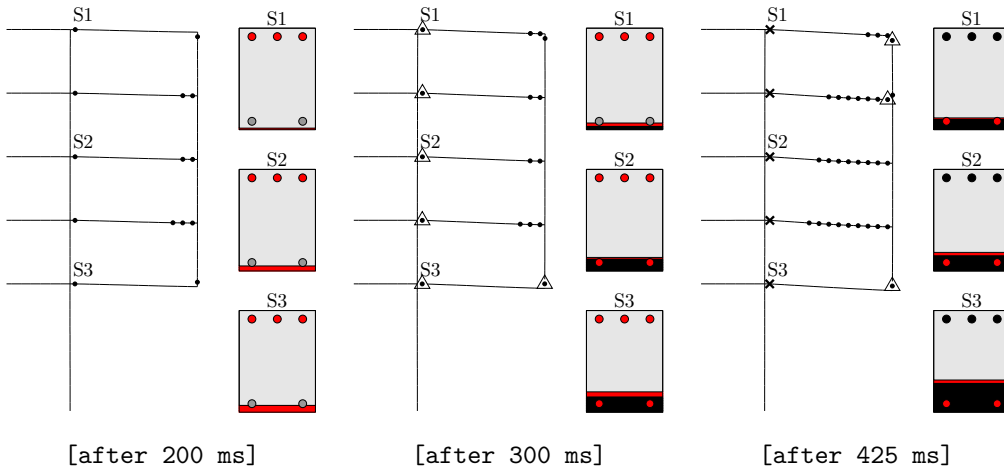


**Figure 4.14:** MO1: response upon consideration of the tensile strength of concrete.

The complete failure of the rightmost bay takes place between 0 and 5 ms (i.e. one time step) later than in the reference test. The failure pattern evolution for the test corresponding to MO1 can be observed in Figure 4.14: no differences are found with respect to the results shown in Figure 4.5. The vertical displacement as a function of time is also compared with the reference test in Figure 4.15, where it can be seen that both curves are practically on top of each other. The previous observation justifies the simplifying assumption commonly made in the literature. As a result, the tensile resistance of concrete will not be considered in the sequel of the present chapter.

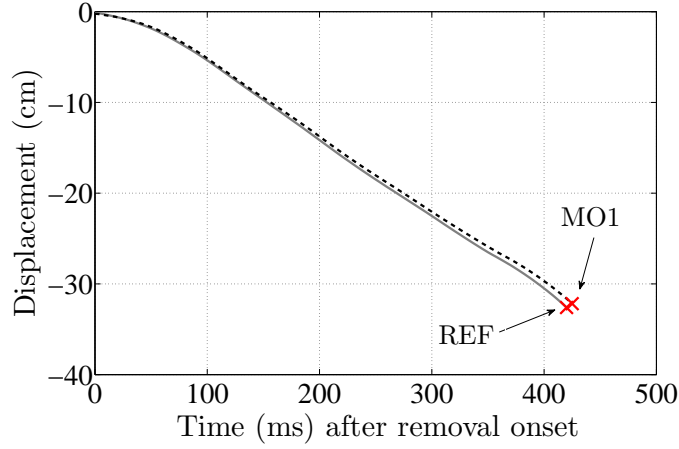


Figure 4.15: MO1: vertical displacement history.

### 4.3.2 Ultimate strain of concrete and steel

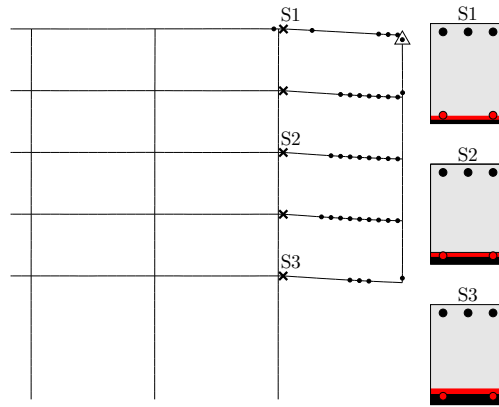
The ultimate strain of concrete in compression used in the reference case of study is  $\epsilon_{c,lim} = -0.35\%$ , which corresponds to the most widely adopted value for unconfined concrete [51,52]. However, the confining effect of the steel stirrups, which are not explicitly modelled in the present study, would induce an increase in the strain limit which depends on the lateral compressive stress and is often calculated as a function of the ratio of shear reinforcement, as explained in Section 3.1.1. Hence, the use of a higher value for the concrete strain limit is motivated in the present analysis since it may result in an enhanced structural resistance to progressive collapse. Applying Eq. (3.4), the increase in  $\epsilon_{c,lim}$  for a given shear reinforcement ratio can be calculated. Eq. (3.6) provides the minimum amount of shear reinforcement, which for the material parameters employed here gives  $\rho_{w,min} = 0.1\%$ . If a ratio of  $\rho_w = 0.2\%$  was considered (thus twice the minimum amount), the ultimate strain corresponding to the confined concrete  $\epsilon_{c,lim}^{conf}$  would be:

$$\epsilon_{c,lim}^{conf} = \epsilon_{c,lim} + \Delta\epsilon_{c,lim} = 0.35\% + 1.4 \frac{\rho_w f_y \epsilon_{s,lim}}{f_{c,st}} = 0.5\%$$

In steel, a strain limit of  $\epsilon_{s,lim} = 4\%$  is adopted as reference value, which corresponds to a ductility level close to class B as described in Eurocode 2 [51]. The highest value prescribed in [51] is  $\epsilon_{s,lim} = 7.5\%$ , corresponding to ductility class C. Nevertheless, a large variability for this parameter is found in literature. The most employed values are comprised between 1% and 10% [42, 48, 51, 52, 55].

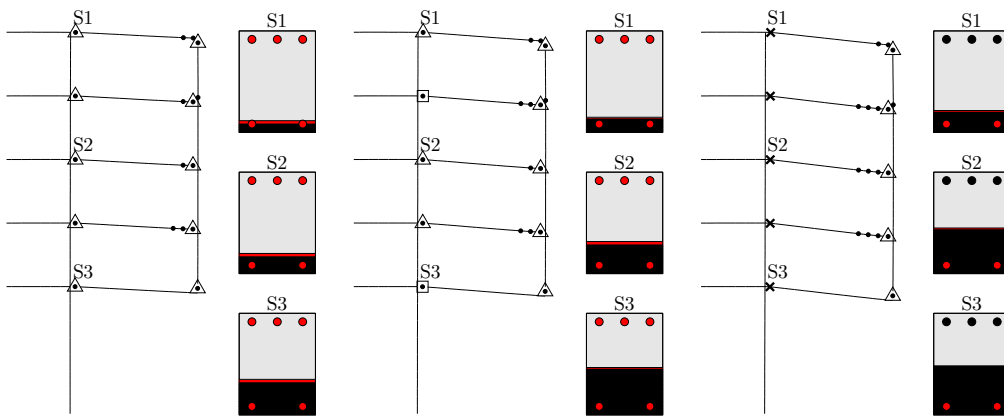
### 4.3 Influence of the material parameters of concrete and steel reinforcement

As indicated in Table 4.4, in the test corresponding to **MO2** the ultimate strain of concrete is increased to  $\epsilon_{c,lim} = -0.5\%$  (the value corresponding to confined concrete with 0.2% shear reinforcement) while the ultimate strain of steel is kept unvaried. In **MO3**, the steel ultimate strain adopted is  $\epsilon_{s,lim} = 10\%$  (resulting in a ductility somewhat higher than class C according to Eurocode 2) and the concrete strain limit is kept equal to  $\epsilon_{c,lim} = -0.35\%$ . Finally, the test for **MO4** is conducted for increased values of both limit strains:  $\epsilon_{c,lim} = -0.5\%$  in concrete and  $\epsilon_{s,lim} = 10\%$  in steel. The tensile strength in concrete is neglected. The results of the three computations are shown in Figures 4.16 to 4.18.



[after 430 ms]

**Figure 4.16:** MO2: response for  $\epsilon_{c,lim} = -0.5\%$ .

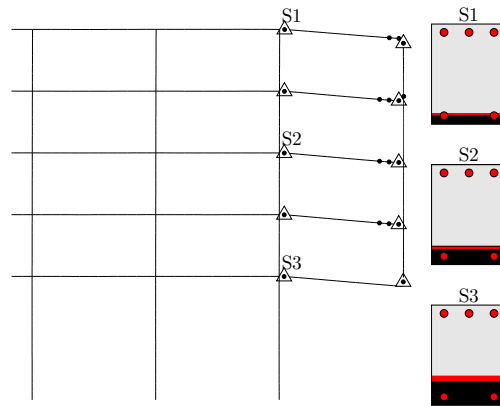


[after 400 ms]

[after 600 ms]

[after 885 ms]

**Figure 4.17:** MO3: response for  $\epsilon_{s,lim} = 10\%$ .



[after 2000 ms]

**Figure 4.18:** MO4: response for  $\epsilon_{c,lim} = -0.5\%$  and  $\epsilon_{s,lim} = 10\%$ .

The following observations can be made out of these figures:

- The change of the ultimate strain of concrete by itself does not influence the global response, as can be seen in Figure 4.16. It has a slightly delaying effect in the concrete crushing initiation. The crushed concrete area in the shown sections is slightly smaller than in the reference test (Figure 4.5). The complete failure of the rightmost bay takes place barely 10 ms later than in the reference test. This justifies the choice of a multilayered model where stirrups (having a confining effect on concrete) are not explicitly represented.
- The increase of the strain limit of steel (Figure 4.17) causes a delay on the appearance of failed sections. For instance, the final collapsed pattern is reached 885 ms after the onset of the column removal, which doubles the time required with respect to the reference case. Note that the failing sections have more than one third of their concrete surface crushed before the failure of the tensile steel rebars takes place, which shows an increase in the efficiency of the RC sections since a better exploitation of the concrete in compression is achieved.
- If both parameters are increased simultaneously (Figure 4.18), the structural collapse is prevented from occurring. The increased ductility of both materials leads to a structural strength gain, favoring the load redistributions.

Figure 4.19 shows the vertical displacement history of the node located at the connection with the removed column, as a function of the parameter combinations. The increase of the ultimate strain for steel leads to a

#### 4.4 Influence of the reinforcement scheme

---

higher ductility at the structural scale, since the displacement at the moment of structural failure doubles the one obtained for the reference case. For this particular case, results show that a computation including large displacements effects would be useful, contrarily to the previous tests where the displacements obtained could be considered small enough to neglect catenary effects.

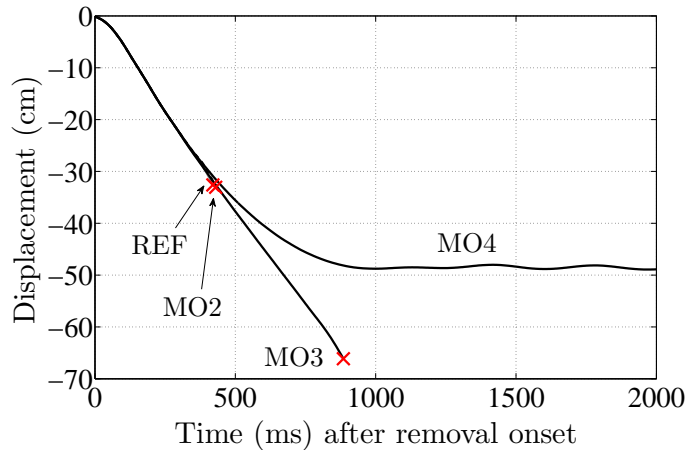


Figure 4.19: MO2 to MO4: vertical displacement history.

#### 4.4 Influence of the reinforcement scheme

The influence of the design options are assessed in the present section. To this end, the sudden column removal will be performed for varying reinforcement dispositions and considering an alternative structural topology.

It is well known that the steel reinforcement arrangement is crucial to guarantee the integrity of a RC structure subject to an abnormal loading scenario. Numerous works have been issued on this subject after the disastrous consequences of the Oklahoma City bombing in 1995 [7, 10, 11]. The Murrah Federal Building was designed and built in accordance with the existing building codes, namely the American Concrete Institute (ACI) *Building Code Requirements for Reinforced Concrete*. The consideration of abnormal loading events (such as blast or earthquake loading) was not required [11]. However, later studies showed that if partial or fully continuous reinforcement had been employed, the structural loss and the number of casualties could have been reduced in a significant manner (up to 80%) [11]. According to the FEMA [10], seismic detailing may improve the structural ability to

resist the extreme loads of a blast and reduce the likelihood of subsequent progressive collapse.

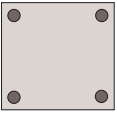
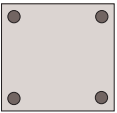
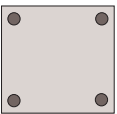
In the present work, it was observed that the loss of a column induces a sudden reversal of the bending moment in the beams at the connection with the failing column, as well as a significant increase of the bending moment and the axial force in the connections with the adjacent columns. If these values of the generalised stresses were to be used for an elastic design of the collapse resistant structure, the originally calculated reinforcement ratios would have to be multiplied by a factor 3 or 4 in some sections of the beams, leading to unrealistic highly overreinforced designs. In this study, in order to remain in a reasonable range of reinforcement amount, which additionally allows for taking into account the load redistributions linked to the plastification of concrete and/or steel, alternative designs will be considered based on different reinforcement arrangements, to analyse the influence of the reinforcement scheme in the structural resistance to progressive collapse.

The minimal amount of longitudinal reinforcement for each cross-section of the reference structure was calculated according to the Eurocode 2 requirements. For the sake of simplicity, only one diameter was considered for the steel rebars ( $\phi = 32$  mm) and only three different RC sections were considered. The reinforcement scheme obtained this way resulted in fully continuous bottom reinforcement and 66% continuous top reinforcement for the beams. For the columns, the reinforcement was also fully continuous and symmetrical (see Figure 4.3). The resulting maximum longitudinal reinforcement ratios were 1.6% (total reinforcement of the columns) and 0.9% (top reinforcement of the beams at the supports), which falls within the normal range. For comparison's sake, other works related to progressive collapse consider ratios of 2% [29] or even 4% [31] in the studied structures.

However, many other different reinforcing arrangements could have been considered for the structure under scrutiny. Table 4.5 gathers the data of the tests conducted for three other combinations of cross-sections A, B and C, which result in similar amounts of reinforcement with respect to the reference case. The number of bars for each section is indicated. Unless specified otherwise, all the bars have a diameter of  $\phi = 32$  mm.

In reinforcement arrangement **RS1**, the difference with respect to the reference one lies in the top reinforcement of Section B: instead of prolonging two out of the three 32 mm bars used for Section A, the minimum reinforcement amount has been considered by employing two 20 mm bars. The aim

**Table 4.5:** Reinforcement schemes (RS) tested.

	Section A	Section B	Section C
<b>REF</b>			
<b>RS1</b>			
<b>RS2</b>			
<b>RS3</b>			

bar diameter  $\phi = 32$  mm unless otherwise specified

here is to investigate the response of a reinforcement arrangement that fulfills the building codes requirements in terms of reinforcement area, where supplementary continuity issues are not considered. For **RS2**, fully continuous reinforcement is provided at the beams. Sections A and B are thus identical. Finally, in the test corresponding to reinforcement scheme **RS3** the beams are provided with not only fully continuous, but also symmetrical reinforcement.

All the tests from Table 4.5, including the reference one, are performed for a higher rise structure as well, which will allow for a generalisation of the conclusions about reinforcement detailing to be drawn in the present analysis. Figure 4.20 depicts the 8-storey 5-bay RC structure employed. It can be observed that this new structure is not only higher, but also the number of bays is lower than in the reference structure, which in principle makes it more prone to progressive collapse for two reasons: 1) the ground columns

support higher compressive loads due to the increased number of floors and 2) the lateral inertia is lower due to the decreased number of bays. The cross-section of the columns needs to be higher in this case. The new sections are  $550 \times 550 \text{ mm}^2$  for the columns and  $600 \times 550 \text{ mm}^2$  for the beams. The same disposition and amount of steel rebars than in the reference structure are employed, which results in slightly inferior reinforcement amounts (the cross-sectional concrete-to-steel surface ratio is higher now). Note that this design fulfills the Eurocode 2 requirements as well.

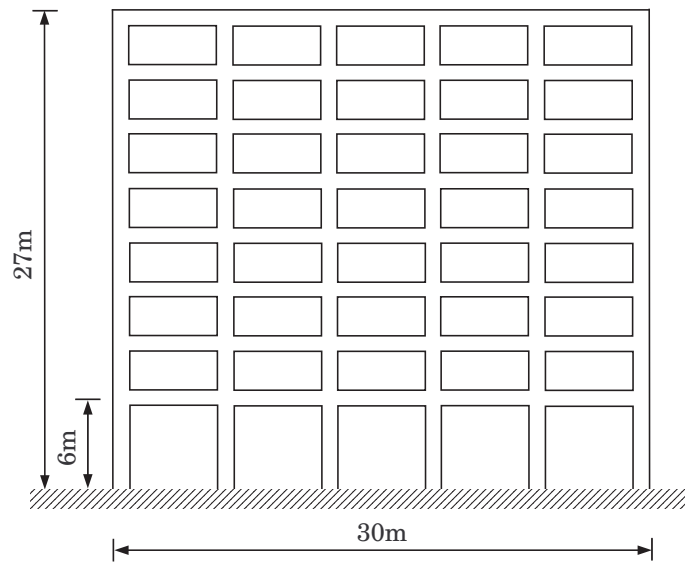


**Figure 4.20:** Additional higher-rise structure used for the present analysis.

The responses of both the low-rise reference structure and the new medium-rise structure for each of the tests are shown from Figure 4.21 to Figure 4.28. The failure pattern is shown either at the time of total failure, if it occurs, or at the end of the time span considered (i.e. 2000 ms after the onset of column removal), if progressive collapse is avoided. Figure 4.29 shows the vertical displacement of the node located at the connexion with the removed column for all the configurations analysed: low-rise structure for exterior and interior column loss, and medium-rise structure for exterior and interior column loss.

For the reference reinforcement arrangement (**REF**), the failure scheme

#### 4.4 Influence of the reinforcement scheme

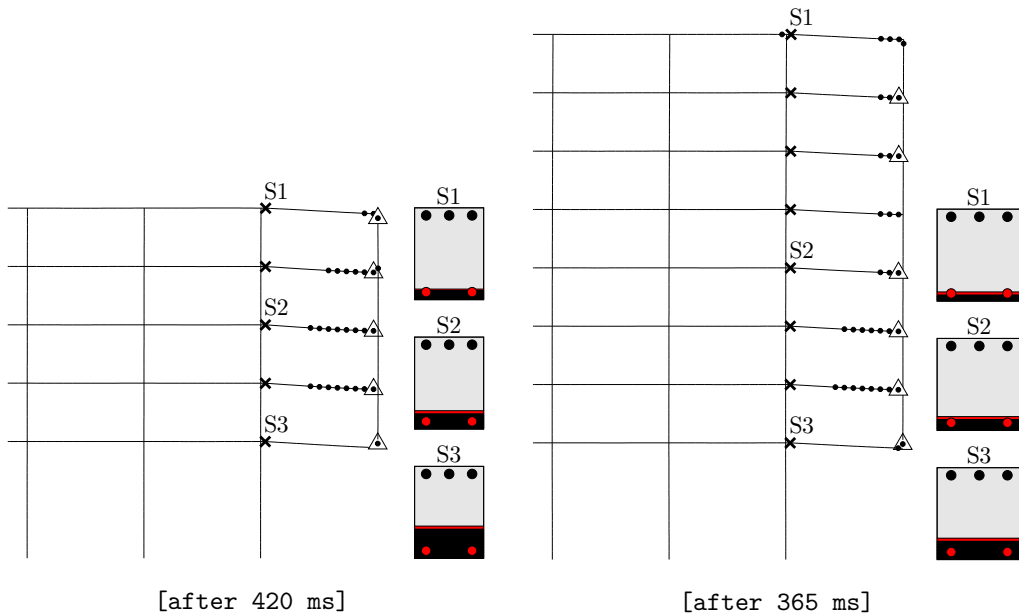


**Figure 4.21: REF: response of both structures.**

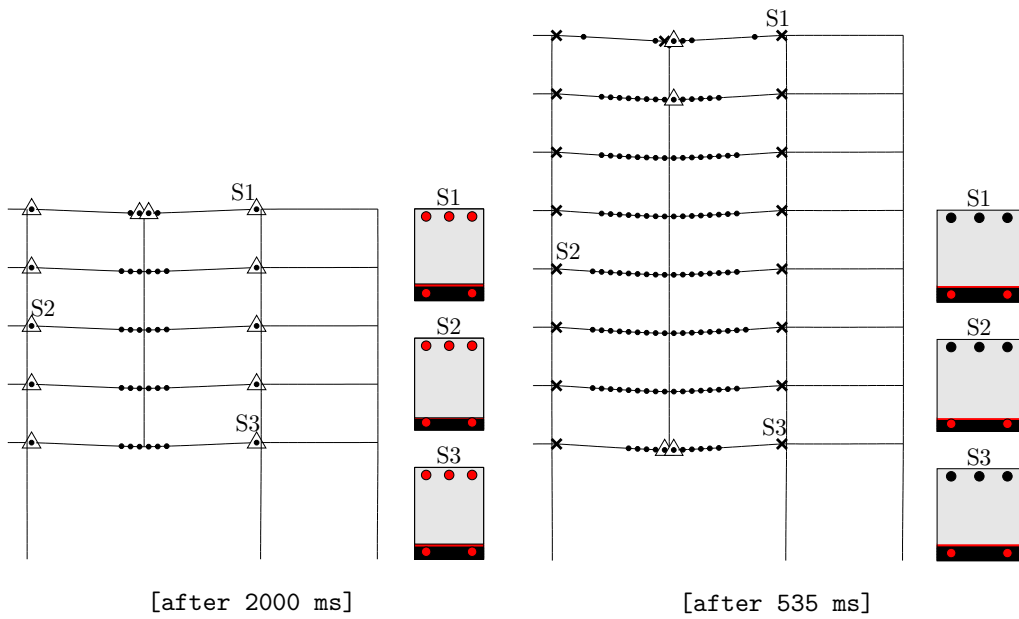


**Figure 4.22: REF: response to an interior column removal.**

after the sudden removal of an exterior column is similar in both structures, as observed in Figure 4.21. The total failure of the rightmost bay occurs somewhat earlier for the higher-rise structure, though. It can be observed that the area of crushed concrete at the moment of failure is approximately the same in the selected elements of both structures. On the contrary, if an

interior column is removed, the higher-rise structure collapses after 535 ms, as opposed to the lower one which resists to the column loss (Figure 4.22). The total collapse of the two adjacent bays in the 8-storey structure takes places later than in the case of an exterior column. This confirms the expected ‘negative’ consequences of adopting a higher-rise structure.

For reinforcement scheme **RS1**, where a strong discontinuity is considered in the top reinforcement, the structural damage mechanism is different: failure occurs at the elements where this discontinuity begins and not at the connection with the adjacent column(s), as can be observed in Figures 4.23 and 4.24. The sectional failure in this case is due to the reversal of the bending moment in the midspan of the beams, where the upper reinforcement amount is insufficient to withstand this load inversion. The total collapse takes place at approximately the same time for both structures. The rupture of the tensile steel rebars happens so promptly that the compressive zone of the beams is very limited and the crushing in concrete has barely initiated by that moment (black area of the sections). Failure is also observed to expand to the adjacent bay(s): the plastification of the top steel bars initiates at the level of the top reinforcement discontinuity.

In reinforcement arrangement **RS2**, fully continuous reinforcement is employed for all the beams and columns. This so-called ‘integrity reinforcement’ is included in the guidelines of the GSA as part of the recommendations for the design of robust structures, with low potential for progressive collapse [1]. According to [11], this feature could have reduced significantly the structural damage if it had been considered in the design of the Murrah’s Federal Building in Oklahoma City. However, the results obtained in the present test are almost identical to the reference one, in which the top reinforcement was made 66% continuous across the beam span. Figures 4.25 and 4.26 show the structural failure pattern for reinforcement **RS2**: no differences are found with respect to the reference test (Figures 4.21 and 4.22). In Figure 4.29 the curves corresponding to the vertical displacement for the tests corresponding to **REF** and **RS2** are coincident.

Reinforcement arrangement **RS3** consists of fully continuous and symmetrical reinforcement for all the elements. The number of top and bottom steel rebars is thus identical. Figures 4.27 and 4.28 depict the response of both structures for an exterior and an interior column loss. This alternative arrangement succeeds in providing structural integrity for all the structural configurations studied. The final displacement of the node at the connection with the removed column is significantly reduced, as can be observed in

#### 4.4 Influence of the reinforcement scheme

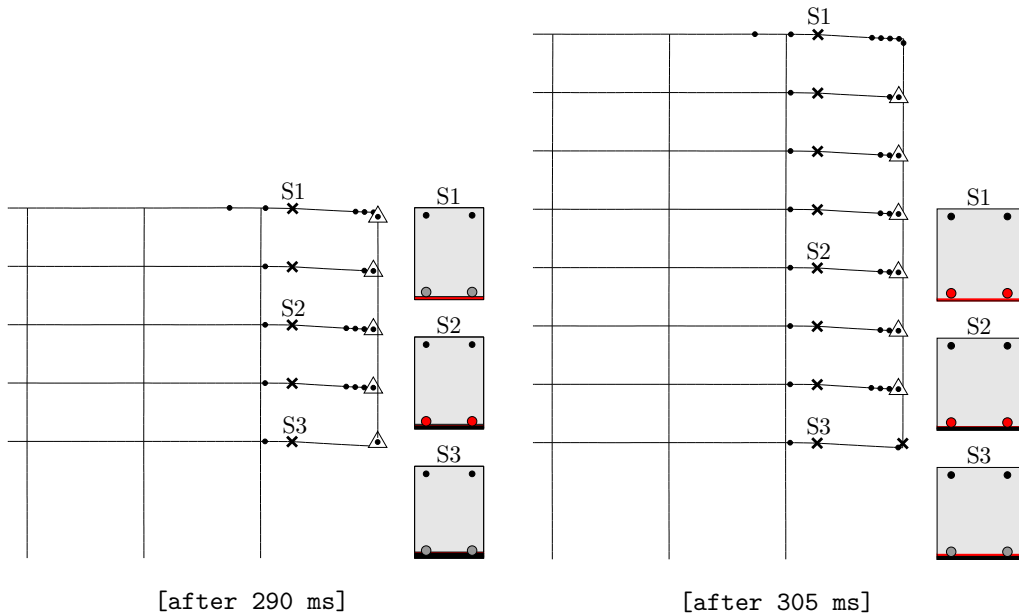


**Figure 4.23: RS1: response of both structures.**

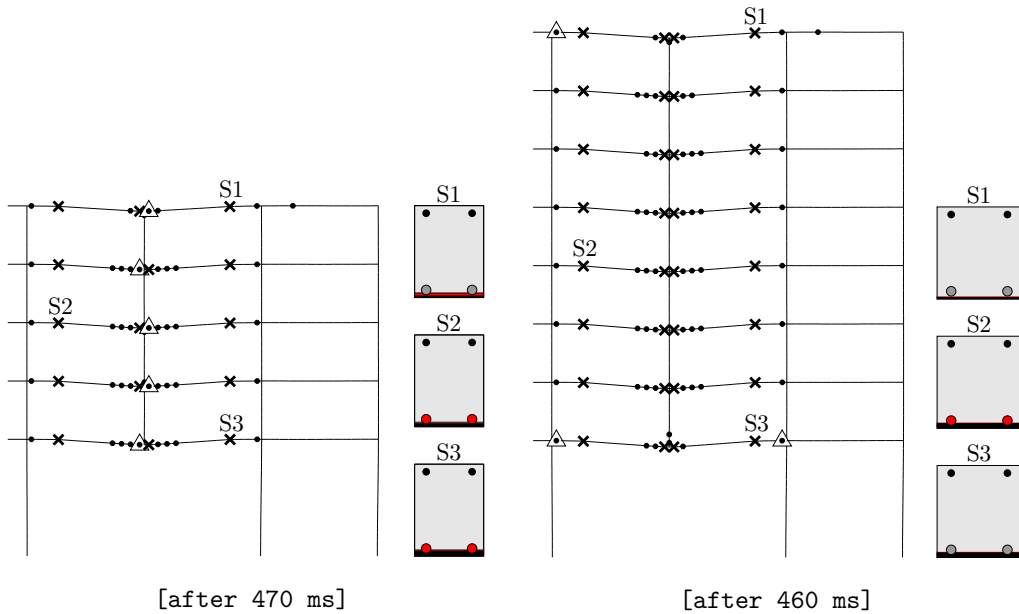


**Figure 4.24: RS1: response to an interior column removal.**

Figure 4.29: the displacement corresponding to the interior column removal in the 5-storey structure (Figure 4.29b) is reduced by 50% with respect to the one obtained for **REF** and **RS2**. The extra reinforcement provided with respect to the previous design **RS2** (i.e. one additional bottom bar), provides the strength enhancement required in the beam connections for the

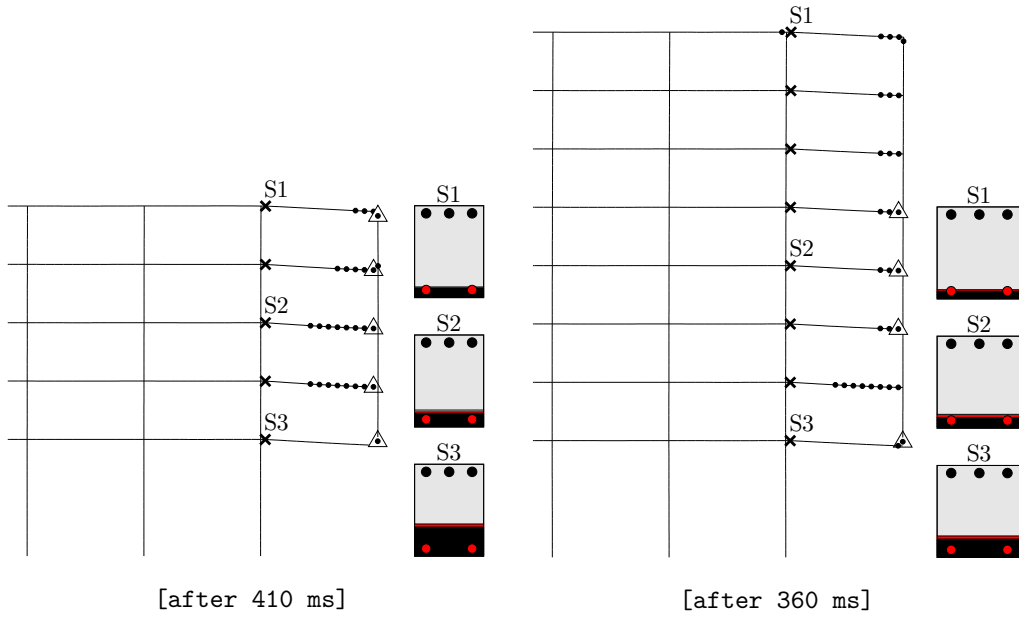


**Figure 4.25: RS2: response of both structures.**

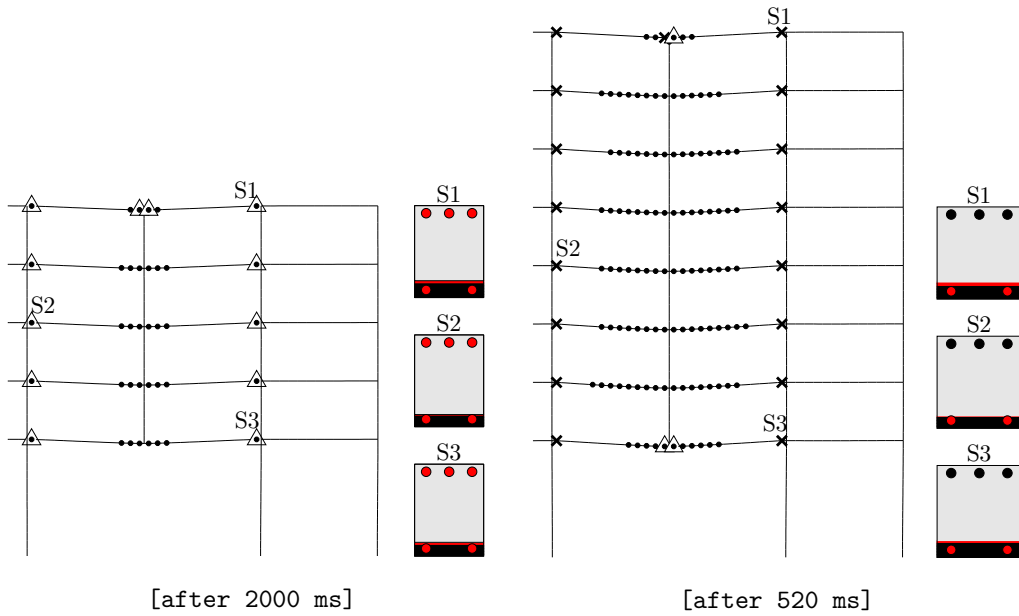


**Figure 4.26: RS2: response to an interior column removal.**

load redistributions to develop. It corresponds however to a much lower reinforcement amount to the one theoretically required for ensuring a collapse resistant (elastic) design. As previously mentioned, the aim here is to study the structural integrity and not its serviceability following a sudden column loss. The symmetrical reinforcement scheme allows for an accommodation of

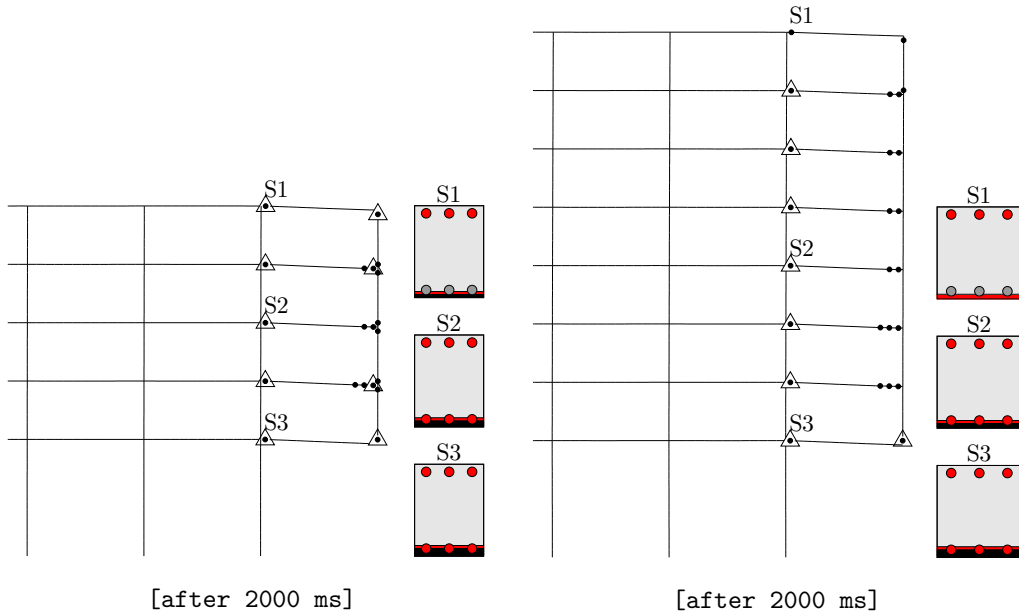


**Figure 4.27: RS3: response of both structures.**

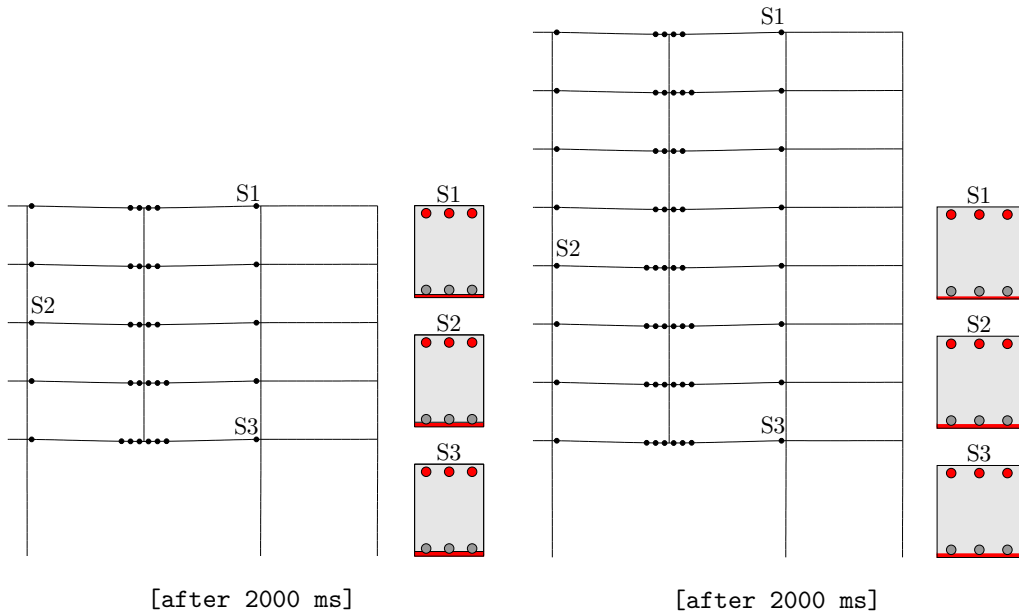
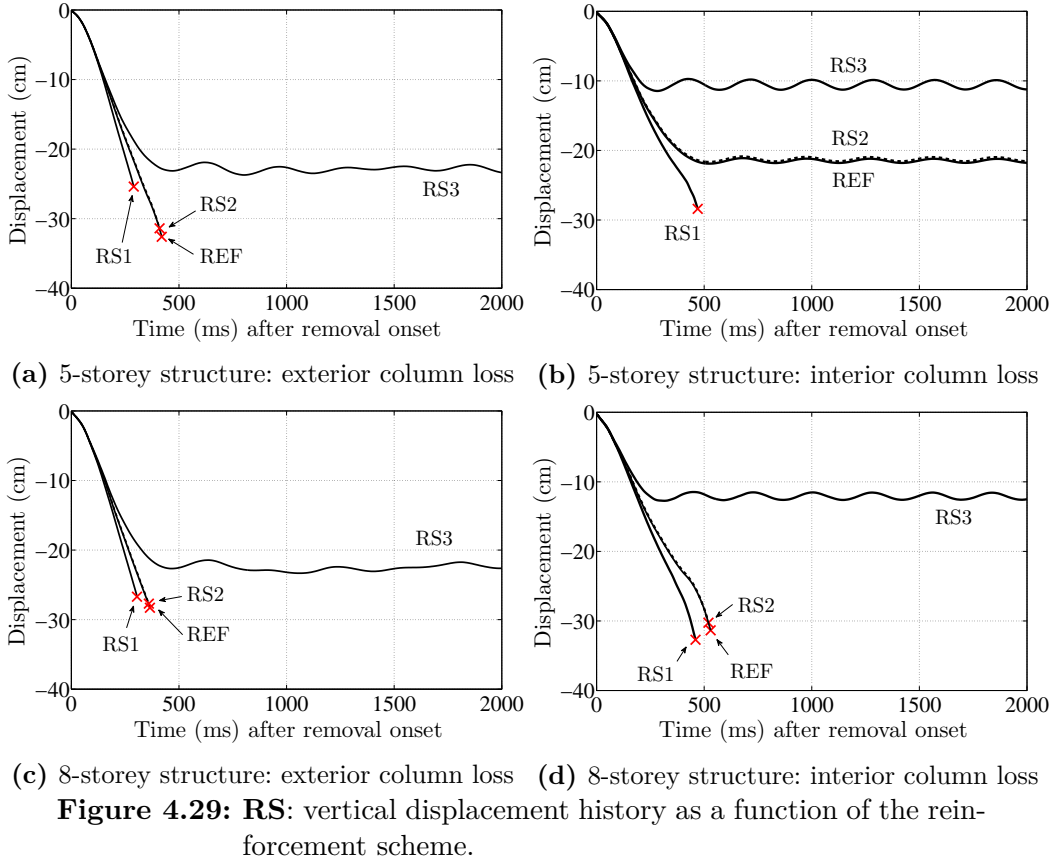


**Figure 4.28: RS3: response to an interior column removal.**

the double span condition. The resulting ‘increased’ and ‘reversed’ bending moments at the beam connections are three to five times larger than the initial values (as seen in Figures 4.8b and 4.12b), which means that the design safety margins introduce the adequate resistance reserve for the structure to withstand such an increase of the design loading conditions.



The partial conclusions drawn out of these design parametric variations are the following:

- Based on the computational modelling assumptions used here, the minimum requirements provided by the standard building codes are insufficient to prevent structural collapse following the sudden loss of a primary load-bearing member. This observation was made in the test corresponding to reinforcement scheme **RS1**, in which the minimal reinforcement ratio was employed for the mid-span sections of the beams.
- Continuous reinforcement over the beam span is essential to accommodate the loss of a support. However, it may not be sufficient for all the possible configurations and loading scenarios (higher-rise structures, internal column loss, low strength materials...) as seen **REF** and **RS2**, where partially and fully continuous reinforcement were provided respectively. The structures collapsed for most of the studied configurations.

- Fully continuous symmetrical reinforcement of the beams appears to be the best design solution to prevent progressive collapse, resulting in the structural robustness required to accommodate the load reversals and the double-span condition (**RS3**).
- These results are general for both low and medium rise structures: almost the same response patterns have been obtained for the two different structures considered here.

### 4.5 Influence of the column removal duration

In this section, the interest is shifted towards the effects of the removal time in the progressive failure scheme of the initial structure. Various column removal times are applied in order to link the rate of column disappearance to the nature of the loading scenario that causes it. Up to now, a sudden column removal technique has been employed, which in practical terms means that the removal is performed in a single time step, thus  $t_r = 5$  ms. This removal time would also correspond to the duration of the impulsive phase of an explosion [78].

Here, in order to represent column removal durations corresponding to initial triggering events other than a blast, different column removal times, indicated in Table 4.6, are adopted. They correspond to the order of magnitude of the time of column removal in a low velocity impact event. According to the bibliography dedicated to the subject of car-crash simulations [86–88], the duration of a vehicle impact on a structure would typically be in the range of several tens or several hundreds of milliseconds (ms). Furthermore, Eurocode 1 (document EN 1991-1-7) in its Annexe C (Dynamic design for impact) provides the guidance for the approximate dynamic design of structures subject to accidental impact by road vehicles, rail vehicles and ships [16]. In this document, the design force due to an impact may be considered as a rectangular pulse whose duration ( $\Delta t$ ) is determined by the mass ( $m$ ) and the equivalent elastic stiffness ( $k$ ) of the colliding object:

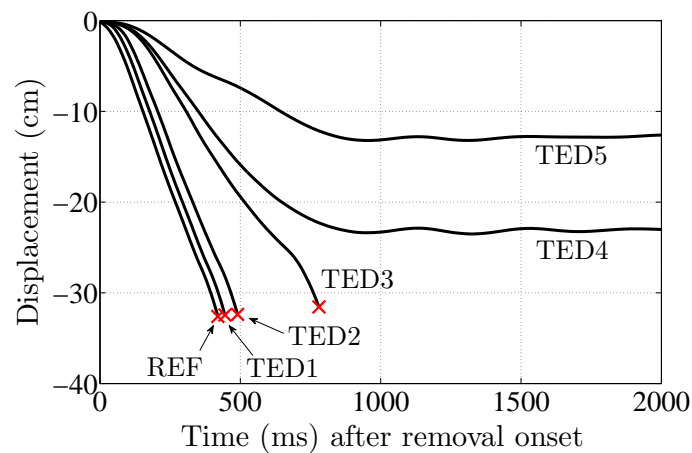
$$\Delta t = \sqrt{m/k}$$

The values of  $m$  and  $k$  are given as a function of the type of vehicle. For a car  $m = 1500$  kg while for a lorry  $m = 20000$  kg. The equivalent stiffness is  $k = 300\text{kN/m}$  for both. These values give an impact duration of 220 ms in the case of a car and 816 ms for a lorry. Based on such values, column removal times of up to 500 ms are tested in the present analysis. The reference structure is employed in this study.

**Table 4.6:** Triggering event durations (TED) tested.

	$t_r$ [ms]
<b>REF</b>	5
<b>TED1</b>	50
<b>TED2</b>	100
<b>TED3</b>	250
<b>TED4</b>	300
<b>TED5</b>	500

The vertical displacement history at the connection with the removed column is depicted in Figure 4.30 for the six considered removal times. The structural failure patterns are reported in Figure 4.31. They show that inertial effects play a major role in the present progressive collapse analysis: higher removal times, and subsequently lower accelerations, can prevent the collapse after the column loss. For instance, for **TED5**, where  $t_r = 500$  ms, only the plastification of the steel bars is observed in some locations. This analysis illustrates to which extent the inertial effects affect the structural response and is consistent with the statement from [41], claiming that the sudden column loss idealisation offers an upper bound on the deformations obtained with respect to event-dependent approaches.

**Figure 4.30:** TED: vertical displacement history as a function of the triggering event duration.

## 4.5 Influence of the column removal duration

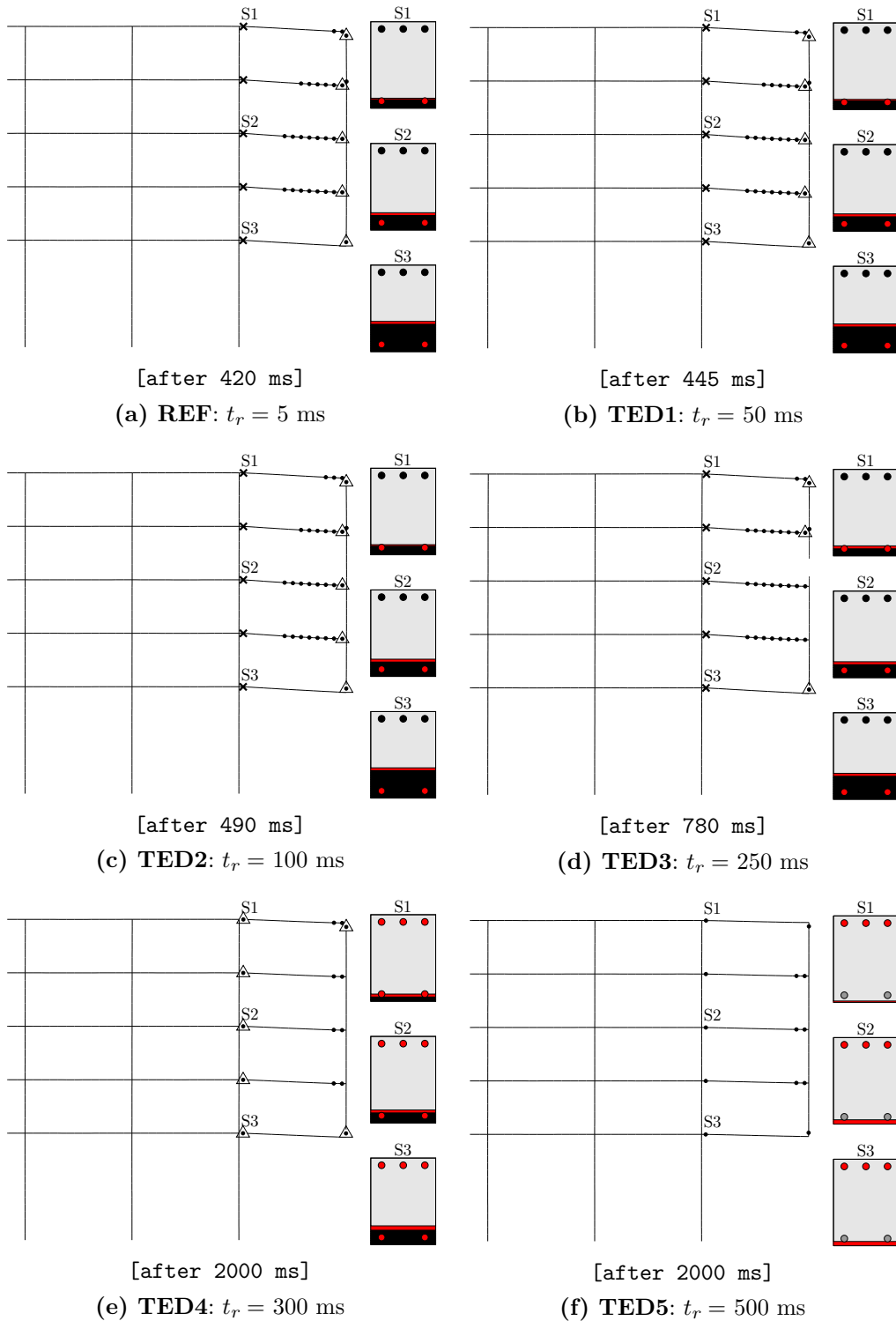


**Figure 4.31: TED: response as a function of the triggering event duration.**

## 4.6 Influence of the design code for progressive collapse verification

The results of the sudden column loss simulation may vary depending on the design code selected to verify the progressive collapse sensitivity of the structure. The GSA prescriptions in terms of load combinations applied to the beams has been employed in the present analysis [1], since it is the technique most often adopted in the literature [21, 22, 24, 28, 29, 32, 33, 35, 36]. The DoD guidelines [15] propose a loading combination that includes 50% of the live loads instead of 25% as suggested by the GSA [1]. The total downward loads applied to the beams in a dynamic computation are thus:

$$\text{Total Loads} = \text{Dead Loads} + 0.5 \times \text{Live Loads}$$

The numerical values for this approach were indicated in Table 4.2 for the studied structure. This analysis procedure is now adopted to verify if the conclusions to be drawn from the previous computations still remain valid with the load combination prescribed by the DoD. The response of the reference 5-storey structure is investigated for two reinforcement arrangements (the reference one (**REF**) and the design **RS3** that provided the better resistance to progressive collapse in Section 4.4), as indicated in Table 4.7.

**Table 4.7:** Study cases depending on the design code (GSA vs DoD).

	Reinforcement scheme	Technique
<b>REF-GSA</b>	REF	GSA
<b>REF-DoD</b>	REF	DoD
<b>RS3-GSA</b>	RS3	GSA
<b>RS3-DoD</b>	RS3	DoD

The results for an exterior column removal are depicted in Figure 4.32. In case **REF-DoD**, the total failure of the rightmost bay takes place 55 ms earlier than in case **REF-GSA**. Apart from this fact, no significant difference is found between both results. In **RS3-DoD**, the reinforcement arrangement RS3 is adopted (see Table 4.5), which was observed to result in the most robust design among the studied reinforcement combinations: while this reinforcement pattern results in a progressive collapse resistant design for the GSA load combination, the structural integrity is not maintained for the DoD approach when an exterior column removal is considered.

## 4.6 Influence of the design code for progressive collapse verification

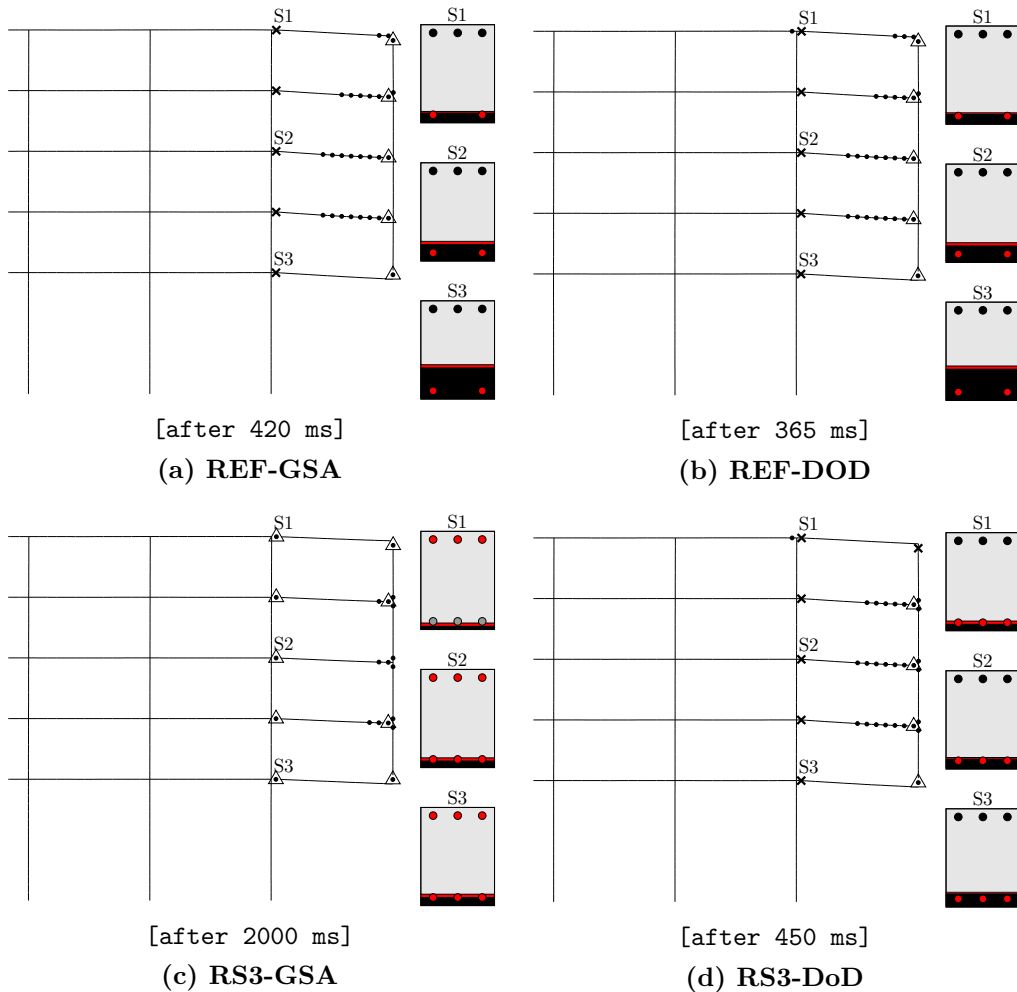


**Figure 4.32: DoD vs GSA: response for an exterior column removal.**

The results for an interior column removal are shown in Figure 4.33. Here again, the results differ substantially from those obtained via the GSA specifications. If the reference design is applied, the collapse of the two bays directly associated with the removed column occurs when 50% of the live loads are applied. In general, the DoD technique leads to more conservative results than the GSA approach for both reinforcement arrangements.

Figure 4.34 depicts the displacement history for both column removals and both load combinations for the two considered designs. These results indicate that the structural response obtained in a sudden column loss analysis may differ depending on the procedure considered, even for the most widely used methods, which shows the importance of the choice of the code standard

#### 4. Numerical Simulations of Progressive Collapse

used for the simulation of progressive collapse.

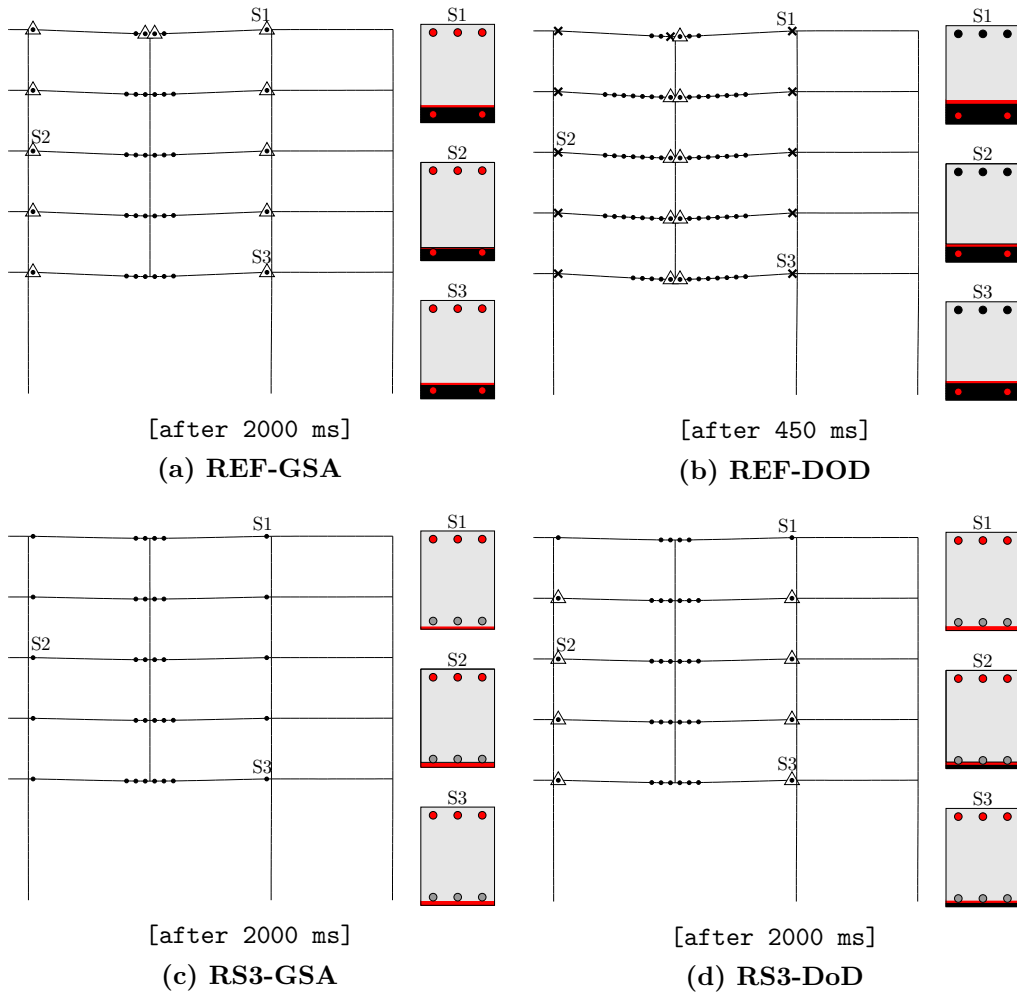
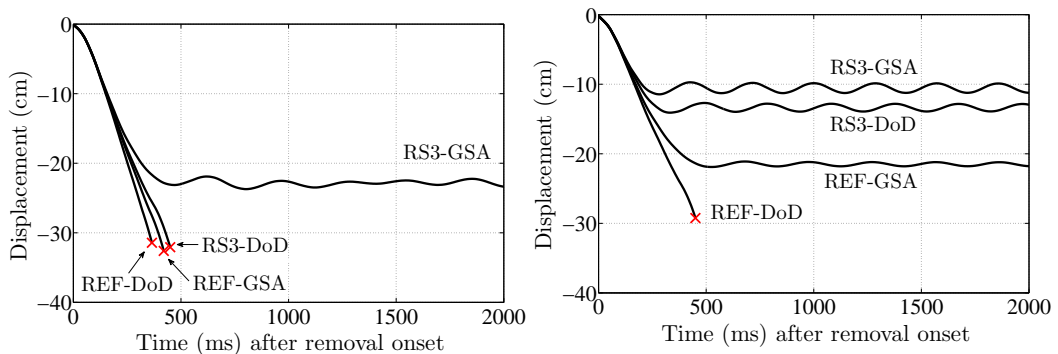


**Figure 4.33: DoD vs GSA: response for an interior column removal.**



(e) Exterior column removal

(f) Interior column removal

**Figure 4.34: DoD vs GSA: vertical displacement history.**

## 4.7 Discussion

The previous progressive collapse simulations show the rate independent response of a RC frame subject to a sudden column loss. This technique is widely used in the framework of progressive collapse verification methods. It consists in the instantaneous removal of a support member in order to represent the direct effects of an abnormal loading event that would result in a full failure of such member. The results of the reference case of study showed the interest in adopting a multilayered beam formulation for the representation of the sectional behaviour of RC beams, due to the important variations (both in time and position) of the generalised stresses and strains during the progressive failure process.

The benefits of the multilayered model adopted in the present work with respect to other closed-form formulations which introduce a number of simplifying hypothesis in the characterisation of the flexural behaviour of RC members is demonstrated. To this end, the reference case of study is repeated by varying the most important design and modelling parameters susceptible to affect the structural failure scheme. The range of these parametrical changes is motivated by the variability found in the literature and always matches realistic values of the studied parameters. The present model allows for a direct consideration of such variations, without the need of a priori identifications for the relationships between generalised stresses and strains and their complex interactions.

The material parameters analysed here, in particular the tensile strength of concrete and the ultimate strains of concrete and steel, do not appear to affect the global response of the RC frame studied in a significant manner. The consideration of the tensile strength of concrete yields to almost identical results with respect to the reference test, where this parameter is ignored. The tensile contribution of concrete could therefore be neglected in the context of rate independent analyses. The increase of the ultimate strain in concrete seems also to have no influence on the results. This structural insensitivity to the ultimate strain of compressive concrete justifies the fact that the stirrups (having a confining effect on concrete and thus a ductility-increasing effect) are not explicitly incorporated in the present work. Concerning the increase of the ultimate strain of steel, it might be responsible for a slight structural enhancement consisting in a more ductile behaviour. Nevertheless, this conclusion should be tempered due to the large displacements involved in the corresponding response, which are a priori incompatible with the geometrically linear approach employed in the present study.

As far as the design options are concerned, various reinforcement arrangements were tested, and this for two different topologies: the 5-storey 8-bay reference structure and a 8-storey 5-bay frame. Several degrees of continuity of the steel rebars are considered. Among all the studied reinforcement patterns, fully continuous symmetrical reinforcement over the beam spans results in the most robust design. Conventional reinforcing complying with the building codes requirements is observed to be unable to provide the structural resilience needed to resist to a sudden column loss. It was also demonstrated that continuous reinforcement over the beam span, which is considered as an essential feature to accommodate the loss of a support according to the GSA [1], may not be sufficient for providing the required resistance to the loss of a supporting element: the partially and fully continuous reinforcement tested in the present study resulted in collapse for most of the configurations analysed.

As expected, the higher-rise structure appears to be more prone to progressive collapse. However, the same trends are observed in the response of both structural topologies.

The location of the removed element has also an effect on the propagation of collapse: the removal of an interior column leads to lesser degrees of structural damage, due to the support provided by the neighboring columns at both sides.

The column removal time, which is varied here to represent different types of extreme loading event resulting in local failure, is also determinant in the structural response. The inertial effects are directly related to this variable: for higher removal times the accelerations involved in the process are smaller and thus the extent of structural damage is lower. This confirms that the sudden column loss idealisation represents a useful design scenario for the assessment of structural robustness, as stated in [41].

All the previous computations were conducted for a particular choice of the loads to be applied to the structure. The load combination prescribed by the GSA was considered: 25% of the live loads were applied. In order to appraise the effect of such a choice, the load combination proposed by the DoD procedure, which considers 50% of the live loads, was evaluated. This combination resulted in an increase of the structural robustness with respect to the previous results. It can be thus concluded that the strategy used for the simulation of the sudden column loss has a significant effect on the results: the DoD might lead to conservative designs with respect to the GSA

guidelines. The latter constitutes the most often adopted approach for the progressive collapse verification [21, 22, 24, 28, 29, 32, 33, 35, 36].

It must be noted that the previous observations should be considered in the context of the simplifying approximations introduced in the present modelling strategy. Regarding the material modelling aspects, a number of features have not been considered for the sake of simplicity and/or since the modelling of all the possible aspects of the material response at the fine scale is out of the scope of the present work. Nevertheless, the introduction of such additional features would allow for a more realistic representation of the material behaviour. For instance, a damage evolution law for the material stiffness degradation as a function of the cumulated plastic strain would provide a better approximation in the unloading phases. It would also allow for reducing the spurious high frequency vibrations in the structural response that increase the computational effort. Moreover, the incorporation of the cyclic response would also result in a better approximation of the material response of concrete and steel, especially considering the dynamic, oscillatory nature of dynamic progressive collapse.

The geometrically linear approximation employed in this work is considered to be partially justified by the rather limited plastic rotations in RC structures. However, it was observed that for certain cases the displacements involved in the progressive collapse process might be considerable. Furthermore, the rotational ductility appears to be a very important parameter for the safe design of RC structures, since it determines the ability of the structure to redistribute moment and fail gradually [49]. Nevertheless, this simplifying hypothesis is assumed to provide with more conservative results/designs, since the a priori favourable catenary effects that follow the large displacement configurations are not taken into account.

The extension of the present two-dimensional approach to three dimensions seems to be the logical next step in order to obtain a more realistic structural response. Note that the single column removal in a 2D representation would correspond to removing a whole row of columns in 3D since the transversal resistance is not taken into account. However, this upgrade is nontrivial both from the computational cost viewpoint, and from the perspective of structural complexities (representation of torsional effects, stiffening effects of the floors...).

Finally, the fully damaged structural elements are not removed from the topology, they remain attached to the structure after reaching complete fail-

#### 4. Numerical Simulations of Progressive Collapse

---

ure. The consequences of such assumption are twofold: 1) they keep transferring stresses to the intact elements in the vicinity and 2) the impact of failing members on adjacent elements is not included.



# 5

## Investigation of the Strain Rate Effects

Strain rate effects in reinforced concrete might be expected to have an influence in the structural response under progressive collapse. In the present chapter, the strain rate dependence in the material behaviour of concrete and steel is studied and modelled. These effects are introduced at the structural level through the multilayered beam formulation. In order to assess the degree of rate dependence in progressive collapse, the results of rate dependent simulations are presented and compared to the rate independent approach. The influence of certain parameters in the rate dependent response is also studied. Rate effects are observed to have an influence on the structural response.

### 5.1 Strain rate effects in RC

For a wide range of triggering events (impact, blast...), progressive collapse is a strongly dynamic process involving rather high strain rates. As a result, the global response of a part or the entire structure is likely to entail dynamic effects, as well as strain rate effects in the material response. Reinforced concrete structures subjected to high loading rates are expected to have a different response than when loaded statically. For instance, concrete shows a strongly rate dependent behaviour, with both compressive and tensile strengths increasing significantly with the strain rate [52, 81, 82], as confirmed by experimental tests carried out by means of the Split Hopkinson Bar [83, 84]. Figure 5.1 illustrates the strain rate effects in the compressive strength of concrete, obtained via experimental tests [81]. It shows the so-called dynamic increase factors (DIF), representing the ratio of dynamic to static strength. This rate dependent strengthening effect is attributed to moisture in capillary pores and micro-inertia [89]. Steel also presents a strain

## 5.1 Strain rate effects in RC

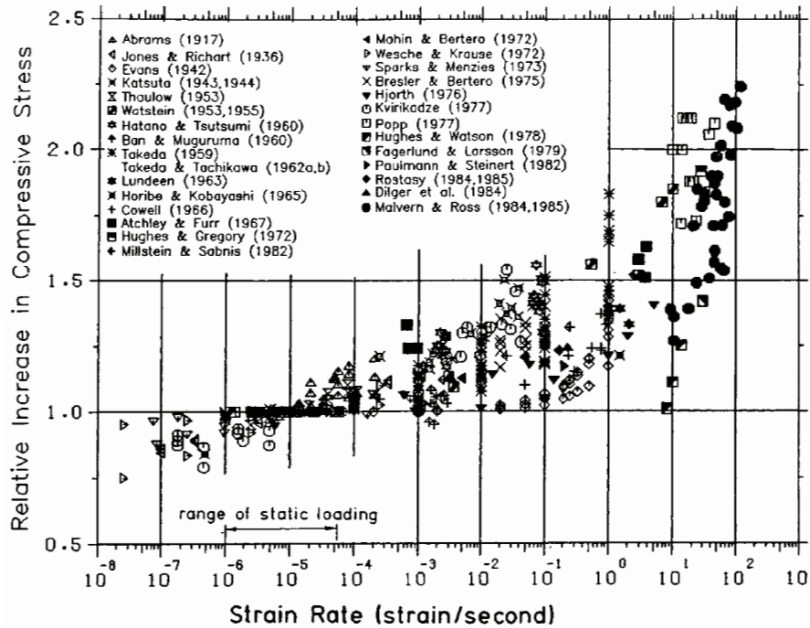


**Figure 5.1:** Strain rate effects on the compressive strength of concrete. Reproduced from [81].

rate sensitive behaviour, although to a lower extent than concrete [85].

Since the structural behaviour under progressive collapse depends considerably on stress redistributions, this material strain rate dependence, leading to an enhancement in the local strength with increasing strain rates, might also induce a different overall response of the whole structure. The multilayer beam formulation is the tool used to assess the need for taking such a strain rate dependent material behavior of the constituents into account in progressive collapse simulations. It indeed allows for the incorporation of the rate effects at the sectional level linking the generalised stresses ( $N$  and  $M$ ) to the generalised strains ( $\bar{\epsilon}$  and  $\chi$ ) and their rates ( $\dot{\bar{\epsilon}}$  and  $\dot{\chi}$ ) implicitly; thereby avoiding the need for a complex identification of approximate closed-form rate dependent sectional evolution laws.

Numerous references on the rate-dependent behaviour of concrete can be found in the literature [89–92], where the strength enhancement at the material level is studied and modelled in the context of small scale structural computations. However, the influence of the viscous effects at the global scale has not yet been investigated in contributions related to structural pro-

gressive collapse. For instance, according to [33] the strain-rate effects are not expected to be significant in the progressive collapse response. Other contributions include these effects analytically, by increasing the strength of concrete and steel as a function of the strain rate [29, 30]. For instance in [30] the strain rate effects in concrete and steel are mentioned to have been taken into account in a computation although no further details are provided in this regard. To the knowledge of the author, no previous work has so far included physically motivated strain rate effects in the material model, for both the elastic and plastic response, in the context of large-scale structural computations. Furthermore, the degree of influence of such effects at the global scale has not yet been investigated in contributions related to structural progressive collapse. In [80], the strain rate effects (introduced via strength amplification factors) in the seismic response of a small RC frame were found to be minor.

Here, the rate dependent effects in the structural response stem from the rate dependence at the material level: strain rate dependent constitutive laws for concrete and steel are defined and introduced in the layers of the multilayered beam, which allows for rate dependent relationships between generalised stresses and strains. In order to justify the development of a rate dependent constitutive model, the value of the strain rates obtained in the sudden column loss simulation have been extracted. Figure 5.2 depicts the evolution of the strain rates in the external layers of Sections S1, S2 and S3 in the previous reference case of study (Figure 4.5).

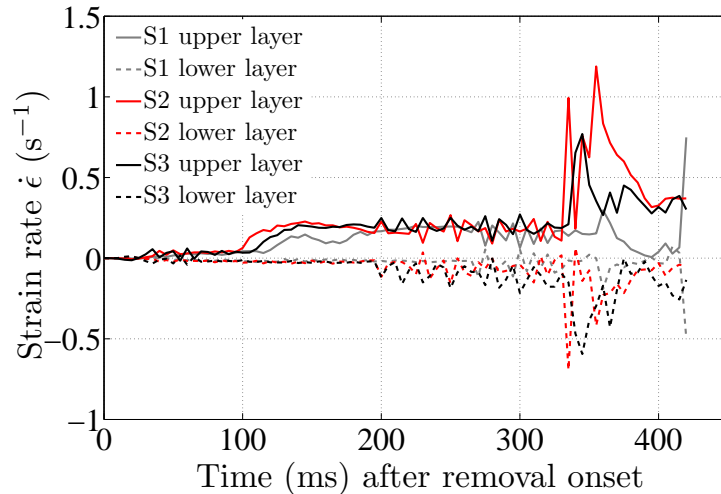


**Figure 5.2: REF:** evolution of the strain rate in the external layers of sections S1, S2 and S3.

The maximum values of the compressive strain rates obtained in all the elements of the structure are also shown in Figure A.1, in the Appendix. Values of up to  $1.1 \text{ s}^{-1}$  are reached in some elements, which according to Figure 5.1 could give rise to a significant local strength enhancement resulting in a potential structural integrity improvement.

## 5.2 Rate dependent response of concrete and steel

The International Federation for Structural Concrete (*fib*) [52] describes the rate dependent behaviour of **concrete in compression** by means of a rate dependent modulus of elasticity and the dynamic increase factors (DIF) on strength, as determined by Malvar and Crawford [82]. The effect of strain rate on Young's modulus and the dynamic increase factors are estimated by:

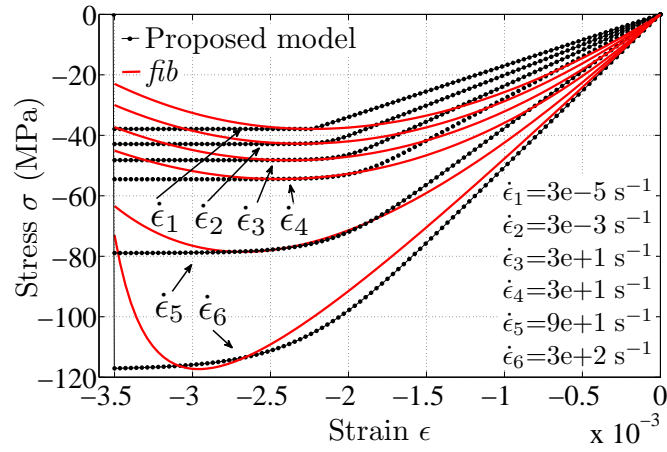
$$\frac{E_c}{E_{c,st}} = \left( \frac{\dot{\epsilon}}{\dot{\epsilon}_{st}} \right)^{0.026} \quad (5.1)$$

$$\text{DIF}_{\text{conc}}^{\text{comp}} = \frac{f_c}{f_{c,st}} = \begin{cases} \left( \frac{\dot{\epsilon}}{\dot{\epsilon}_{st}} \right)^{1.026\alpha_s} & \text{for } \dot{\epsilon} \leq 30 \text{ s}^{-1} \\ \gamma_s \left( \frac{\dot{\epsilon}}{\dot{\epsilon}_{st}} \right)^{1/3} & \text{for } \dot{\epsilon} > 30 \text{ s}^{-1} \end{cases} \quad (5.2)$$

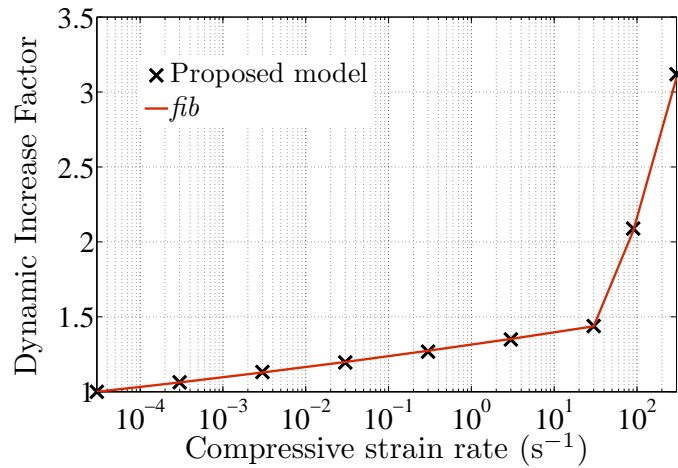
where  $E_c$  is the compressive Young's modulus at strain rate  $\dot{\epsilon}$ ;  $E_{c,st}$  the compressive static Young's modulus;  $f_c$  the compressive strength at strain rate  $\dot{\epsilon}$ ;  $f_{c,st}$  the static compressive strength (37.9 MPa for a C30 concrete);  $\dot{\epsilon}$  a strain rate between  $3 \cdot 10^{-5} \text{ s}^{-1}$  and  $300 \text{ s}^{-1}$ ;  $\dot{\epsilon}_{st}$  the compressive 'static' strain rate of  $3 \cdot 10^{-5} \text{ s}^{-1}$ ;  $\log(\gamma_s) = 6.156 \alpha_s - 2$ ;  $\alpha_s = 1/(5 + 9f_{c,st}/10^7)$ .

Based on these dynamic increase factors, a strain rate dependence is introduced both in the elastic and in the plastic domain of the proposed bilinear model explained in Chapter 3, to match the previous *fib* prescriptions in terms of peak stress and strain at peak stress. This allows for preserving the crushing energy (area under the compressive stress-strain curve) as shown in Figure 5.3a, where the simplified bilinear model used here is compared to the response as proposed by the *fib*. The compressive stress-strain curves for a C30 concrete type are depicted for various strain rates. The rate dependent curves suggested by the *fib* have been constructed following the static stress-strain expression based on relationships (3.1), (3.2) and (3.3), and the rate dependent expressions for the Young's modulus (Eq. (5.1)) and the DIFs on the compressive strength (Eq. (5.4)). A rate dependent Young's modulus is adopted, an important feature due to its influence in the load distributions involved in progressive collapse analyses. It must be noted that the long-term time-effects on the material characteristics of concrete (such as creep or

shrinkage) are not considered in this model, since they are out of the scope of the present research. The ultimate compressive strain (-0.35%) corresponding to the crushing strain of concrete will be considered constant independently of the strain rate, as no evolution of this parameter was evidenced in [60]. The dynamic increase factors for a C30 concrete type obtained with the proposed model are in good agreement with the prescriptions of the *fib* [52], as observed in Figure 5.3b. The details of the rate dependent constitutive model proposed in this work, as well as the stress update algorithm, will be given in the next section.



(a) Stress-strain diagram



(b) Dynamic increase factors

**Figure 5.3:** Strain rate dependent model for concrete in compression.

The **tensile behaviour of concrete** is also rate dependent. The tensile contribution of concrete was observed to be negligible in the previous rate

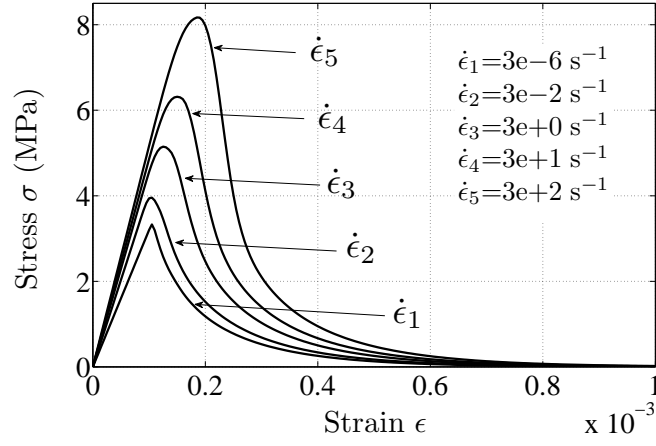
independent computations. In order to investigate whether the strength enhancement resulting from the strain rate effects lead to a more significant influence of the tensile strength, a rate dependent model for tensile response is also developed. The expression for the rate dependence of Young's modulus and the tensile strength, given by the *fib* [52], are:

$$\frac{E_t}{E_{t,st}} = \left( \frac{\dot{\epsilon}}{\dot{\epsilon}_{st}} \right)^{0.026} \quad (5.3)$$

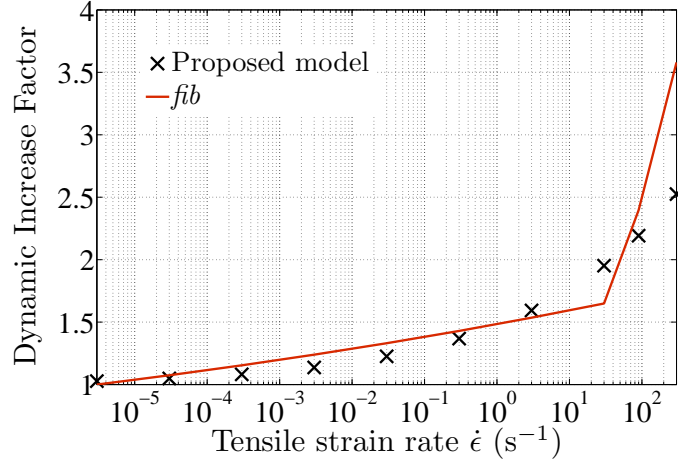
$$\text{DIF}_{\text{conc}}^{\text{tens}} = \frac{f_t}{f_{t,st}} = \begin{cases} \left( \frac{\dot{\epsilon}}{\dot{\epsilon}_{st}} \right)^{1.016\delta_s} & \text{for } \dot{\epsilon} \leq 30\text{s}^{-1} \\ \beta_s \left( \frac{\dot{\epsilon}}{\dot{\epsilon}_{st}} \right)^{1/3} & \text{for } \dot{\epsilon} > 30\text{s}^{-1} \end{cases} \quad (5.4)$$

where  $E_t$  is the tensile Young's modulus at strain rate  $\dot{\epsilon}$ ;  $E_{t,st}$  the tensile static Young's modulus;  $f_t$  the tensile strength at strain rate  $\dot{\epsilon}$ ;  $f_{t,st}$  the static tensile strength (3.25 MPa for a C30 concrete);  $\dot{\epsilon}$  a strain rate between  $3 \cdot 10^{-6} \text{ s}^{-1}$  and  $300 \text{ s}^{-1}$ ;  $\dot{\epsilon}_{st}$  the tensile 'static' strain rate of  $3 \cdot 10^{-6} \text{ s}^{-1}$ ;  $\log(\beta_s) = 7.11\delta_s - 2.33$ ;  $\delta_s = 1/(10 + 6f_{c,st}/10^7)$ .

In what refers to the rate dependence of the tensile fracture energy  $G_f$ , the *fib* merely states that the value of this parameter increases with increasing stress and strain rate [52], however no quantitative information is given. Numerous studies have been carried out to assess the rate dependence of  $G_f$ , from which different conclusions are derived. According to [62] the fracture energy barely depends on the strain rate. In [56], experimental tests are carried out and the fracture energy is considered to remain constant for medium levels of the loading rate, whereas for high values of the loading rate it does increase but not in a significant manner. The ultimate strain is shown to be practically rate independent. For other authors [57–61], the rate dependence in the fracture energy is considered to be more significant and different expressions as a function of the strain/loading rate are suggested. In this contribution, in order to limit the rate dependence of the fracture energy to a certain extent, the model parameters are set such that the stress decreases to reach a zero value at the fixed ultimate strain of  $\epsilon_u = 10/00$  whatever the value of the strain rate, as observed in Figure 5.4a. The DIFs are also shown in Figure 5.4b. The model proposed here matches the DIF previsions from the *fib* (based on those obtained by Malvar et al. [85]) in a reasonable way for the range of strain rates that are considered here (up to  $2 \text{ s}^{-1}$ ).



(a) Stress-strain diagram



(b) Dynamic increase factors

**Figure 5.4:** Strain rate dependent model for concrete in tension.

For **steel**, Young's modulus is assumed to be rate independent, as observed by Malvar et al. [85]. The DIFs corresponding to the yield stress and the ultimate stress for steel obey the following expressions according to [85]:

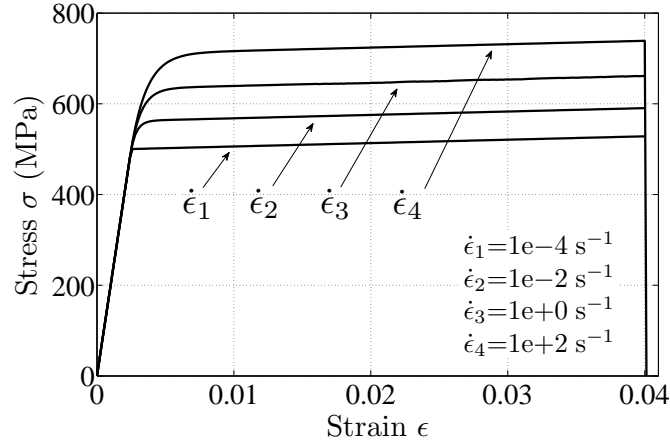
$$\text{DIF}_{\text{steel}}^y = \frac{f_y}{f_{y,st}} = \left( \frac{\dot{\epsilon}}{\dot{\epsilon}_{st}} \right)^{\alpha_y} \quad (5.5)$$

$$\text{DIF}_{\text{steel}}^u = \frac{f_u}{f_{u,st}} = \left( \frac{\dot{\epsilon}}{\dot{\epsilon}_{st}} \right)^{\alpha_u} \quad (5.6)$$

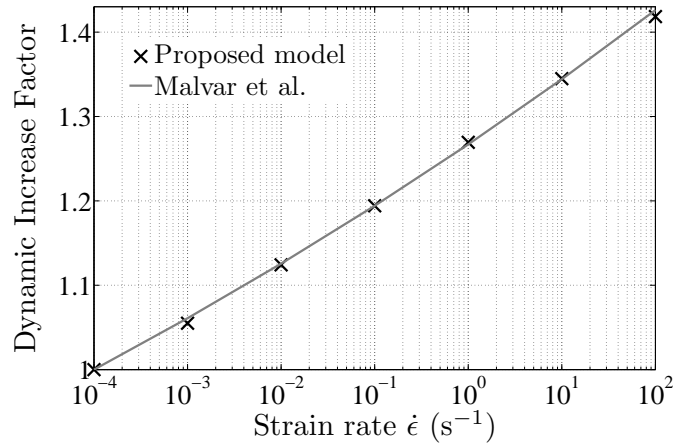
with  $f_y$  the yield stress at strain rate  $\dot{\epsilon}$ ;  $f_{y,st}$  the static yield stress (here 500 MPa);  $f_u$  the ultimate stress at strain rate  $\dot{\epsilon}$ ;  $f_{u,st}$  the static ultimate stress (here 530 MPa);  $\dot{\epsilon}$  a strain rate between  $10^{-4} \text{ s}^{-1}$  and  $225 \text{ s}^{-1}$ ;  $\dot{\epsilon}_{st}$  the 'static' strain rate of  $10^{-4} \text{ s}^{-1}$ ;  $\alpha_y = 0.074 - 0.040f_y/414$ ;  $\alpha_u = 0.019 -$

## 5.2 Rate dependent response of concrete and steel

$0.009f_y/414$ . The parameters of the constitutive model (which will be detailed in next section) are adjusted to match the previous recommendations in terms of  $DIF_{steel}^y$ .



(a) Stress-strain diagram



(b) Dynamic increase factors

**Figure 5.5:** Strain rate dependent model for steel.

Figure 5.5 shows the rate dependent stress-strain curves of the proposed model and the corresponding DIFs. It can be observed that the plastic slope of the stress-strain relationships remains constant independently of the strain rate. However, the DIFs predicted in [85] for the yield stress are significantly higher than those for the ultimate stress. In order to guarantee that the resulting values of the ultimate stress do not overestimate the previous rate dependent previsions, the ultimate-to-yield stress ratio in the proposed model ( $f_{u,st}/f_{y,st} = 1.06$ ) is lower than the minimum value recommended in Eu-

rocode 2 [51] for a steel ductility class B ( $f_{u,st}/f_{y,st} \geq 1.08$ ). The ultimate strain, which is not observed to vary as a function of the strain rate [85], is taken equal to  $\epsilon_{s,lim}$  4% as in the rate independent model. In order to represent the failure of steel, the stress is set to zero for strains exceeding this value, regardless of the value of the strain rate.

### 5.3 Rate dependent constitutive model

A natural way to include the strain rate effects in a material model is the introduction of viscous terms in the constitutive law. For instance, Pedersen et al. [89] developed a rate dependent macroscopic material model based on the microscopic and mesoscopic behaviour of concrete. According to the authors, the rate dependence of concrete behaviour is assumed to be linked to the moisture in micro- and nano-pores of the material for intermediate rates, while for higher rates the observed strength increase in concrete would be due to a change of the failure mechanisms and to the effect of micro-/meso-inertia. In the present contribution, rate dependent one-dimensional constitutive laws for concrete and steel are used in the layers of the layered beam model. The Perzyna's viscoplastic model [94, 95] is adopted for the behaviour of both constituents. This model is widely employed for the characterisation of the strain rate effects in concrete [89, 91–93]. In such a model, the viscoplastic strain rate  $\dot{\epsilon}^{vp}$  is expressed as a function of the yield function  $f$  defined in Eq. (3.10):

$$\dot{\epsilon}^{vp} = \frac{1}{\eta} \left\langle \frac{f}{\bar{\sigma}_0} \right\rangle^N \frac{df}{d\sigma} \quad (5.7)$$

where  $\bar{\sigma}_0$  (MPa) is the initial yield stress;  $f$  (MPa) is the yield function which accounts for the overstress ( $\sigma - \bar{\sigma}$ );  $\eta$  (s) and  $N$  (-) are viscosity parameters, with  $N \geq 1$  an integer number; and  $\langle \rangle$  denotes the Macaulay brackets. The previous relation implies that the applied stress  $\sigma$  can exceed the yield stress  $\bar{\sigma}$  in a viscoplastic approach, contrarily to the rate independent plastic case (where  $\sigma \leq \bar{\sigma}$ ). Figure 5.6 describes the typical stress–strain relationship in a viscoplastic model.

Note that the parameter  $\eta$  may depend on the strain rate  $\eta(\dot{\epsilon})$  to match the material response reported in the literature in terms of DIFs. The Young's modulus may also be a rate dependent function, as previously explained ( $E(\dot{\epsilon})$ ). Rewriting Eq. (5.7) in an incremental fashion, the residual in Eq. (3.14)

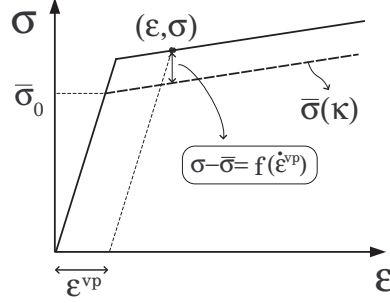


**Figure 5.6:** Typical stress-strain relationship of an elasto-viscoplastic model.

now reads:

$$\{R(\sigma_{n+1}, \kappa_{n+1})\} = \left\{ \begin{array}{l} \sigma_{n+1} - \sigma_{n+1}^{trial} + E(\dot{\epsilon}_{n+1})\Delta\kappa_{n+1} \\ \eta(\dot{\epsilon}_{n+1})\Delta\kappa_{n+1} - \Delta t_{n+1} \left\langle \frac{f(\sigma_{n+1}, \kappa_{n+1})}{\bar{\sigma}_0} \right\rangle^N \frac{df}{d\sigma} \Big|_{n+1} \end{array} \right\} = 0 \quad (5.8)$$

where Eq. (3.9) and the approximation  $\dot{\kappa} = \Delta\kappa/\Delta t$  have been used, with  $\Delta t$  the time step. As in the rate independent approach, this residual is a function of two variables:  $\sigma$  and  $\kappa$ .

### 5.3.1 Particularities of the rate dependent model parameters

The expressions and/or values for the parameters of the rate dependent model are provided in Table 5.1. It can be observed that some of these parameters depend on the strain rate. For instance, the use of strain rate dependent functions for the material parameters, instead of constant values, constitutes the main originality of the present formulation. Their analytical expressions are given in the Appendix.

For **concrete in compression**, the rate dependence needs to be introduced both in Young's modulus  $E_c(\dot{\epsilon})$  and in the viscoplastic parameter  $\eta_c(\dot{\epsilon})$ , to obtain a good agreement with the previsions reported in the *fib* in terms of stress-strain relationships and DIFs, which were shown in Figures 5.3. The expression for  $E_c(\dot{\epsilon})$  is different from the rate dependent formula proposed by the *fib* in Eq. (5.1), since in the present simplified bilinear model an equivalent reduced elastic modulus is adopted (Figure 5.3a), instead of the 'real' Young's modulus (the initial slope of the stress-strain curve proposed by the *fib* model). Hence, the rate dependent expression for this parameter differs

**Table 5.1:** Material parameters of the rate dependent constitutive models for steel and concrete

<b>steel</b>		
$N_s$	$\eta_s$ [s]	
1	$\eta_s(\dot{\epsilon})^*$ (Fig. 5.11)	

\* numerical expression in Appendix

<b>concrete</b>		
compression		
$E_c$ [GPa]	$N_c$	$\eta_c$ [s]
$E_c(\dot{\epsilon})^*$ (Fig. 5.7a)	1	$\eta_c(\dot{\epsilon})^*$ (Fig. 5.7b)
tension		
$E_t$ [GPa]	$N_t$	$\eta_t$ [s]
$E_t(\dot{\epsilon})^*$ (Fig. 5.10a)	5	$\eta_t(\kappa_t)^*$ (Fig. 5.10b)

\* numerical expression in Appendix

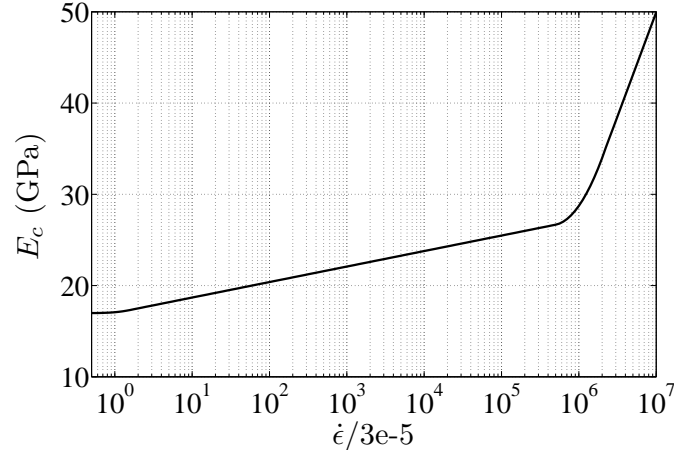
from the *fib* formula. As for the viscoplastic parameter  $\eta_c$ , a rate independent choice would not allow approximating the predictions in terms of DIFs (in Figure 5.3b). Hence the need to adopt a rate dependent function for this parameter as well. Parameters  $E_c(\dot{\epsilon})$  and  $\eta_c(\dot{\epsilon})$  are depicted in Figure 5.7.

In **tension**, the rate dependence of the Young's modulus  $E_t(\dot{\epsilon})$  is directly taken from Eq. (5.1), since the 'real' elastic modulus is adopted for the tensile response. The viscoplastic parameter  $\eta_t$  is considered rate independent for the sake of simplicity, which yields a slightly worse yet still reasonable agreement with the DIFs provided by the *fib* (in Figure 5.4b), for the strain rate range considered in this work (values up to  $2 \text{ s}^{-1}$  were obtained in the reference test from previous chapter). As explained in Section 3.1.2, the post-peak tensile stress-strain curve is modelled by using a softening evolution law for the yield stress, in order to represent the strength decrease due to cracking. This softening being an exponential function, the overstress induced by the present viscoplastic model would prevent the tensile stress from vanishing for a constant viscoplastic strain rate ( $\dot{\epsilon}^{vp} = \text{const}$ ). For instance, it can be easily yielded from Eq. (5.7) that if  $\dot{\epsilon}^{vp}$  is constant, then the overstress ( $\sigma - \bar{\sigma}$ ) included in the yield function  $f$  (see Eq. (3.10)) will also be constant. Figure 5.8 illustrates this phenomenon.

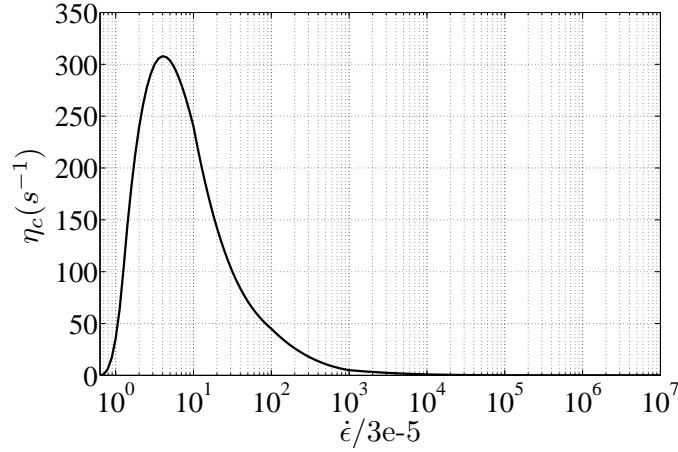
Adopting a constant viscoplastic parameter  $\eta_t$  in tension would therefore result in a considerable increase of the fracture energy for increasing strain

### 5.3 Rate dependent constitutive model

---



(a) Young's modulus in compression  $E_c(\dot{\epsilon})$ .



(b) Viscoplastic parameter  $\eta_c(\dot{\epsilon})$ .

**Figure 5.7:** Model parameters for concrete in compression.

rates, due to the growth of both the stress level and the ultimate strain (strain at which the stress vanishes). To avoid this, here  $\eta_t$  is made a decreasing function of the accumulated tensile plastic strain  $\kappa_t$ , in such a way that the overstress vanishes at the ultimate strain  $\epsilon_u = 10/00$ . Thus,  $\eta_t$  drops exponentially from its initial value to zero, in order to retake the classical (rate independent) plastic approach for strains exceeding the ultimate strain. By doing so, the rate dependence on the fracture energy is only related to the tensile strength enhancement, and not to the pathological residual stress in the post-peak branch. Figure 5.8 shows the different stress-strain curves obtained for a constant viscoplastic parameter and a parameter  $\eta_t$  which vanishes with  $\kappa_t$ . It must be noted that this feature (i.e. the evolution of  $\eta_t$  on the cumulated strain  $\kappa_t$ ) is also an original contribution to the physically-based

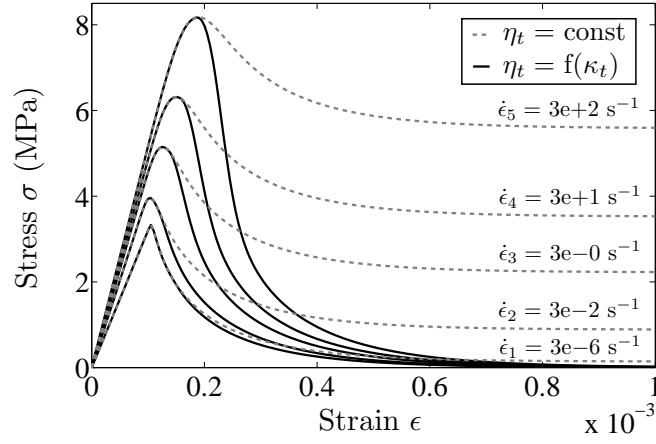


**Figure 5.8:** Rate-dependent tensile response of the model for concrete as a function of the choice for  $\eta_t$ .

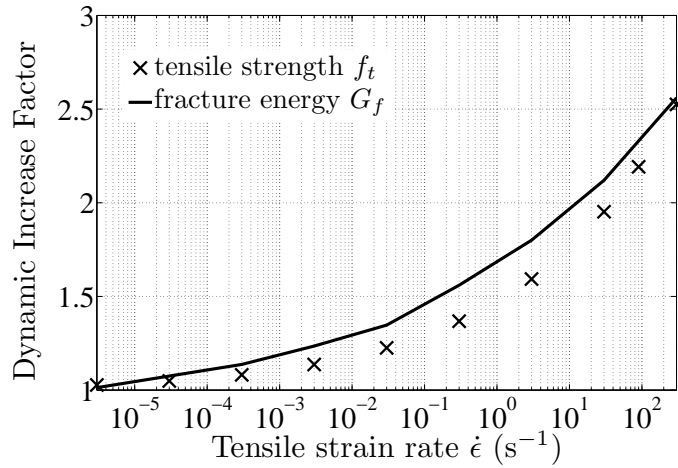
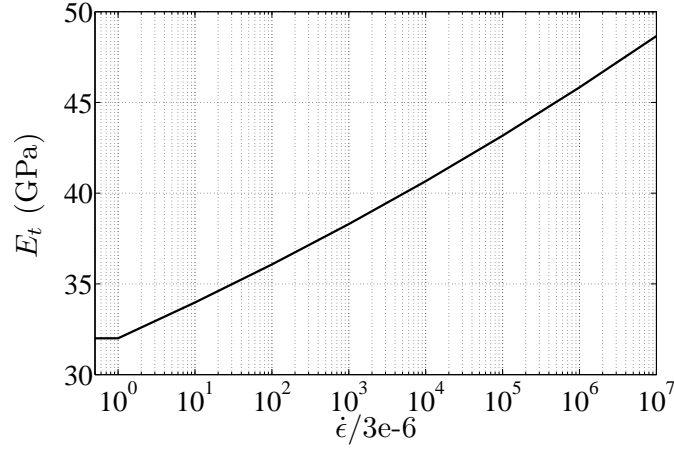


**Figure 5.9:** DIFs of the fracture energy  $G_f$  as a function of  $\dot{\epsilon}$ .

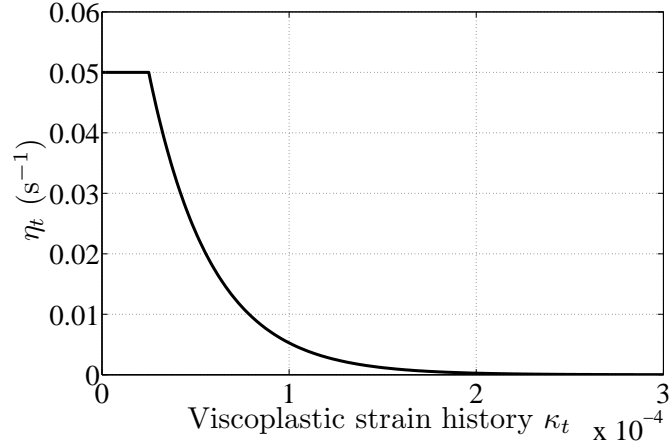
modelling of the rate dependent tensile response in concrete. In Figure 5.9, the evolution of the fracture energy  $G_f$  as a function of the strain rate obtained with the proposed model in terms of DIFs is illustrated. It can be observed that the corresponding DIFs for  $G_f$  are close to the values of the DIFs for the tensile strength of concrete. The tensile Young's modulus  $E_t(\dot{\epsilon})$  and the evolution of parameter  $\eta_t$  as a function of the viscoplastic strain history parameter  $\kappa_t$  are shown in Figure 5.10.

### 5.3 Rate dependent constitutive model

---



(a) Young's modulus in tension  $E_t(\dot{\epsilon})$ .



(b) Viscoplastic parameter  $\eta_t(\kappa_t)$ .

**Figure 5.10:** Model parameters for concrete in tension.

For **steel**, the Young's modulus adopted in the present study is rate independent, accordingly to the observations from [85]. The viscoplastic parameter  $\eta_s$  varies as a function of the strain rate ( $\eta_s(\dot{\epsilon})$ ) to match the DIFs predicted by [85] (Figure 5.5b). Parameter  $\eta_s(\dot{\epsilon})$  is depicted in Figure 5.11.

A perturbation technique is used to evaluate the material tangent operator  $H$  consistent with the return-mapping algorithm. This avoids the analytical derivation of the constitutive equations with respect to the strain  $\epsilon$ , a non-trivial task due to the multiple dependence of parameters  $E_c(\dot{\epsilon})$ ,  $\eta_c(\dot{\epsilon})$ ,  $\eta_t(\kappa_t)$  and  $\eta_s(\dot{\epsilon})$ .

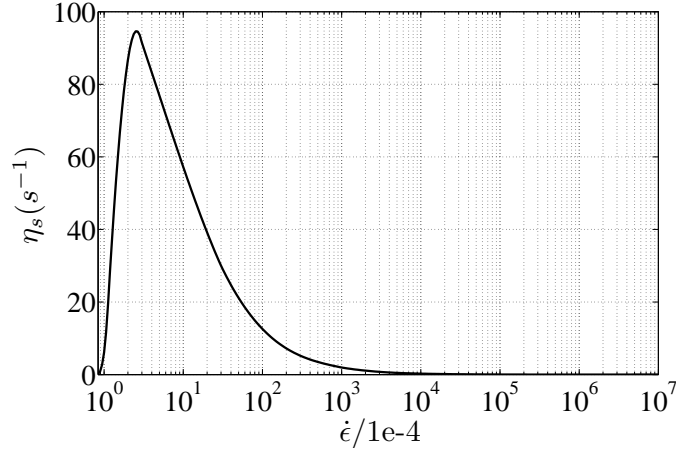


**Figure 5.11:** Parameter  $\eta_s(\dot{\epsilon})$  in steel.

## 5.4 Rate dependent multilayered approach

The introduction of the previous rate dependent constitutive equations in the layered beam formulation provides rate dependent relationships between the beam generalised stresses  $\{\Sigma^{gen}\}$  and strains  $\{E^{gen}\}$ :

$$\{\Sigma^{gen}\} = f(\{E^{gen}\}, \{\dot{E}^{gen}\}) \quad (5.9)$$

To obtain such relationships, the layer-wise strain rates are computed from the generalised strain rates  $\{\dot{E}^{gen}\} = \{\dot{\epsilon}, \dot{\chi}\}$  as follows:

$$\dot{\epsilon}_i = \dot{\epsilon} - \bar{y}_i \dot{\chi} \quad (5.10)$$

These strain rates are used to calculate the layer-wise stresses by applying the rate dependent constitutive laws  $\sigma_i(\epsilon_i, \dot{\epsilon}_i)$ , as illustrated in Figure 5.12.

An analytical version of such a rate dependent multilayered approach is presented in [47], where the strain rate dependence is introduced in a simply supported RC slab under blast loading by multiplying the layer-wise stresses  $\sigma_i(\epsilon_i)$  by their corresponding dynamic increase factors  $DIF(\dot{\epsilon}_i)$ . The rate dependence of concrete in the elastic region is not taken into account in [47], contrarily to the present formulation.

## 5.4 Rate dependent multilayered approach

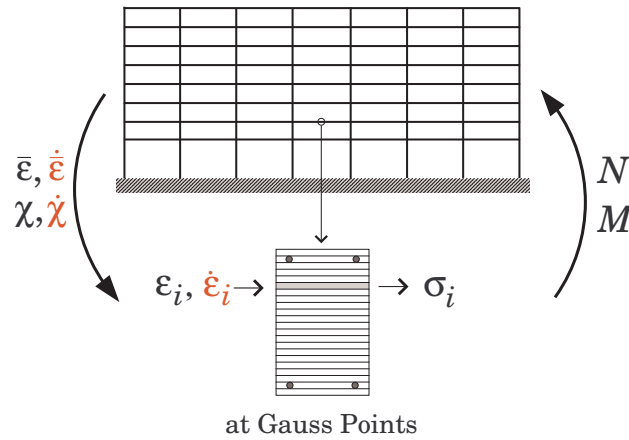


**Figure 5.12:** Rate dependent multilayered approach.

### 5.4.1 Application: rate dependent moment-curvature relationships for a given RC section

To illustrate the rate-dependent response of reinforced concrete at the cross-sectional level, a RC beam section is subjected to a simple bending test where curvature is applied at different rates. The values of the curvature rates used in this test are in the same order of magnitude as those obtained in the rate independent structural computations in the previous chapter. Figure 5.13 shows the evolution of the curvature rate in sections S1, S2 and S3 from the reference case of study.

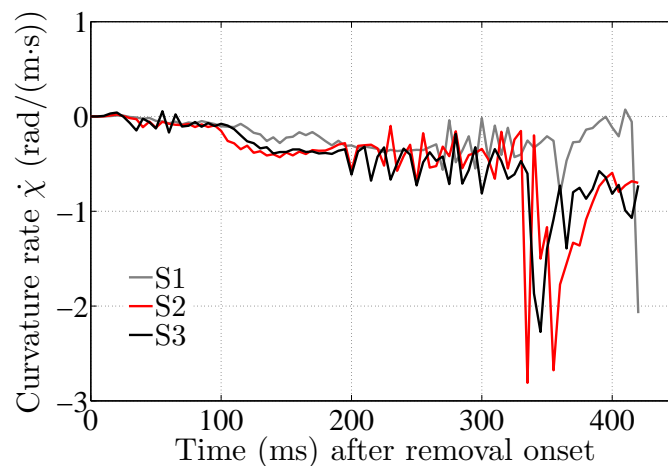


**Figure 5.13:** Evolution of the curvature rates in the reference case of study.

It can be observed that the maximum values are reached at the end of the computation, when collapse is imminent and the structure is in an advanced state of degradation. In order to obtain the range of rates which are related exclusively to the column removal (before significant structural damage has occurred), the maximal values reached in all the elements of the structure until 250 ms after the column removal onset have been extracted. The maximal value obtained is  $\dot{\chi} = 0.73 \text{ rad}/(\text{m}\cdot\text{s})$ .

The present test is sketched in Figure 5.14: a uniform curvature is created along the beam length by applying an angular displacement  $\theta$  at both ends. This angular displacement is incrementally increased at a constant rate  $\dot{\theta}$ . The curvature rate  $\dot{\chi}$  is calculated as:

$$\dot{\chi} = \frac{\delta\dot{\theta}}{\delta x} = \frac{2\dot{\theta}}{L} \quad (5.11)$$

with  $L$  the beam length. Two beam cross-sections are used: Scheme A corresponds to Section A of the reference case of study in the previous chapter (Figure 4.3); Scheme B contains the same upper reinforcement, but for the lower one the 32 mm diameter bars are substituted by 20 mm diameter ones. Inertial effects are not taken into account here since the aim is to focus on the strain rate effects. The material parameters are those indicated in Tables 3.2 and 5.1. Tensile strength of concrete is taken into account, together with its corresponding rate effects. The obtained rate dependent bending

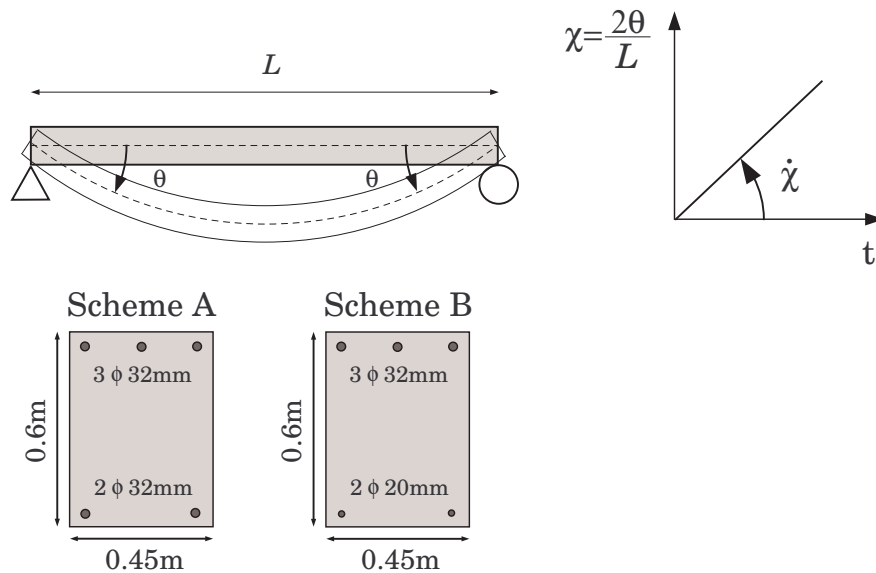
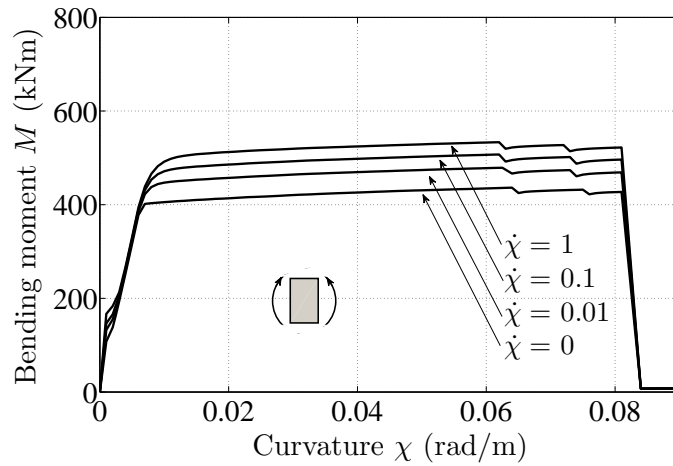


**Figure 5.14:** Rate dependent uniform bending test description.

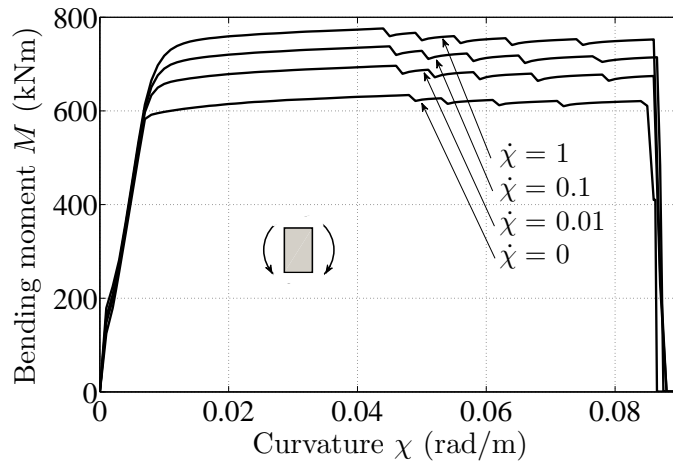
## 5.4 Rate dependent multilayered approach

moment–curvature relationships for Scheme A are shown in Figure 5.15, for both positive and negative bending.

Crushing of concrete occurs first, followed by the failure of the tensile rebars. It can be observed that the use of a rate dependent model for concrete and steel leads to a significant enhancement in the sectional behaviour for the rates considered in the present study. Logically, the section exhibits higher resistance for negative bending, since the upper reinforcement ratio is larger than the lower one. The crushing of compressive concrete is observed to initiate earlier for increasing rates.



(a) Positive bending



(b) Negative bending

**Figure 5.15:** Scheme A: Bending moment–curvature diagrams as a function of the curvature rate.

The final state of the section for Scheme A for as a function of the curvature rate is depicted in Figure 5.16 for positive and negative bending. The sectional failure is identical for the various curvature rates adopted in the case of positive bending, while for negative bending the area of concrete under compression (in particular the plastic red zone) increases slightly as a function of the curvature rate. This result might be a consequence of the absolute strength enhancement in the upper steel bars (in tension) due to the strain rate effects, which is higher than in the bottom steel bars and is thus balanced by an increased area of concrete under compression.

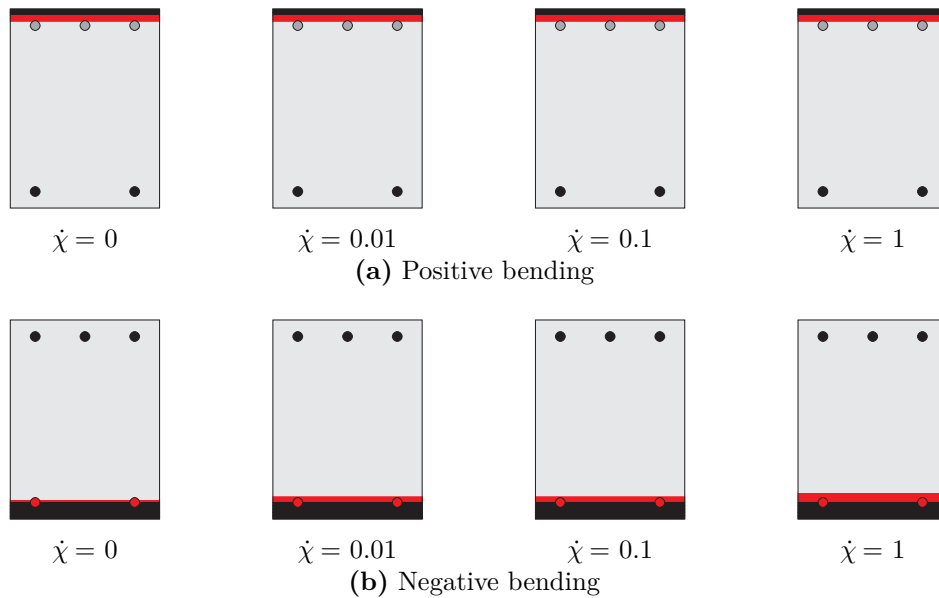
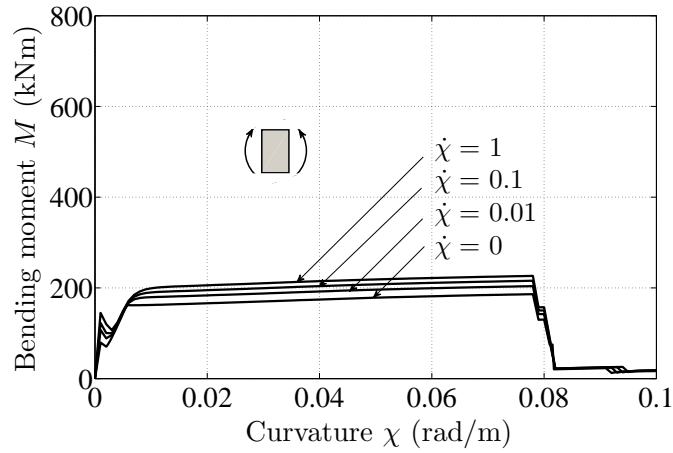


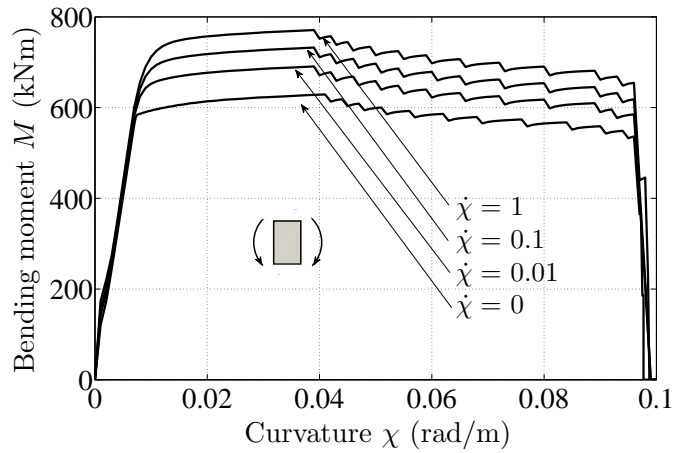
**Figure 5.16:** SchemeA: sectional final state as a function of the curvature rate.

The results corresponding to Scheme B are depicted in Figure 5.17 for the moment–curvature relationships and in Figure 5.18 for the final state of the section as a function of the curvature rate. The same generic observations as for the previous scheme are valid for this less reinforced configuration. The level of sectional resistance under positive bending is lower than under positive bending, since the amount of bottom reinforcement is much lower to the top one. For this reinforcement arrangement the positive moments are also inferior to those obtained with Scheme A, as expected from the reduction of the lower reinforcement area. Due to this fact, the fracture of the tensile steel bars occurs before the initiation of concrete crushing. For negative

## 5.4 Rate dependent multilayered approach



(a) Positive bending



(b) Negative bending

**Figure 5.17:** Scheme B: Bending moment–curvature diagrams as a function of the curvature rate.

bending, however, the crushing takes place earlier than for Scheme A, which is also due to the lesser amount of bottom reinforcement. Although the same level of bending moment is obtained for both schemes, Scheme B presents a slightly more ductile response: the rupture of the steel bars occurs later than for Scheme A. The same phenomena is observed as for the rate independent response of these sections (Chapter 3).

Concerning the final state of the section for the different curvature rates, the main difference with respect to Scheme A is that the crushed concrete area is lower for positive bending and higher for negative bending. The same global rate effects are obtained for Scheme B: for positive bending the sec-

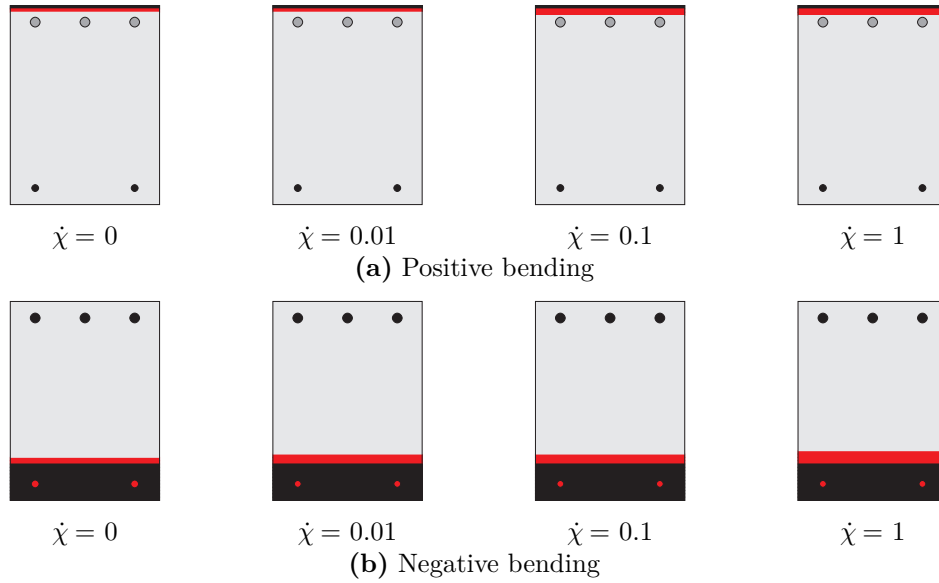


**Figure 5.18:** Scheme B: sectional final state as a function of the curvature rate.

tional failure pattern is less rate-sensitive than for negative bending. However, a better exploitation of the concrete material is observed for negative bending in Scheme B with respect to Scheme A: the rate effects induce an increase of the compressive part of the section. As for Scheme A, the strength enhancement in tensile steel due to the strain rate effects appears to be compensated by increasing the area of concrete under compression. Since the bottom reinforcement in Scheme B is lower than in Scheme A, this increase is more significant than in the previous case.

The dynamic increase factors of the maximal bending moment (thus before crushing) as a function of the curvature rate are gathered in Figure 5.19. They are practically identical for both schemes. For positive bending the DIFs are slightly inferior for Scheme B, although this is only a minor difference. The increase of the rotational strength takes values up to 23%, as can be seen in the figure. This is thus the order of magnitude of the flexural resistance enhancement that may be expected in a rate dependent progressive collapse simulation. Note that this enhancement could play a crucial role in situations of sudden bending moment increase and/or reversal at the beam-to-column connections after the loss of a bearing member.

## 5.5 Time integration scheme for the strain rate dependent approach

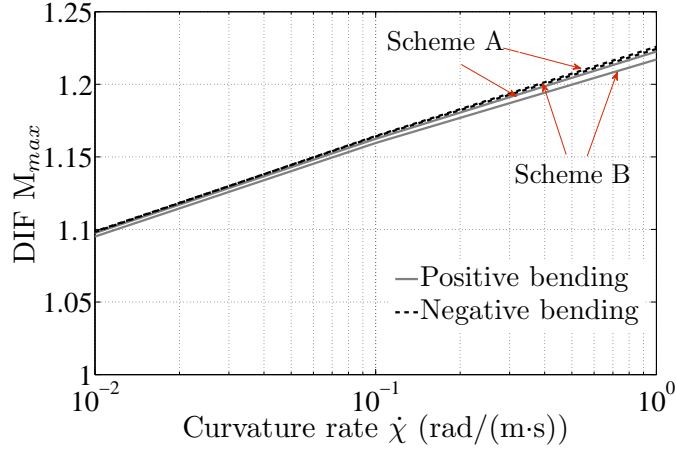


**Figure 5.19:** Dynamic Increase Factors for the maximum bending moment.

## 5.5 Time integration scheme for the strain rate dependent approach

At the structural scale, the equilibrium equations now read:

$$\{f^{int}(\{q\}, \{\dot{q}\})\} + [M]\{\ddot{q}\} = \{f^{ext}\} \quad (5.12)$$

where the internal forces  $\{f^{int}\}$  are also a function of the displacement rates  $\{\dot{q}\}$ :

$$\{f^{int}(\{q\}, \{\dot{q}\})\} = \sum_e \int_{V_e} [B]^t \{ \Sigma^{gen}(\{E^{gen}\}, \{\dot{E}^{gen}\}) \} dV \quad (5.13)$$

Note that the new structural tangent operator  $[K_t^*]$  (defined as the variation of the internal forces with respect to the displacements) now contains inherently a viscous damping term which stems from the rate dependence of the internal forces. The development of this new structural tangent operator yields:

$$\begin{aligned} [K_t^*] &= \frac{\partial \{f^{int}(\{q\}, \{\dot{q}\})\}}{\partial \{q\}} = \\ &= \frac{\partial \{f^{int}(\{q\}, \{\dot{q}\})\}}{\partial \{q\}} \Big|_{\{\dot{q}\}=cst} + \frac{\partial \{f^{int}(\{q\}, \{\dot{q}\})\}}{\partial \{\dot{q}\}} \Big|_{\{q\}=cst} \frac{\partial \{\dot{q}\}}{\partial \{q\}} \end{aligned} \quad (5.14)$$

By making use of the definitions of tangent stiffness matrix  $[K_t]$  and tangent damping matrix  $[C_t]$ , which denote the variation of the internal forces with

respect to the displacements and the velocities respectively, the expression of the tangent operator is given by:

$$[K_t^*] = [K_t] + [C_t] \cdot \frac{\partial \{\dot{q}\}}{\partial \{q\}} \quad (5.15)$$

The non-vanishing of the viscous damping matrix  $[C_t]$  is fulfilled by the rate dependence of the internal forces  $\{f^{int}(\{q\}, \{\dot{q}\})\}$ , which allows for their derivability with respect to the displacement rate  $\{\dot{q}\}$ , contrarily to a rate-independent approach where this term would vanish and  $[K_t^*] = [K_t]$  (as seen in Section 3.4). This means that the strain rate dependent nature of the material constitutive equations provides a certain amount of damping at the structural level, contrarily to classical rate independent approaches where a numerical damping of constant value is assumed exclusively, as it is the case of most contributions to progressive collapse [24, 35, 42].

The flowchart of the time integration scheme for the rate dependent approach is provided in Figure 5.20. The difference with respect to the rate independent case is that now the velocities  $\{\dot{q}\}$  are used to compute the internal forces  $\{f^{int}\}$ .

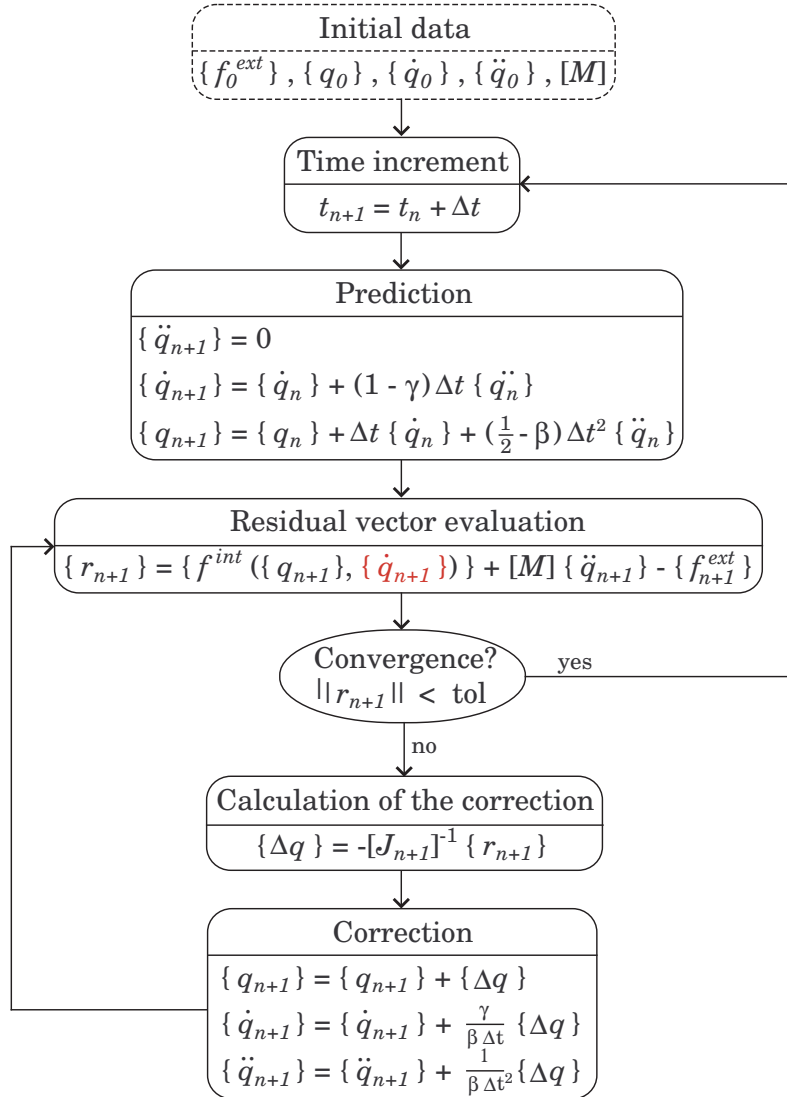


**Figure 5.20:** Dynamic integration scheme for the rate dependent approach [67].

## 5.6 Rate dependent simulations of progressive collapse

In this section, the strain rate effects in the progressive collapse simulation are analysed. First, a rate dependent version of the reference test from previous chapter (described in Section 4.2) is performed. Additionally, some of the tests carried out previously for varying design and modelling options will



## 5.6 Rate dependent simulations of progressive collapse

---

the material strength-enhancement due to the strain rate effects prevents collapse from occurring, as opposed to the rate independent case where the entire rightmost bay collapses.

The sectional strength degradation is thus lower in the rate dependent case, as can be observed in the figures for both column removal locations. It must be pointed out that the sectional damage at the supports (sections S1, S2, S3, etc.), which in the rate independent case occurs in a single element, is now extended over several elements. For instance, this damage is also propagated to the adjacent bay (where yielding of the steel bars occurs in one element), contrarily to the rate independent case, in which the fracture of the rebars prevents a load propagation to the neighbouring (and thus intact) elements.

This result suggests that the introduction of the rate dependence implies a modification in the load redistributions over the residual structure: the corresponding strength increase at the material level might result in a further expansion of the alternate load path. The viscous effects would hence play a delocalising role in the structural damage. For instance, the inclusion of viscous terms in the material constitutive laws is sometimes adopted in the literature in order to introduce an internal length that avoids mesh-sensitivity problems [69, 89].

For an interior column removal, the degree of sectional failure is lesser when the strain rate effects are considered: the area of crushed concrete is

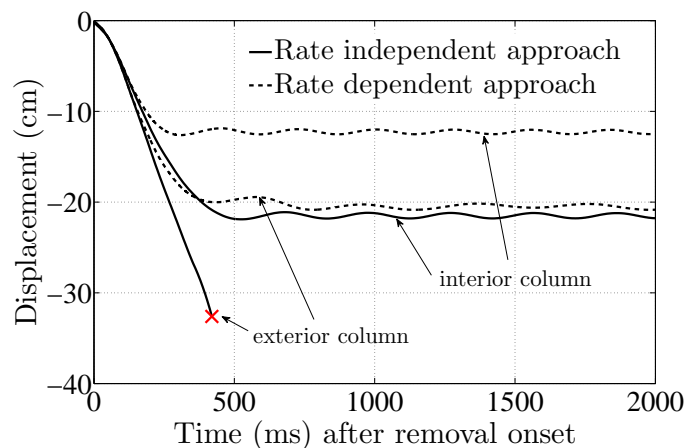


**Figure 5.23: REF:** vertical displacement history for the rate dependent approach.

reduced. Nevertheless, the final response patterns are similar in both cases, in which progressive collapse is avoided. The vertical displacement history at the point of connection with the removed column is shown in Figure 5.23: even for an interior column removal, the displacement is decreased in a significant manner (almost by 50%) upon consideration of the rate effects.

The evolution of the axial force  $N$  and bending moment  $M$  are depicted in Figures 5.24 and 5.25 respectively for an exterior removal, and in Figures 5.26 and 5.27 for an interior removal. Since complete sectional failure does not place at any point of the structure, the level of  $N$  and  $M$  is almost the same

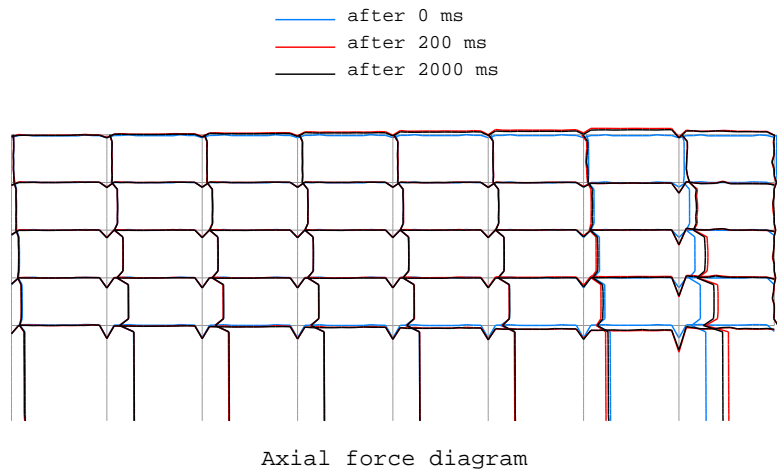


**Figure 5.24:** Evolution of  $N$  for an exterior column removal.

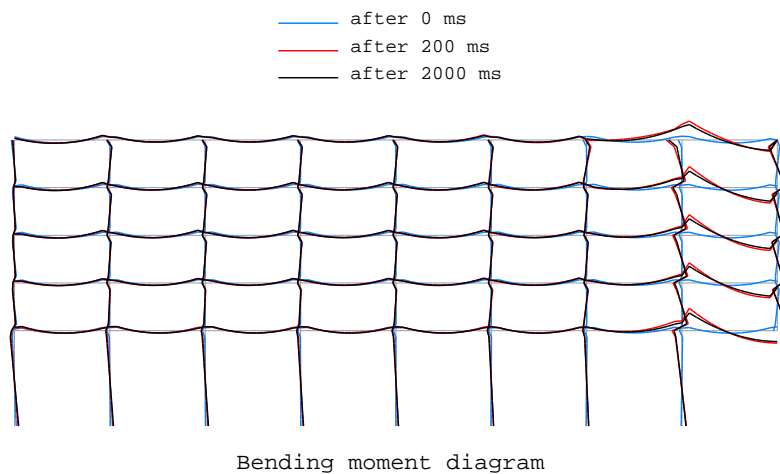


**Figure 5.25:** Evolution of  $M$  for an exterior column removal.

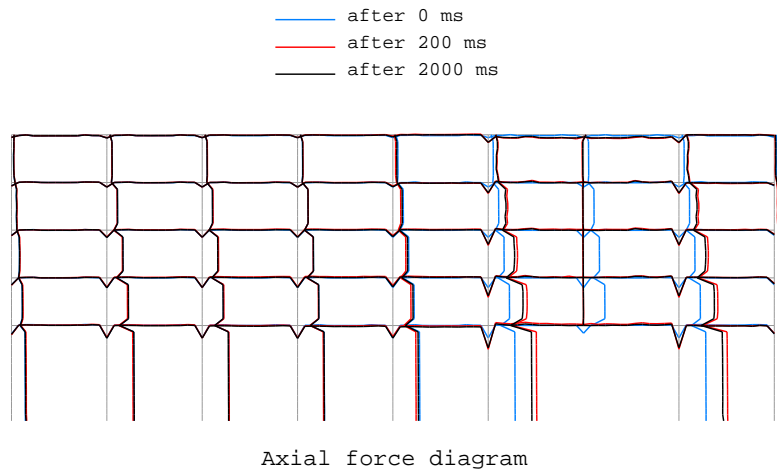


**Figure 5.26:** Evolution of  $N$  for an interior column removal.

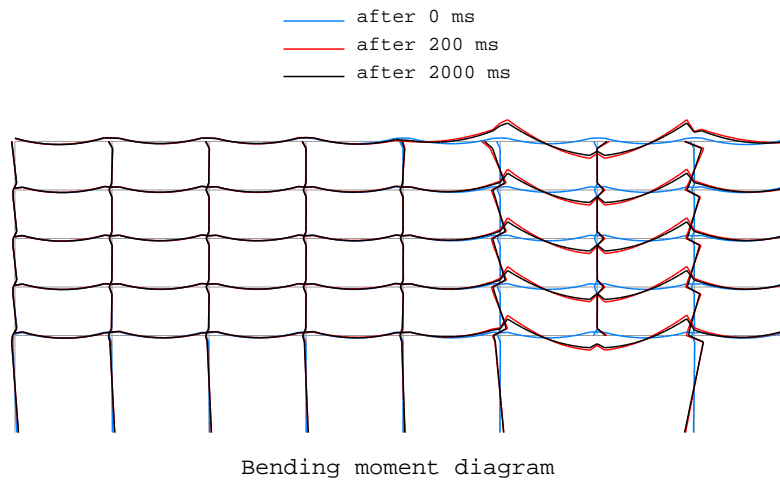


**Figure 5.27:** Evolution of  $M$  for an interior column removal.

at 200 ms and 2000 ms after the removal onset, due to the stabilisation of the structural loads.

Figure 5.28 compares the evolution of the strain rate of the upper and lower layers  $\dot{\epsilon}$  of section S3 during the rate dependent and rate independent computations for an exterior column removal. Note that the highest values in the rate independent case are due to the onset of structural degradation, contrarily to the rate dependent case, in which the highest rates are obtained at the transient phase and decrease with the time as the structure reaches a stable state.

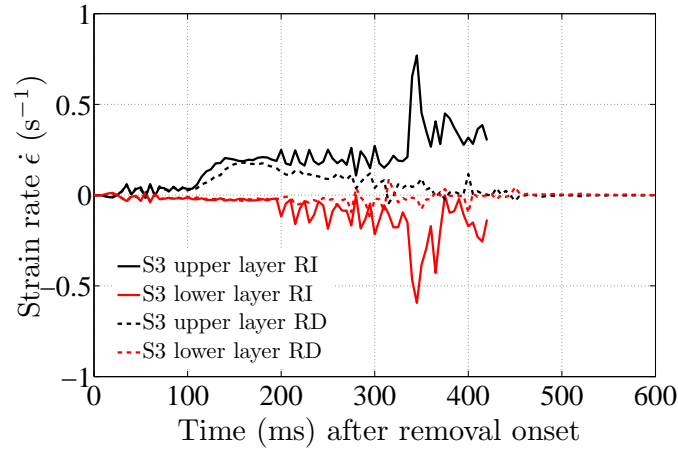


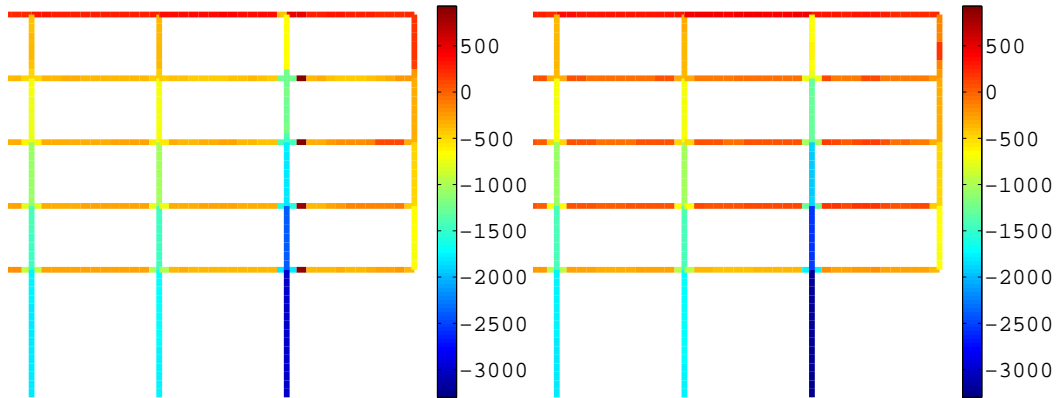
**Figure 5.28: REF:** evolution of the strain rate in the extreme layers of section S3.

The maximum axial force and bending moment obtained in all the elements of the structure along the computation are depicted in Figures 5.29 and 5.30 for an exterior column removal. The rate independent approach shows a localisation of the loads in the elements where failure occurs. In the rate dependent results, this localisation is lower since the total sectional failure does not occur: a load redistribution along the bay directly associated with the failing column is obtained. It can also be observed that the axial load is propagated leftwards through the horizontal beams in a more uniform way than in the rate independent case, where the axial load is strongly concentrated at the supports due to the sectional failure.

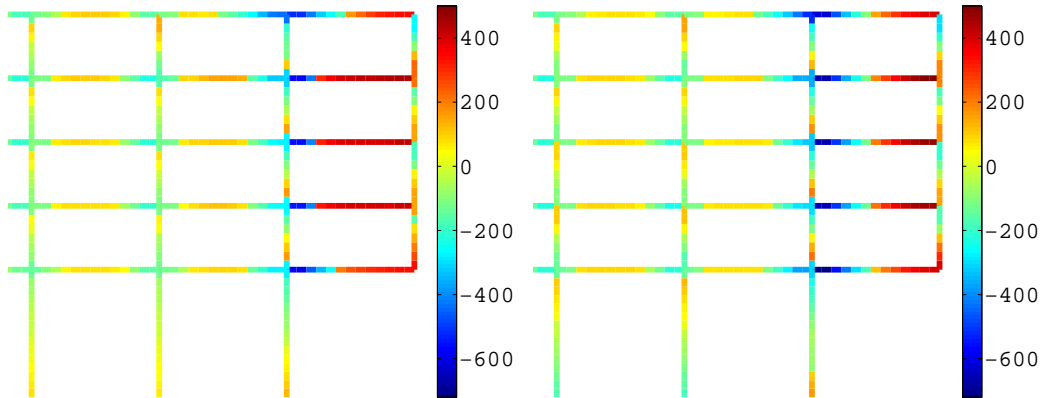
The rate dependent results obtained for the higher-rise structure analysed in the previous chapter are also provided. Figures 5.31 and 5.32 show the structural failure pattern for an exterior and interior column removal, respectively. The rate dependent response is compared to the previous rate independent results.

While in the rate independent computation the sudden column loss led to the entire collapse of the bays directly associated with the failing column (for both column locations), the material strength-enhancement provided by the strain rate effects result in an increased resistance to collapse.

The sectional strength degradation is almost identical in the rate independent and rate dependent simulations for an exterior column removal, while



(a) Rate independent approach (b) Rate dependent approach  
**Figure 5.29:** Maximum values of  $N$  (kN) obtained for an exterior removal.



(c) Rate independent approach (d) Rate dependent approach  
**Figure 5.30:** Maximum values of  $M$  (kNm) obtained for an exterior removal.

this difference becomes more considerable for an interior column removal. As in the previous frame, the sectional damage at the supports is extended over several elements (two in this case). Contrarily to the previous frame, the damage is not transmitted to the adjacent bays.

The evolution of the vertical displacement of the node at the connection with the removed column is depicted in Figure 5.33. Again, the difference between the level of displacement obtained for an exterior and for an interior column removal become evident. The obtained displacements are slightly larger than those obtained for the 5-storey structure, as expected.

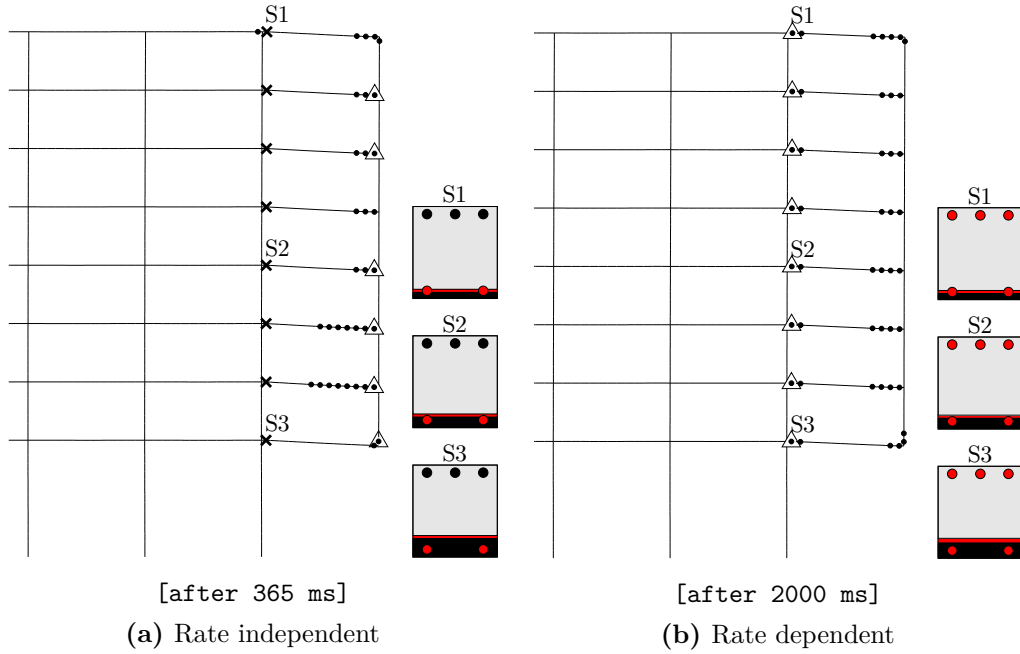


**Figure 5.31: REF: response of the 8-storey frame.**

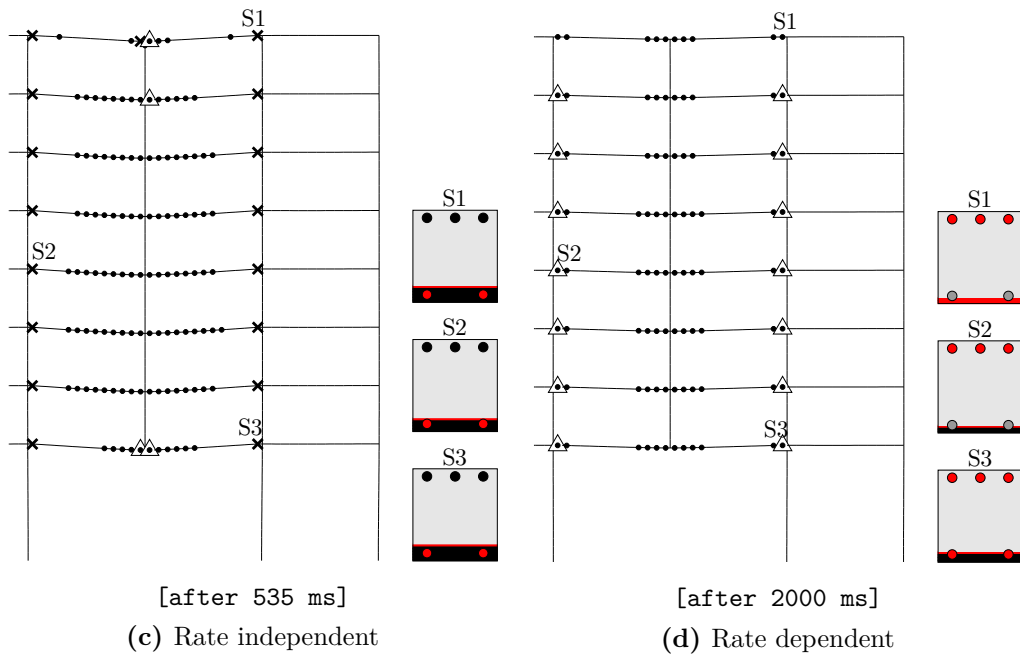


**Figure 5.32: REF: response of the 8-storey frame to an interior column removal.**

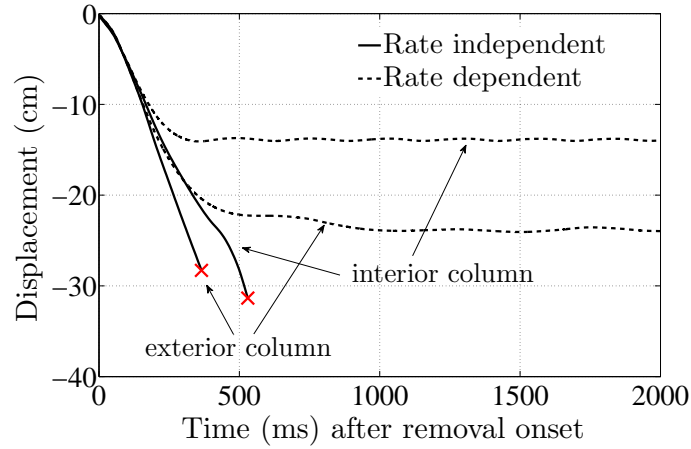


**Figure 5.33: REF:** rate dependent vertical displacement of the 8-storey frame.

### 5.6.2 Analysis of the individual contribution of the material features to the global rate effects

The material strain rate effects are observed to lead to an improvement of the structural response to progressive collapse. The objective now is to assess the individual contribution of each source of rate dependence to the rate-related structural strength enhancement. In the present work, the rate dependence is introduced at the material level by way of several parameters:

- A rate dependent Young's modulus in concrete  $E(\dot{\epsilon})$
- The viscoplastic parameters  $\eta$  and  $N$ , which introduce the rate dependence in the plastic domain of concrete and steel. Moreover, parameter  $\eta$  is here a rate dependent function:  $\eta(\dot{\epsilon})$ .

The reference case of study for an exterior column removal is conducted by considering the following individual sources of strain rate effects, where the corresponding test name is indicated in brackets for clarity:

- Rate dependence in the response of concrete in compression, both elastic and plastic domains (**RDconEP**).
- Rate dependence in the response of steel (**RDst**).
- Rate dependence in the response of steel and in the elastic domain of concrete in compression (**RDst+RDconE**).

- Rate dependence in the response of steel and in the plastic domain of concrete in compression (**RDst+RDconP**).

The final structural response for each of these combinations is depicted in Figure 5.34 for an exterior column removal. These results are gathered in Figure 5.35, in terms of vertical displacements as a function of the individual material contributions to the total strain rate effects. The results of the fully rate independent and fully rate dependent versions of the reference case of study are also shown.

The exclusive consideration of the rate effects in concrete in compression (**RDconEP**) yields a result quite similar to the rate independent case:

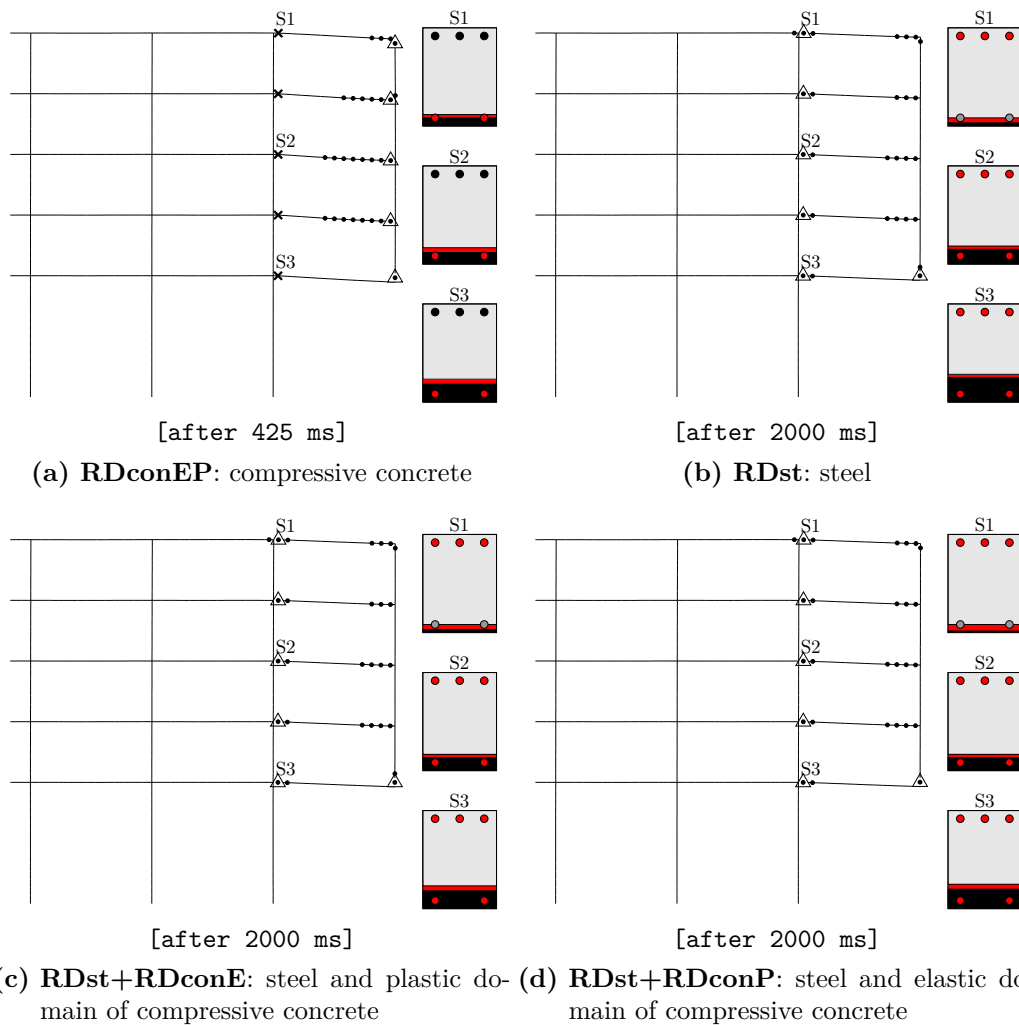


**Figure 5.34:** Individual material contributions to the global rate effects.

## 5.6 Rate dependent simulations of progressive collapse

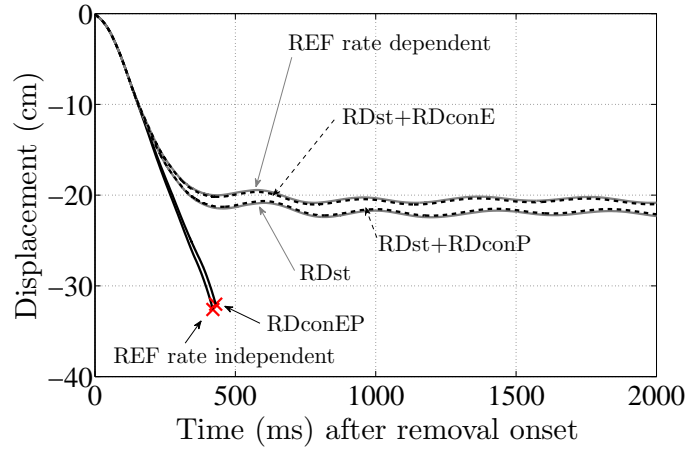


**Figure 5.35:** Vertical displacement history as a function of the individual material contributions to the global rate effects.

progressive collapse occurs in an identical way and approximately at the same time as in the rate independent computation. However, the mere consideration of the strain rate effects in steel (**RDst**) results in a structural enhancement which prevents collapse from happening. If the rate dependence in the plastic domain of compressive concrete is added to the rate effect in steel (**RDst+RDconP**), a negligible contribution to the structural enhancement is observed. For instance, both curves are practically coincident. On the contrary, the addition of the rate dependence in the Young's modulus of concrete (**RDst+RDconE**) has a more significant effect at the global scale: the corresponding curve is almost on top of the one obtained for a full consideration of the rate effects in steel and in compressive concrete.

From these results it can be deduced that the strain rate effects in steel play the major role in the structural response. The reasons for this phenomenon might be various. The major explanation would be the similar amount of steel reinforcement at both sides (tensile and compressive) for the sections considered here. This feature implies that the sectional response is mostly determined by the steel bars. A lower amount of compressive reinforcement would favour the exploitation of compressive concrete to counterbalance the axial load induced by the tensile bars. However, as it was concluded in previous chapter, a design including symmetrical reinforcement constitutes the most robust alternative to resist to a sudden column loss. The higher resistance and ductility of steel with respect to concrete could also account for this observation: the absolute gain in the dissipated energy (area under the stress-strain curve) due to the strain rate effects is much

higher in steel than in concrete.

### 5.6.3 Influence of the tensile strength of concrete

Since the tensile resistance of concrete was ignored in the previous rate dependent computations, the test is now repeated upon consideration of the tensile contribution, to assess the influence of the rate effects of concrete in tension. All the possible sources of material rate dependence are thus included. The results are shown in Figure 5.36, where also the rate independent response including the tensile strength (i.e. the test corresponding to material options **MO1** as named in Chapter 4) is depicted for sake of comparison.

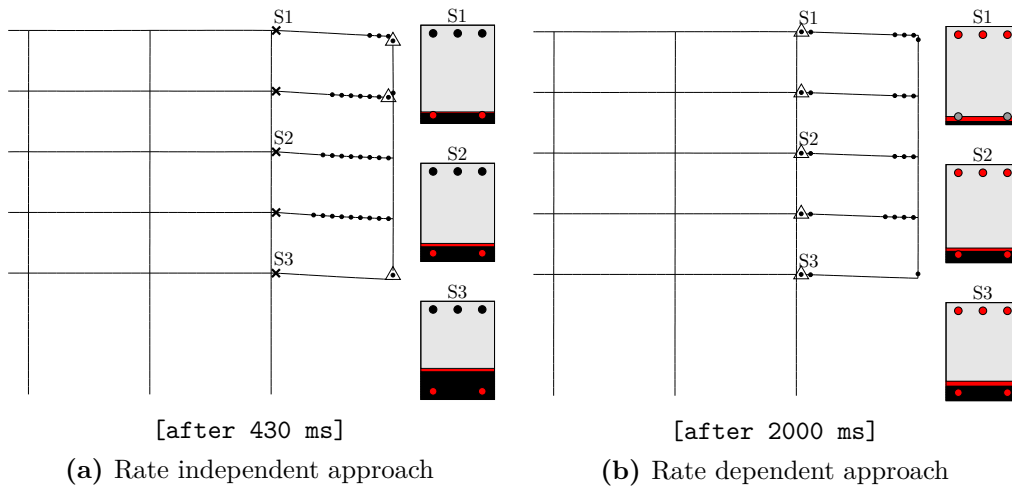


**Figure 5.36:** MO1: Response upon consideration of the tensile strength of concrete.

At a glance, both structural patterns are quite similar to those obtained without considering the tensile resistance of concrete (Figure 5.21). However, the corresponding vertical displacement curves shown in Figure 5.37 provide a more representative illustration of the contribution of the tensile response of concrete. It can be observed that, upon introduction of the strain rate effects, the difference between the consideration and non-consideration of the tensile resistance becomes more significant. The increase of the fracture energy with the strain rate might account for this phenomenon. In this particular case, and for the concrete type considered in this work, this effect does not make a strong difference in the structural failure scheme since collapse is avoided in the rate dependent case.

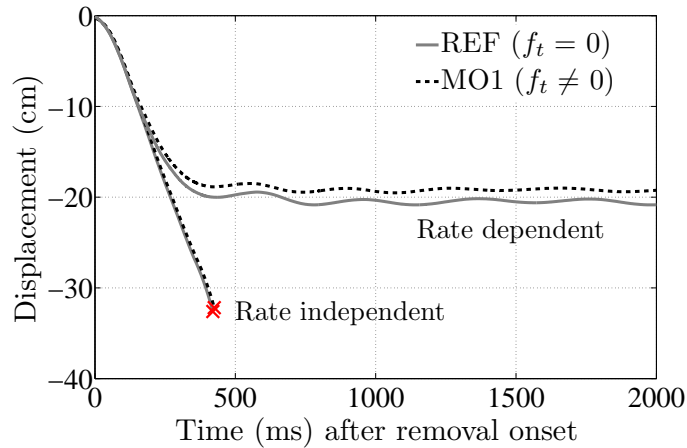


**Figure 5.37:** MO1: Vertical displacement history upon consideration of the tensile strength of concrete.

#### 5.6.4 Influence of the ultimate strain of concrete

The influence of the ultimate strain of compressive concrete (i.e. the crushing strain) was observed not to have a significant effect on the rate independent structural response. The result of the computation corresponding to the material options **MO2** (where the ultimate strain of concrete was  $\epsilon_{c,lim} = 0.5\%$ ) was the collapse of the bay directly associated with the removed column (see Figure 4.16), as it was also the case for the reference set of material parameters **REF**. The rate dependent version of the reference case of study has shown an increase of the structural resistance to progressive collapse. The strain rate effects in such computation have been observed to stem mainly from the rate dependence in the steel material, due to the higher ductility in steel among other possible reasons. In order to investigate the influence of the ductility in compressive concrete (in other words the ultimate strain) in the structural strain rate effects, a rate dependent version of the test carried out in the previous chapter for **MO2** is also studied. The corresponding results are shown in Figure 5.38, where the response is compared to the reference case **REF**.

Upon consideration of the the strain rate effects, the ductility of concrete appears to have a significant influence in the sectional response, as opposed to the rate independent approach. The absolute increase of the crushing energy (area under the compressive stress-strain curve) related to the rate effects is larger now that the ultimate strain takes a higher value, which allows for a better exploitation of compressive concrete. An increase of the red area



response in a negative manner, since it would result in a low ductility class, which is not recommended for plastic analysis according to the Eurocode 2 [51]. In the latter document, the recommended steel classes for plastic analyses are Classes B and C.

### 5.6.5 Influence of the reinforcement scheme

The rate effects in steel are observed to be determinant in the structural rate dependent response due to the highly symmetrical character of the RC sections adopted for the reference structure, which limits the participation of compressive concrete in the load balance. In the previous chapter, a less reinforced design complying with the design code requirements was also studied, which resulted in a less symmetric arrangement (design **RS1**). In this scheme only the bottom rebars were continuous along the beam span, while the top reinforcement at the midspan was much lower than in the supports (see Table 4.5). The results of the rate dependent computation corresponding to such an arrangement are shown in Figure 5.40 for an exterior column removal and in Figure 5.41 for an interior column removal.

Contrarily to the reference design, for which collapse is avoided when the rate dependence is introduced in the computation (regardless of the location of the removed column), in this less-reinforced design the strength enhancement provided by the rate effects appears to be insufficient to prevent collapse in the case of an exterior column removal. For an interior removal, the difference between the rate independent and rate dependent approaches is significant, however. It was observed that, in a rate independent approach, the lower amount of upper reinforcement was not capable of resisting the bending moment reversal that occurs in the midspan. In the present rate dependent case, the rate effects allow for this reversal to occur without further consequences. For instance, the degree of final structural damage seems lower here than for the reference design (Figure 5.21): crushing of concrete does not take place in this case as opposed to the reference result. The reason for this phenomenon would be the fact that the upper reinforcement ratio of the sections in the most advanced state of damage is much inferior now than in the reference design. The bending moment reversal observed in these elements inverts the role of the materials in the section: the upper rebars, which were designed to withstand a compressive load, are now subject to tension. Since the lower reinforcement is much superior to the one theoretically needed in the compressive zone, it prevents concrete from contributing to the moment equilibrium. The vertical displacement history for both column removals is depicted in Figure 5.42 and compared to the rate independent case.

## 5. Investigation of the Strain Rate Effects

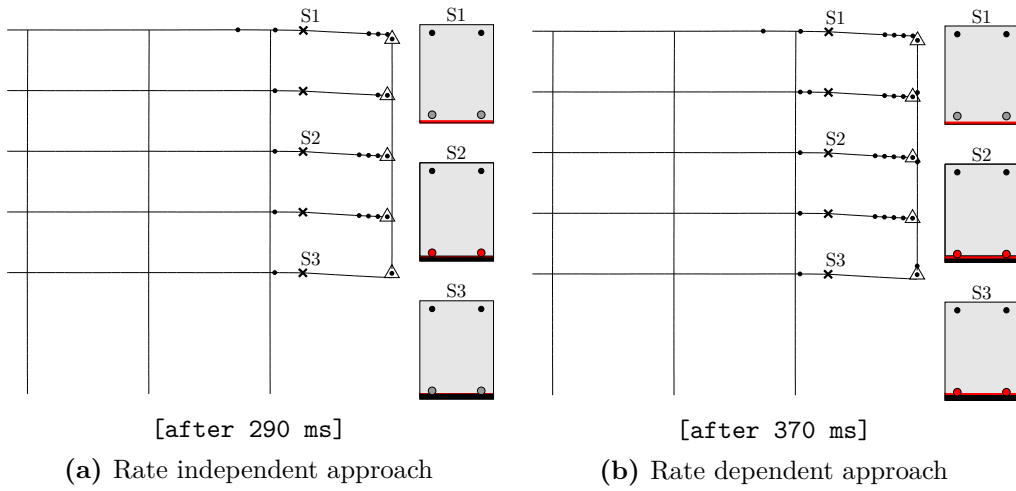


**Figure 5.40: RS1: response to an exterior column removal.**

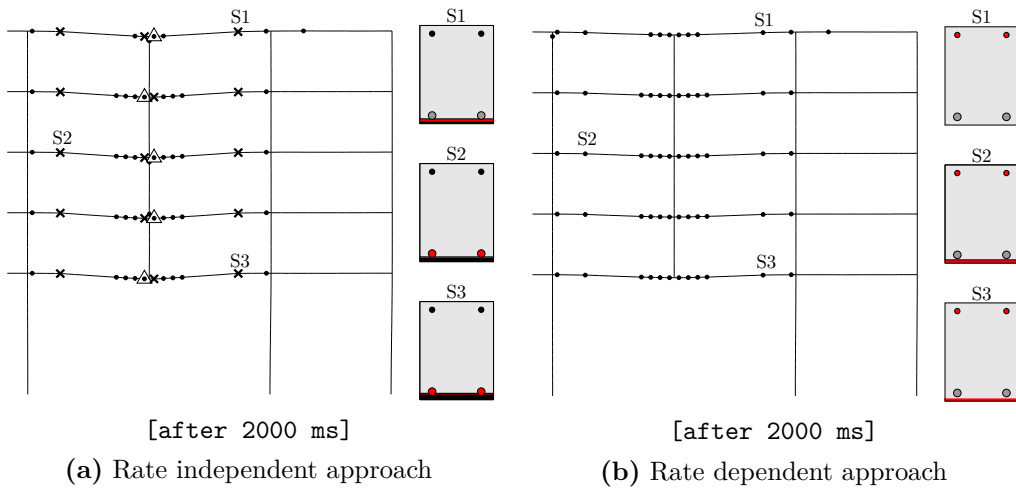


**Figure 5.41: RS1: response to an interior column removal.**

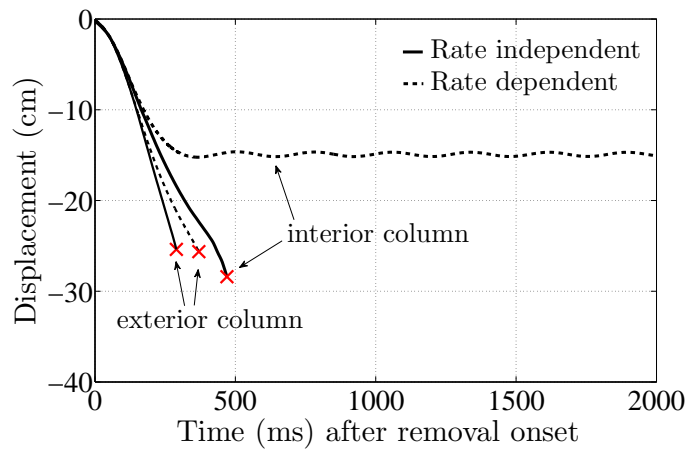


**Figure 5.42: RS1: Vertical displacement history.**

### 5.6.6 Influence of the column removal duration

In the previous chapter it was confirmed that the classically adopted rate independent approach leads to a more important structural failure evolution as the column removal time decreases, due to the increase of the inertial effects. The sudden column loss technique was then confirmed to provide an upper bound on the deformations obtained with respect to an approach where the duration of the triggering event is accounted for. In a rate dependent approach as adopted here, shorter column removal times give rise to higher strain rates as well, which implies that inertial effects and strain rate effects may act in opposite ‘directions’ and that the competition between them should be scrutinised: while the inertial effects favour the propagation of the failure in the structure, the strain rate effects limit the degree of localised failure due to their strength enhancing character. To determine whether the sudden column loss approach can also be considered as a suitable design tool when strain rate effects are involved, and with the aim of assessing the influence of the duration of the triggering event that causes local failure in the structural rate effects, the column loss simulation is conducted for longer removal times (**TED1** to **TED5**). Figures 5.43 to 5.45 depict the structural failure pattern for three removal times:  $t_r = 50$  ms, 250 ms and 300 ms. The rate independent results are also indicated.

For all the considered removal times, collapse is not observed to occur when the strain rate effects are incorporated. The degree of structural damage varies as a function of the removal time, as it was the case in the rate independent approach. However, the introduction of the rate effects compensates partially the inertial effects and makes the response less sensitive to a decrease of the removal time with respect to the rate independent computations, as observed in Figure 5.46: the distance between the vertical displacement curves as a function of the removal time is smaller than in the rate independent case. For instance, the same level of displacement is observed for  $t_r = 5$  ms (**REF**) and  $t_r = 50$  ms (**TED1**). This phenomenon is also observed for durations **TED4** and **TED5** ( $t_r = 300$  and 500 ms respectively): while the gap between the corresponding displacements is of approximately 10 cm in the rate independent computation, this difference is reduced to barely 3 cm in the rate dependent test (thus less than one third of the previous gap). The displacement observed in the rate dependent test for **TED3** ( $t_r = 250$  ms) equals the displacement obtained for a removal time of  $t_r = 500$  ms (**TED5**) in the rate independent case.

5. Investigation of the Strain Rate Effects

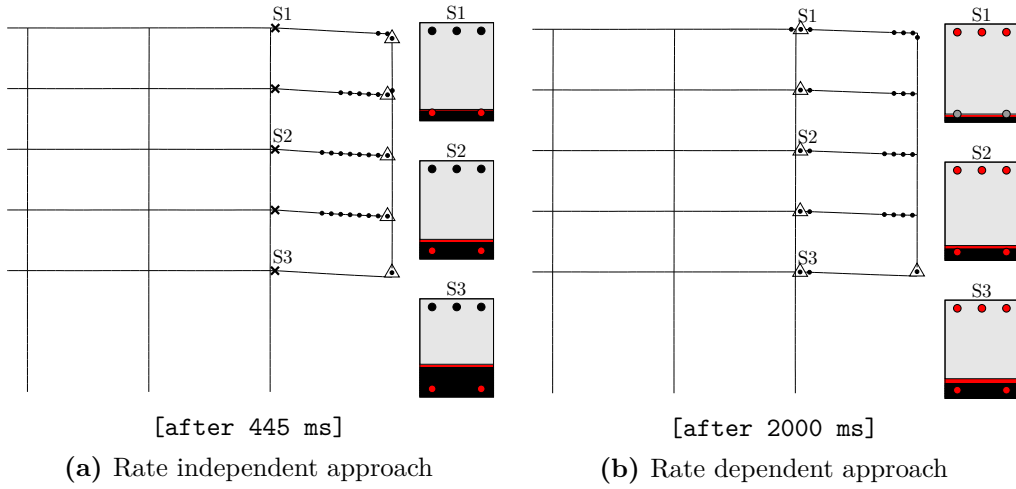


**Figure 5.43: TED1:** removal time  $t_r = 50$  ms.

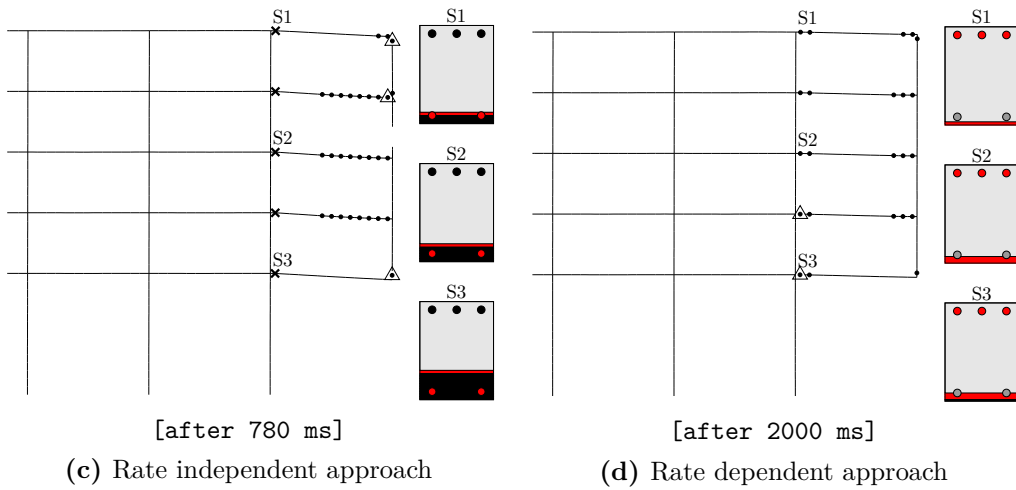


**Figure 5.44: TED3:** removal time  $t_r = 250$  ms.

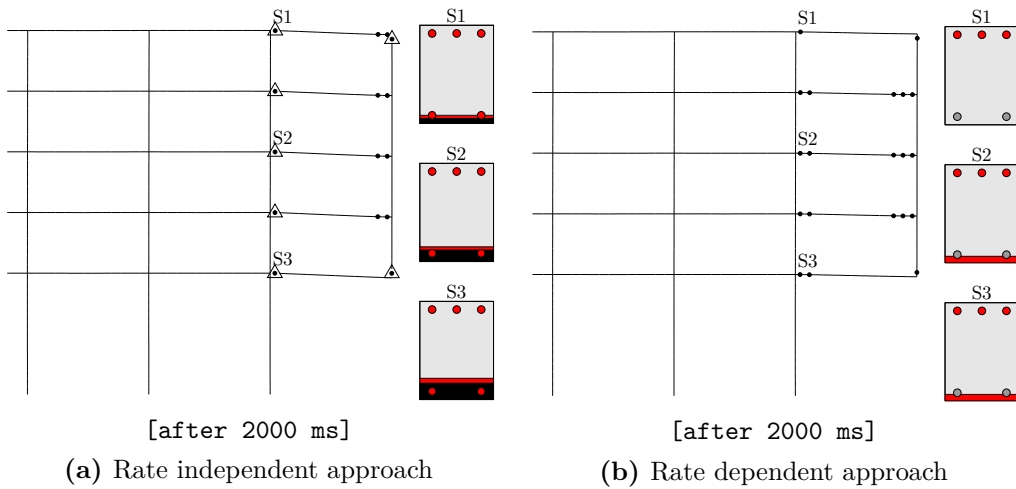


**Figure 5.45: TED4:** removal time  $t_r = 300$  ms.

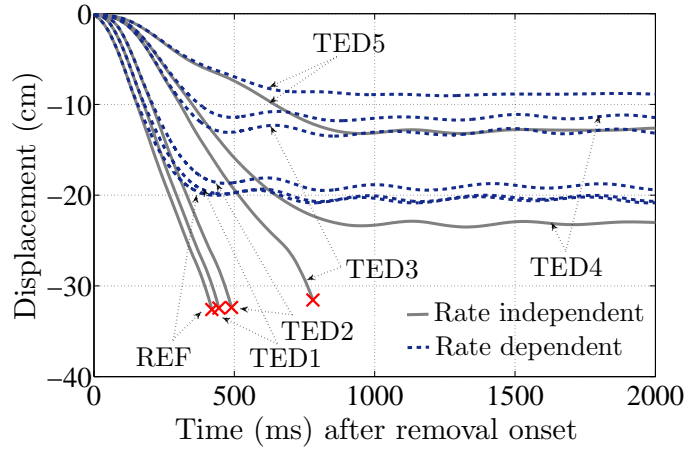


**Figure 5.46: TED:** Vertical displacement history as a function of the removal time.

In light of the previous results, it can be concluded that the material rate dependence should be taken into consideration in analyses where the strain rates are likely to be significant, as it is the case of blast loads or high velocity impact events. Finally, the results obtained confirm that the use of the sudden column loss idealisation (where an instantaneous removal of the column is assumed) to obtain an upper bound on the deformation demands [41] is also applicable to the rate dependent case, since the largest deformations are obtained for the lowest removal time.

### 5.6.7 Influence of the design code

The influence of the strategy (GSA vs DoD) adopted for the rate independent response to progressive collapse was investigated in the previous chapter. The DoD technique [15] was observed to provide with more conservative results than the GSA guidelines [1]. In this section, the load combination proposed by the DoD (thus 50% of the live loads) is applied, in order to generalise the conclusions drawn for the rate independent approach. The responses depicted in Figures 5.47 and 5.48 indicate that the same trend is obtained in the rate dependent case.

If an exterior column is removed, the collapse of the associated bay occurs 585 ms after the onset of the removal, as opposite to the result obtained for a load combination including 25% of the live loads, in which the structural integrity was maintained. For an interior removal, the collapse does not occur and the difference between the results of both techniques is less significant.

Although the pattern of structural damage is almost identical, the crushing of compressive concrete in the critical sections is more advanced in the computations including the DoD prescriptions (**REF-DoD**): the black zone corresponding to the layers having reached the ultimate strain is larger. The vertical displacements in Figure 5.49 indicate that the difference between both approaches is lower when the strain rate effects are involved. However, the DoD guidelines still produce significantly more conservative results than the GSA approach.

## 5.6 Rate dependent simulations of progressive collapse

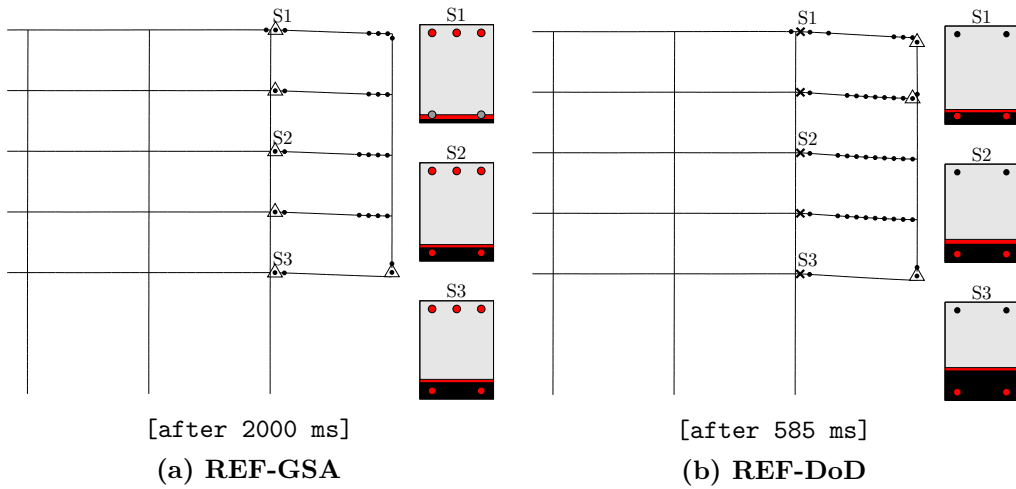


**Figure 5.47: DoD vs GSA: Rate dependent response for an exterior column removal.**

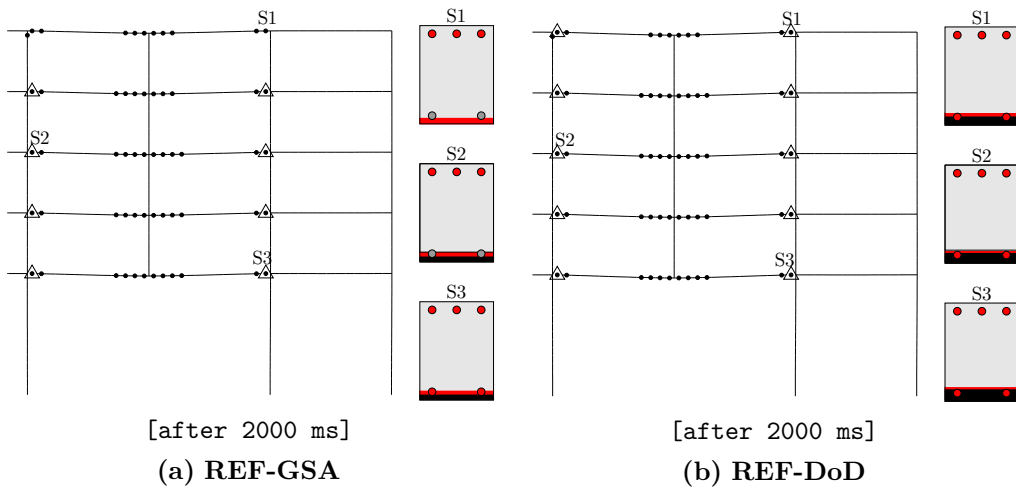


**Figure 5.48: DoD vs GSA: Rate dependent response for an interior column removal.**

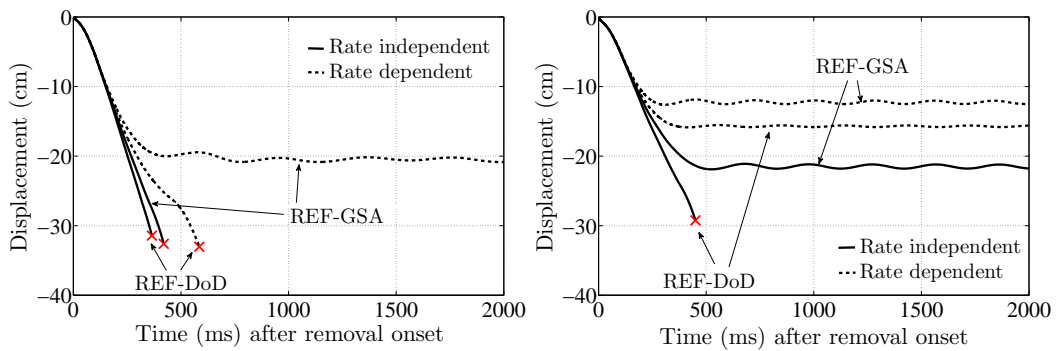


**Figure 5.49: DoD vs GSA: Vertical displacement history.**

## 5.7 Discussion

The strain rate effects in concrete and steel material behaviour, reported in the literature by means of experimental tests, are expected to have an influence in the progressive collapse response of RC structures, due to the high strain rates involved in such a phenomenon. The previous simulations show the structural response of a RC frame to a sudden column loss, where the strain rate effects are incorporated in the constitutive equations for concrete and steel. The influence of various parameters and/or modelling features in the rate dependent response is also analysed. In general, the strength-enhancing nature of the rate effects results in an increased resistance to progressive collapse in most of the studied cases, with respect to the rate independent computations in the previous chapter. Similar observations are made for the 5-storey and 8-storey frames. However, the results obtained here would suggest that the introduction of the rate dependence implies a modification in the load redistribution following the loss of a bearing member. The local strength increase related to the rate effects might lead to a further expansion of the alternate load path across the remaining structure in order to seek an equilibrium state. This effect was expected, since material laws including viscous terms are used in the literature as localisation limiters, so that localisation is reached on a physically based size.

In particular, the strain rate effects in steel appear to play the major role in the structural response, for the set of material parameters and reinforcement schemes employed in the present study. The similar amount of steel reinforcement at both sides (tensile and compressive) for the sections considered here could account for this phenomenon. This feature limits the contribution of concrete to the axial load and moment equilibrium in the section, which is mostly satisfied by the steel bars. Steel determines thus the sectional performance. Regarding the individual contribution of compressive concrete to the global rate effects, the rate dependence would stem mostly from the rate effects in the elastic domain (i.e. the rate dependent Young's modulus), rather than from the plastic region (thus the viscoplastic terms). The rate-related 'stiffening' in concrete has as effect a decrease of the displacements in the structure.

The contribution of tensile concrete is also assessed in the rate dependent response. It is observed that the difference between the consideration and non-consideration of the tensile resistance becomes more significant when strain rate effects are included. While this effect was negligible in a rate independent approach, it might not be the case in the rate dependent one.

This might be due to the increase of fracture energy involved in the rate dependent approach.

The influence of the ultimate strain of concrete in compression has been also observed to become more relevant when the strain rate effects are considered. The additional increase in the area under the stress-strain curve due to the rate effects results in a better exploitation of the concrete part of the RC sections. A high ductility concrete is thus recommended for a collapse resisting design.

Although the influence of the strain rate effects in concrete appear to be minor with respect to steel, their consideration can be recommended in a general fashion. It is important to note that the present work is focused on a standard type of concrete (C30). The modelling of the strain rate effects for other concrete types (for example high strength concrete or fiber-reinforced concrete) might yield to different conclusions. Such a modelling would require: 1) to obtain the DIFs corresponding to the new type of concrete considered (based on experimental tests) and 2) the complex parametric identifications shown in Section 5.3.1. Note that the values of the model parameters used in this work are exclusively valid for a C30 concrete type.

As far as the reinforcement arrangement is concerned, the design scheme **RS1** studied in the previous chapter has also been tested with the aim of investigating whether a lower steel-to-concrete ratio allows for a better exploitation of the strain rate effects in the concrete part of the section, or whether, adversely, the strain rate effects in steel are insufficient for providing an improvement of the structural response. This less reinforced configuration has resulted in progressive collapse in the case of an exterior column removal. For an interior removal, the rate effects allow for the bending reversal to occur without further consequences. Although a slight gain of resistance is observed, it can be confirmed in a general manner that a discontinuous arrangement is less prone to accommodating the double span condition, and therefore should be avoided in the context of collapse resistant design of structures.

The influence of the column removal time was studied, in order to account for the nature of the collapse-triggering event in the rate dependent response. The sudden column loss technique is often adopted in the related literature since it a priori provides the worst case scenario, in which maximum deformations are obtained. This conclusion being confirmed in the rate independent case, the aim was now to generalise it to the rate dependent simulations, in

which the increase of the loading rate (in this case shorter removal times) might be expected to have a positive influence in the structural strength due to the enhancement provided at the material level by the strain rate effects. The degree of structural damage is observed to vary as a function of the removal time, as it was the case in the rate independent approach. However, the introduction of the rate effects compensates partially the inertial effects and makes the response less sensitive to a decrease of the removal time with respect to the rate independent computations. The difference between the results obtained for different removal times is less significant. Nevertheless, these results confirm that the use of the sudden column loss idealisation (where an instantaneous removal of the column is assumed) to obtain an upper bound on the deformation demands [41] is also applicable to the rate dependent case.

Concerning the strategy adopted for the verification of the structural integrity, the DoD technique is also confirmed to produce significantly more conservative results than the GSA approach, as expected. Nevertheless, the GSA technique appears to be the most often employed in the literature [21, 22, 24, 28, 29, 32, 33, 35, 36].

The adopted modelling strategy, based on a multilayered beam model, allows a natural incorporation of the strain rate effects from the material level to the structural scale. The flexibility of the present formulation is again demonstrated, as opposed to the simplified closed-form approaches, where accounting for the strain rate effects in the relationships between generalised stresses and strains, as well as in bending moment–axial load interactions would be non-trivial.

Although the validity of the previous observations is linked to the modelling options considered here and therefore limited to the two-dimensional representation of RC structures, the strain rate effects observed with the present approach are supposed to remain general. The rate dependent structural effects, which stem from physically-based material laws, are expected to get reproduced in more complete approaches, with additional modelling features such as 3D representation, consideration of shear failure, cyclic modelling of the concrete and steel response or topological removal of the failing elements.



## 6

# Concluding Remarks and Recommendations

This chapter summarises the challenges of the modelling of RC structures for progressive collapse simulations and presents the main contributions of the present thesis. An overview of the results obtained from the tests conducted for different modelling and design parameters are given. Practical recommendations for the design and/or modelling against progressive collapse are extracted. Finally, future prospects for improving the adopted modelling strategy are proposed.

### 6.1 Challenges of the research

Progressive collapse is a phenomenon characterised by a disproportionate structural damage, typically originated by the local failure of a primary structural component. This subject has dragged the attention of the civil engineering research community after the disastrous consequences of well-know progressive collapse scenarios occurred in the last decades. Most of the general building codes have included since guidelines for the evaluation of the potential for progressive collapse, which are based on simplified analysis approaches or merely provide ‘good practice rules’ for the progressive collapse resistant design of structures. The present research work aimed at contributing to the detailed computational modelling of reinforced concrete frames in the framework of progressive collapse simulations. Among the different general approaches to the progressive collapse verification of structures, the ALP was adopted in the present work: the ability of the structure to find an alternate load path in order to redistribute loads among the remaining elements is studied.

The main challenge of the present study was reported in Chapter 2. It lies in a more realistic characterisation of the response of RC members for large-scale structural computations purposes. The complexity of such a task stems from the heterogeneous nature of the beams cross-sections, which are composed of two materials (i.e. concrete and steel) with different constitutive material behaviour. Besides, strain localisation issues may be obtained at the structural level due to the softening nature of the sectional response. A proper representation of the characteristic length where the deformation is localised is essential for a realistic modelling of the structural failure, as a correct estimation of the dissipated energy is required. Furthermore, an additional complexity arises from the computational modelling of the material response of concrete. This material presents multiple peculiarities that need to be taken into account for a proper constitutive modelling: different response in tension and compression, discrete failure in tension, confining effect of the transversal reinforcement, characterisation of the strain rate effects, etc. Regarding the latter feature, a physically-based modelling of the strain rate effects for progressive collapse analysis purposes has not yet been dealt with in the literature. However, these effects may be expected to play an important role in the load redistributions. Concerning the steel reinforcements, a correct modelling of their response is also required. With this respect, a realistic representation of its ductility is of major importance to reproduce the actual rotational capacity of the RC sections.

## 6.2 Main contributions

The overall response of a RC member is therefore directly determined by the aforementioned material properties of the constituents, in both the elastic and plastic range, as well as the design options, such as the amount and position of the steel reinforcing bars. The multilevel approach developed here allows dealing with the present complexity: a multilayered beam formulation is adopted, where the structural members are discretised through a finite number of layers for which one-dimensional constitutive relations are described. The response at the structural scale is systematically derived from the response at the constituents level, contrarily to the alternative closed-form approaches where the assumption of (strongly simplified) analytical relationships between generalised stresses and strains at the sectional level is based on an off-line identification of such generalised constitutive laws, as a function of the modelling and/or design parameters. In the present multilevel strategy, the related identification problem is not necessary, since it directly accounts for any variation of the design and/or material parameters. Fur-

thermore, it allows considering the strain rate effects at the structural level whenever a rate dependent material approach is adopted. Additionally, a progressive sectional strength degradation can be obtained as a consequence of the progressive failure of the constitutive layers, resulting in complex nonlinear sectional responses exhibiting softening even for simplified 1D constitutive laws for the constituents. Conversely, all these advantages are naturally counterbalanced by the higher computational cost involved in a multiscale approach. Nevertheless, this computational effort is justified by the gain in flexibility with respect to closed-form solutions.

### 6.2.1 Rate independent non-linear constitutive models

Chapter 3 presented the non-linear constitutive models adopted for the rate independent material characterisation of concrete and steel, as well as the numerical algorithm used for the integration of such equations. The parametric identification was made based on the prescriptions of the International Federation for Structural Concrete and Eurocode 2. Bilinear stress-strain models are proposed for concrete in compression and steel in which failure criteria are established in terms of ultimate strains, so that the stress level drops down to zero after these values are reached. Standard types are chosen for the materials (C30 concrete and S500 steel bars). The ductility of the steel bars would correspond to class B described in Eurocode 2. The cyclic nature of the steel response was not characterised in the present work. The introduction of this feature would provide a better estimation of the sectional response under the unloading phases related to the bending reversals and the gradual sectional failure. In tension, the brittle behaviour of concrete is modelled via a softening evolution law. The fracture energy involved in the cracking process is obtained by multiplying the area under the stress–plastic strain curve by the characteristic length. A realistic value for this parameter was considered for the type of concrete studied here. A research on the different empirically-based expressions for the estimation of the characteristic length of RC concrete was carried out.

### 6.2.2 Multilayered beam approach

The description of the multilayered beam approach was given in Chapter 3. The performance of the proposed methodology was illustrated by means of a bending test on a RC section, which showed the interactions between axial load and bending moment for a monotonic loading sequence. A design variable was also tested (amount of bottom reinforcement) in order to highlight the multiple interdependences that play a role in the sectional response. Note

that such interactions become much more complex in a progressive collapse scenario, on account of the oscillatory character of the evolution of  $N$  and  $M$  in the sections, as observed from the numerical computations in Chapter 4. It should be emphasized again that a closed-form formulation would on no account be able to include such multiple and time-dependent interactions in a progressive collapse simulation. The adequacy of the present formulation was illustrated by an experimental comparison. The reasonable agreement obtained confirms that realistic cross-sectional behaviours can be reproduced even for one-dimensional constitutive laws.

### 6.2.3 Numerical simulations

The algorithm for the time integration of the structural equations in dynamics was also presented, based on Newmark's formulation. In Chapter 4, the sudden column loss methodology was applied for the progressive collapse verification of a RC frame designed according to the Eurocode 2 prescriptions, in terms of minimum reinforcement amounts for regular design. This event-independent technique consists in the instantaneous removal of a load-bearing element in the studied structure. The objective of such technique is to simulate the initial localised damage resulting from an abnormal loading event and which could potentially give rise to progressive collapse. It constitutes a useful tool for the assessment of the structural robustness and is often used in the context of ALP approaches. A reference case of study was presented and additional tests were conducted for variations of the main design and material parameters that govern the structural response, to assess their effects on the progressive collapse response analysis. All the studied parameters were varied in a realistic range of values.

### 6.2.4 Investigation of the strain rate effects

Strain rate effects may be expected to have an influence in the progressive collapse response of RC structures, due to the high strain rates involved in this phenomenon. However, the investigation of their influence on a progressive collapse analysis has not yet been analysed in the related literature. Moreover, such effects are seldom included in progressive collapse analyses. Chapter 5 described the effects of the strain rate on the material response of concrete and steel. A strain rate dependent material formulation has been developed for the constituents, where the rate dependence is introduced in the elastic and plastic domains of the material response. The corresponding constitutive equations were provided, based on the DIF (dynamic increase factors) reported in the literature, issued from experimental tests. In order

to reproduce such rate-related enhancement at the material level, the parameters of the proposed elasto-viscoplastic model had to be adjusted. This adjustment implied the introduction of rate-dependent terms in the expressions of such parameters. Furthermore, the viscoplastic parameter for tensile concrete had to be made a vanishing function of the cumulated plastic strain, so that the rate dependent increase of the fracture energy would take realistic values. The latter non-trivial modelling features, to the best knowledge of the author, constitute an originality of the present formulation. The adopted multilayered strategy allows for a natural incorporation of the strain rate effects from the material level to the structural scale in a physically-based manner, contrarily to the phenomenological approaches currently found in the literature, in which the rate dependence is introduced by multiplying the material strength by the corresponding increase factors, as a function of the strain rate. In such approaches, the rate effects in the elastic behaviour are not taken into account. Rate dependent bending moment–curvature relationships for a particular RC section were obtained, considering two types of reinforcement schemes, to illustrate their effects at the sectional level. Once again, the advantages of the multilevel approach in comparison to closed-form formulations is pointed out: the (non-trivial) off-line identification of such rate dependent interactions would be required in such analytical approaches. Strain rate dependent simulations of the sudden column loss were conducted and, as in the previous rate independent analysis, the influence of various parameters and/or modelling features in the structural response was assessed.

### **6.3 Overview of the results**

The observations made from the tests conducted for varying modelling and design parameters are summarised next.

#### **6.3.1 Influence of the material parameters**

##### **Tensile strength of concrete**

The consideration and the non-consideration of the tensile strength of concrete yielded almost identical results in the rate independent case. The differences become more significant in the rate dependent case, which is probably due to the increase of the fracture energy induced by the rate effects.

### **Ultimate strain of concrete**

An increase of the ultimate strain in concrete appeared to scarcely have any influence on the results. This influence has been also observed to become more relevant when the strain rate effects are considered. The additional increase in the area under the stress-strain curve (i.e. the crushing energy) due to the rate effects results in a better exploitation of the concrete part of the RC sections.

### **Ultimate strain of steel**

The increase of the ultimate strain of steel was responsible for a slight structural enhancement in the rate independent study. Nevertheless, the large displacements obtained for a high value of this parameter suggest that a geometrically non-linear formulation would be a more appropriate computational tool. Upon consideration of the strain rate effects, the displacement are considerably reduced. Furthermore, the study of the present parameter was not required in the rate dependent case, since the failure of the steel bars did not occur in any element of the reference structure.

### **6.3.2 Influence of the reinforcement scheme**

In order to test the influence of the reinforcement scheme on the progressive collapse resistance, various reinforcement arrangements were analysed. Since the GSA prescriptive guidelines recommend the use of continuous steel reinforcement for the accommodation of the bending reversal and double-span condition that follow the loss of a supporting member, different levels of reinforcement continuity were tested. A design strictly complying with the regular building code requirements (with no specific provisions for abnormal loading events) showed a strong sensitivity to progressive collapse. Furthermore, the partially and fully continuous reinforcement patterns analysed also resulted in collapse for most of the configurations. On the contrary, fully continuous and symmetrical reinforcement schemes were observed to provide with the required robust design: the same amount of top and bottom reinforcement allowed the structure to resist the bending moment reversal occurring at the connection with the removed column and the strong increase of the bending moment at the adjacent supports.

### **6.3.3 Influence of the simulation options**

#### **Column location**

The progressive collapse scenario was also observed to affect the structural response: the removal of an interior column led in general to lower degrees of structural damage with respect to an exterior column removal, due to the support provided by the neighboring elements at both sides. The catenary effects, which were not considered in the present work since a geometrically linear formulation was adopted, would be expected to contribute to this phenomenon, acting as ‘tie forces’ that allow the transfer of loads from the damaged portion of the structure to the undamaged portion [15].

#### **Column removal time**

As far as the ‘sudden column loss’ strategy is concerned, which considers an instantaneous removal of the failing element, the degree of adequacy of such an approach was assessed in this work. This threat-independent methodology widely used for the vulnerability assessment of structures is assumed to give an upper bound on the deformations obtained with respect to an event-dependent approach. To corroborate the latter statement, the column removal time was increased to account for the actual duration of the abnormal loading event that results in a full column removal (extension to take into account in a simplified manner the nature of the triggering event). The removal time was observed to be determinant in the structural response. Since the inertial effects involved in the dynamic response are lower for longer removal times, the degree of structural damage and the displacements observed are significantly reduced in the rate independent case. In the rate dependent study, the degree of structural damage also decreased with longer removal times. However, the introduction of the rate effects was observed to compensate partially the inertial effects: the response seems less sensitive to a decrease of the removal time with respect to the rate independent computations. The difference between the results obtained for different removal times was lower. Nevertheless, these results confirm that the use of the sudden column loss idealisation to obtain an upper bound on the deformation demands is valid for both the rate independent and rate dependent approaches.

#### **Load combination**

The load combination adopted for the simulation of the sudden column loss has a significant effect on the results: the DoD procedure, which considers 50% of the live loads, might expectedly lead to conservative designs with

respect to the GSA guidelines, which suggests to include only 25% of the live loads in the computations. The same observations were made for both approaches (rate dependent and rate independent).

### 6.3.4 Influence of the strain rate effects

It was observed that the strength-enhancing nature of the rate effects resulted in a structural robustness improvement with respect to the rate independent computations, for the studied two-dimensional frames. On the other hand, the introduction of viscous terms in the constitutive relations resulted in a delocalisation of the structural damage. The local strength increase caused by the rate effects would allow for a further expansion of the loads in the residual structure. The strain rate effects might act as a double-edged sword: while they provide an enhanced material response, they could lead to a spread of the structural damage. Nevertheless, from the viewpoint of the integrity of the studied structures, they were found to have a positive effect on the structural resistance for the structures studied here.

The individual contribution of each possible source of rate dependence was analysed. The strain rate effects in steel appeared to play the major role in the structural response. This phenomenon is due to the similar amount of top and bottom reinforcement in the sections considered here. This feature limits the contribution of concrete to the axial load and moment equilibrium in the section, which is mostly satisfied by the steel bars. Regarding the individual contribution of compressive concrete to the global rate effects, the rate effects in the elastic domain would play a major role with the respect to those stemming from the viscoplastic terms. The stiffening nature of the rate effects reduced the magnitude of the displacements in the structure.

The influence of the material parameters in the structural response was observed to increase when the strain rate effects are considered. It is the case of the tensile strength of concrete and the ductility of compressive concrete and steel. The increase of such parameters was ‘amplified’ by the enhancing nature of the rate effects. Other parameters (here in particular the removal time), appear to affect the structural response in a lesser degree upon consideration of the strain rate effects. Under variations of the removal time, as previously explained, the strain rate effects and the inertial effects act in opposite directions. The competition between them resulted in a lower influence of the column removal time in the observed response.

## 6.4 General recommendations

In light of the results obtained in the present research work, the following set of practical recommendations for progressive collapse simulations and/or design can be derived:

### 6.4.1 Material properties

Materials with high ductility are recommended for a collapse resisting design. As for seismic design, it is important that a structure can reach a given level of deformation before failure occurs. More particularly, a ductile reinforcing steel is essential to fulfill such a requirement: classes B or C according to the Eurocode 2 prescriptions are thus required.

The ductility of concrete was observed to have only a slight influence in the results. However, it should be emphasized that the present work is focused on a standard type of concrete (C30) and on a particular range of reinforcement ratios. The modelling of the behaviour (including the strain rate effects) of other concrete types with higher strength and/or ductility properties could yield different effects. To this regard, the use of other concrete types with enhanced properties (such as fiber-reinforced concrete [96]) might improve the global response of the beams. In particular, the use of high resistance concrete might have a positive effect on the structural robustness, due to the higher Young's modulus of such enhanced concrete types. It must be however emphasized that the modelling of the strain rate effects for other concrete types would require, on the one hand, to obtain the corresponding DIFs and, on the other hand, a subsequent complex parametric identification to adjust the constitutive model to those DIFs (as seen in Section 5.3.1).

The effect of the consideration of the tensile contribution of concrete to the sectional strength is negligible when the strain rate effects are not taken into account and it becomes more relevant in a rate dependent approach due to the increase of the fracture energy. For conventional concrete types, the tensile contribution of concrete could be ignored in the context of rate independent analyses, since the observed effect might not compensate the modelling and computational effort. On the contrary, the use of higher strength concrete types would most probably result in an amplification of the contribution of tensile concrete to the sectional response.

### 6.4.2 Reinforcement scheme

A minimum level of continuity must be provided in both the upper and lower reinforcement. Nevertheless, this requirement does not guarantee a collapse resisting design. In order to ensure the ability of the structure to withstand the bending reversals, the same amount of upper and lower reinforcement would be desirable. Therefore, a conventional reinforcement scheme might not provide the robustness required for the accommodation of the double-span condition that follows the loss of a supporting element. However, it was observed that for discontinuous reinforcement schemes the collapse region is limited by the location of the strongest discontinuity. The sectional failure is so abrupt that the loads are not transferred to the neighbouring elements (Figures 4.23 and 4.24).

### 6.4.3 Load combination

No particular directions can be given with respect to this point. The choice of the load combination to be applied in a progressive collapse simulation will definitely have an influence on the degree of conservatism of the resulting design. Since the DoD guidelines prescribe 50% of the live loads (i.e. variable loads) to be applied to the structure for the simulation, the level of damage obtained using this strategy is higher than the one resulting from an application of the GSA prescriptions, which includes 25% of the live loads. Although the GSA load combination is the most often found in the current collapse-related literature, it should be borne in mind that the DoD prescriptions are most likely to provide with more robust designs.

### 6.4.4 Modelling of the triggering event

The sudden column loss technique is a useful simplified tool for the verification of the structural integrity. Its application is thus recommended since it provides the worst-case scenario with respect to threat-dependent approaches where the column removal time is related to the nature of the abnormal loading event that results in a full column removal. Of course, a detailed characterisation of the triggering event would offer the most accurate and realistic solution, if the response of the structure to a very specific loading scenario was the objective of the simulation. Nevertheless, the computational time required for such a detailed approach would be prohibitive, due to the small step size needed for a thorough simulation of a short-time duration event (such as blast loading). The choice of the sudden column loss technique rises from the impossibility of rationally examining all potential sources of collapse initiation. The main purpose is to analyse the progressive spread of

damage after localised failure has occurred in order to mitigate the potential for progressive collapse, not necessarily to prevent collapse initiation from a specific cause [1]. It is hence considered to offer a reasonable balance between the usefulness of the results and the computational effort.

### 6.4.5 Strain rate effects

The strain rate effects should be taken into account in a progressive collapse analysis and/or design, since they are responsible not only for a local strength enhancement but also for a delocalisation of the structural damage, which could bring to an extension of the collapse region. Although the influence of the strain rate effects in concrete appear to be minor with respect to steel, their consideration can be recommended in a general fashion, since the observations made here cannot be generalised for other types of concrete and/or reinforcement configurations. To test the influence of the strain rate effects for other concrete types, the corresponding DIFs would need to be characterised and, based on such rate dependent expressions, a subsequent parametric identification would need to be conducted (as in Section 5.3.1) for the model to reproduce correctly such strain rate effects.

### 6.4.6 Other numerical aspects

The confining effect of the stirrups in compressive concrete is an optional simulation feature. In the present work, the stirrups were not explicitly modelled. This simplification was justified by the fact that the sensitivity of the response to an increase of the ultimate strain of concrete was not significant. In general, this effect may be considered negligible for beams under bending, as observed in the present work.

A three-dimensional representation of the RC structures is recommended. Note that the single column removal in a two-dimensional representation would correspond to removing a whole row of columns in 3D since the transversal resistance is not taken into account. This simplified approach might thus lead to conservative results. Moreover, torsional effects are not considered in a 2D formulation.

## 6.5 Future prospects

On account of the complexity of the present multilevel problem, a number of simplifying assumptions had to be adopted in the modelling strategy. Further developments could be of interest in order to enhance the possibilities of the

current approach.

From the point of view of the **material modelling**, various aspects have not been considered for the sake of simplicity and because the detailed modelling of the material response was not the main objective of the present work. A balance had to be struck between the modelling effort and the performance of the model for the study purposes. For example, a damage evolution law for the stiffness degradation in concrete as a function of the cumulated plastic strain would certainly provide a better approximation in the unloading phases. It would also allow for reducing the spurious high frequency vibrations in the structural response that increase the computational effort. Additionally, the incorporation of the cyclic response in steel and concrete would also allow for a more realistic representation of the material behaviour in loading reversals. Finally, the modelling of the bond-slip effects between the steel bars and the concrete matrix, to account for the loss of adherence between them, should also be a target of future investigations.

Concerning the **structural representation** aspects, a planar representation of the structure has been employed as an initial approach to the problem. The extension to a three-dimensional approach seems to be the logical next step in order to obtain a more realistic structural response, as previously mentioned. However, this extension is non-trivial both from the computational cost viewpoint, and from the perspective of structural complexities (representation of torsional effects, stiffening effects of the floors, etc.).

The **geometrically linear formulation** adopted here is partially justified by the small-range displacements obtained in most of the computations. Nevertheless, it was observed that for certain cases in which a higher ductility was considered in the material response, the displacements involved in the progressive collapse process were considerable (material option MO4 in Section 4.3.2). This assumption might be also in contradiction with the fact that, as mentioned in the present dissertation, the rotational ductility is considered as a very important structural feature to ensure a robust design, since it allows for a further load redistribution and a gradual structural degradation [49]. Hence, the adoption of a geometrically non-linear formulation should be investigated since, additionally, it would allow for a consideration of the catenary effects, which are considered an essential characteristic to be fulfilled by the residual structure according to the DoD and the British code guidelines [15]. In [39] it was demonstrated numerically that the catenary effects in a RC structure subject to a sudden column loss resulted in an increasing resistance of the beams.

The **shear reinforcement** has not been explicitly modelled. An implicit, phenomenological way of taking them into account was considered by increasing the concrete ultimate strain. The results however showed no significant differences in the structural response. Nevertheless, further investigations on the way of introducing this feature in the simulations should be done.

The Bernoulli **beam approximation** adopted in the present formulation is unable to account for the shear deformation, the cross-sections remaining plane and perpendicular to the longitudinal axis of the beam. This choice implies that shear failure is not considered. In this work the studied designs were considered to be properly designed against shear failure, as prescribed by the GSA [1]. In order to obtain a more complete approach, in which different failure modes could be incorporated, the upgrade to a Timoshenko beam element formulation would be recommended. In [45], the formulation of a Timoshenko multifiber beam element was elaborated and applied for a small-scale analysis.

Finally, the fact that the **failed elements are not removed** from the topology and thus remain attached to the structure implies a residual load transfer onto the intact elements in the vicinity. Moreover, the impact of failing members on adjacent elements is not included. The degree of computational sophistication required for the modelling of such features was out of the scope of the present thesis work.

**Benchmark tests** should be performed in order to compare the results of the present approach with other methodologies and/or experimental tests and to confirm the adequacy of the adopted hypotheses. Moreover, a benchmarking strategy would determine the pertinence of including the latter additional simulation features in the present formulation.

Although the aforementioned improvements could add an extra value to the present methodology, the global effects observed with the present approach are supposed to remain general and are expected to be reproduced in a more complete approach: the adopted constitutive modelling is based on empirically-based observations and realistic values of the material properties. Besides, the approximations are expected to yield conservative results as previously mentioned. Moreover, the flexibility of the present strategy allows an extension to other fine-scale constitutive laws, including a different material response and/or additional modelling features, such as damage or a better representation of the material response under cyclic loading.



## References

- [1] United States General Services Administration (GSA), *Progressive collapse analysis and design guidelines for new federal office buildings and major modernization projects*. Washington DC, 2003.
- [2] Nair R.S., Preventing Disproportionate Collapse. *Journal of Performance of Constructed Facilities ASCE* 20(4), 309–314, 2006.
- [3] Ellingwood B.R., Dusenberry D.O., Building design for abnormal loads and progressive collapse. *Computer-Aided Civil and Infrastructure Engineering* 20(3), 194–205, 2005.
- [4] Ellingwood B.R., Leyendecker E., Approaches for design against progressive collapse. *Journal of the Structural Division ASCE* 104(ST3):413–423, 1978.
- [5] Ellingwood B.R., Mitigating Risk from Abnormal Loads and Progressive Collapse. *Journal of Performance of Constructed Facilities* 20(4), 315–323, 2006.
- [6] [http://www.imacleod.com/msa/supllinfo\\_ch2\\_photo.php](http://www.imacleod.com/msa/supllinfo_ch2_photo.php), last consulted on February 2, 2011.
- [7] Osteraas J.D., Murrah building bombing revisited: a qualitative assessment of blast damage and collapse patterns. *Journal of Performance of Constructed Facilities* 20(4), 330–335, 2006.
- [8] [http://www.oklahomacitynationalmemorial.org/uploads/documents/Alfred P Murrah.pdf](http://www.oklahomacitynationalmemorial.org/uploads/documents/Alfred_P_Murrah.pdf), last consulted on February 2, 2011.
- [9] <http://www.apfn.org/apfn/murrah.jpg>, last consulted on February 2, 2011.
- [10] Corley W.G., Sozen M.A., Thornton C.H., Mlakar P.F., The Oklahoma City Bombing: Improving Building Performance Through Multi-Hazard

## References

---

- Mitigation. Federal Emergency Management Agency Mitigation Directorate, *FEMA Report 277*, 1996.
- [11] Corley G.W., Applicability of Seismic Design in Mitigating Progressive Collapse. National Workshop on the Prevention of Progressive Collapse, Chicago, July 2002.
- [12] Bažant Z.P., Verdure M., Mechanics of Progressive Collapse: Learning from World Trade Center and Building Demolitions. *Journal of Engineering Mechanics* 133(3), 308–319, 2007.
- [13] Starossek U., Wolff M., Design of collapse-resistant structures. JCSS and IABSE Workshop on Robustness of Structures, Watford, UK, November 2005.
- [14] Starossek U., Progressive collapse of structures: Nomenclature and procedures. *Structural Engineering International* 16(2), 113–117, 2006.
- [15] Department of Defense (DoD). Unified Facilities Criteria (UFC): *Design of buildings to resist progressive collapse*, UFC 4-023-03. Washington DC, 2009.
- [16] EN 1991-1-7, *Eurocode 1 : Actions on structures - Part 1-7: General Actions - Accidental actions*, 2006.
- [17] Mohamed O.A., Progressive Collapse of Structures: Annotated Bibliography. *Journal of Performance of Constructed Facilities* 20(4), 418–425, 2006.
- [18] Grierson D.E., Xu L., Liu Y., Progressive-failure analysis of buildings subjected to abnormal loading. *Computer-Aided Civil and Infrastructure Engineering* 20, 155–171, 2005.
- [19] Vlassis A.G., *Progressive collapse assessment of tall buildings*, Ph.D. thesis. Department of Civil and Environmental Engineering, Imperial College London, 2007.
- [20] Izzuddin B.A., Vlassis A.G., Elghazouli A.Y., Nethercot D.A., Progressive collapse of multi-storey buildings due to sudden column loss - Part I: Simplified assessment framework. *Engineering Structures* 30, 1308–1318, 2008.
- [21] Izzuddin B.A., Vlassis A.G., Elghazouli A.Y., Nethercot D.A., Progressive collapse of multi-storey buildings due to sudden column loss - Part II: Application. *Engineering Structures* 30, 1424–1438, 2008.

- 
- [22] Menchel K., *Progressive collapse: comparison of main standards, formulation and validation of new computational procedures*, Ph.D. Thesis. Université Libre de Bruxelles. Belgium, 2008.
- [23] Kim J., Kim T., Assessment of progressive collapse-resisting capacity of steel moment frames. *Journal of Constructional Steel Research* 65, 169–179, 2009.
- [24] Tsai M.-H., Lin B.-H., Investigation of progressive collapse resistance and inelastic response for an earthquake-resistant RC building subjected to column failure. *Engineering Structures* 30, 3619–3628, 2008.
- [25] Kaewkulchai G., Williamson E.B., Dynamic behaviour of planar frames during Progressive Collapse. 16th ASCE Engineering Mechanics Conference. University of Washington. Seattle, USA, 2003.
- [26] Kaewkulchai G., Williamson E.B., Beam element formulation and solution procedure for dynamic progressive collapse analysis. *Computers and Structures* 82, 639–651, 2004.
- [27] Ruth P., Marchand K.A., Williamson E.B., Static equivalency in progressive collapse alternate path analysis: reducing conservatism while retaining structural integrity. *Journal of Performance of Constructed Facilities* 20(4), 349–364, 2006.
- [28] Kim H.-S., Kim J., An D.-W., Development of integrated system for progressive collapse analysis of building structures considering dynamic effects. *Advances in Engineering Software* 40, 1–8, 2009.
- [29] Shi Y., Li Z.-X., Hao H., A new method for progressive collapse analysis of RC frames under blast loading. *Engineering Structures* 32, 1691–1703, 2010.
- [30] Weerheijm J., Mediavilla J., van Doormaal J.C.A.M., Explosive loading of multi storey RC buildings: Dynamic response and progressive collapse. *Structural Engineering and Mechanics* 32(2), 193–212, 2009.
- [31] Luccioni B.M., Ambrosini R.D., Danesi R.F., Analysis of building collapse under blast loads. *Engineering Structures* 26, 63–71, 2004.
- [32] Kwasniewski L., Nonlinear dynamic simulations of progressive collapse for a multistory building. *Engineering Structures* 32, 1223–1235, 2010.

- [33] Bao Y., Kunnath S.K., El-Tawil S., Lew H.S., Macromodel-based simulation of progressive collapse: RC frame structures. *Journal of Structural Engineering ASCE* 134(7), 1079–1091, 2008.
- [34] Khandelwal K., El-Tawil S., Sadek F., Progressive collapse analysis of seismically designed steel braced frames. *Journal of Constructional Steel Research* 65, 699–708, 2009.
- [35] Fu F., Progressive collapse analysis of high-rise building with 3-D finite element modeling method. *Journal of Constructional Steel Research* 65, 1269–1278, 2009.
- [36] Galal K., El-Sawy T., Effect of retrofit strategies on mitigating progressive collapse of steel frame structures. *Journal of Constructional Steel Research* 66, 520–531, 2010.
- [37] Vlassis A.G., Izzuddin B.A., Elghazouli A.Y., Nethercot D.A., Progressive collapse of multi-storey buildings due to failed floor impact. *Engineering Structures* 31(7), 1522–1534, 2009.
- [38] Sasani M., Sagiroglu S., Gravity Load Redistribution and Progressive Collapse Resistance of 20-Story Reinforced Concrete Structure following Loss of Interior Column. *ACI Structural Journal* 107(6), 636–644, 2010.
- [39] Sasani M., Werner A., Kazemi A., Bar fracture modeling in progressive collapse analysis of reinforced concrete structures. *Engineering Structures* 33(2), 401–409, 2011.
- [40] Abruzzo J., Matta A., Panariello G., Study of mitigation strategies for progressive collapse of a reinforced concrete commercial building. *Journal of Performance of Constructed Facilities* 20(4), 384–390, 2006.
- [41] Gudmundsson G.V., Izzuddin B.A., The ‘sudden column loss’ idealisation for disproportionate collapse assessment. *The Structural Engineer* 88(6), 22–26, 2008.
- [42] Menchel K., Massart T.J., Rammer Y., Bouillard P., Comparison and study of different progressive collapse simulation techniques for RC structures. *Journal of the Structural Division ASCE* 35(6), 685–697, 2009.
- [43] Anthoine A., Guedes J., Pegon P., Non-linear behaviour of reinforced concrete beams: from 3D continuum to 1D member modelling. *Computers and Structures* 65(6), 949–963, 1997.

- 
- [44] Davenne L., Ragueneau F., Mazars J., Ibrahimbegovic A., Efficient approaches to finite element analysis in earthquake engineering. *Computers and Structures* 81, 1223–1239, 2003.
- [45] Mazars J., Kotronis P., Ragueneau F., Casaux G., Using multifiber beams to account for shear and torsion. Applications to concrete structural elements. *Computer Methods in Applied Mechanics and Engineering* 195, 7264–7281, 2006.
- [46] Oliveira R.S., Ramalho M.A., Corrêa M.R.S., A layered finite element for reinforced concrete beams with bond-slip effects. *Cement and Concrete Composites* 30, 245–252, 2008.
- [47] Jones J., Wua C., Oehlers D.J., Whittaker A.S., Sunc W., Marksa S., Coppola R., Finite difference analysis of simply supported RC slabs for blast loadings. *Engineering Structures* 31(12), 2825–2832, 2009.
- [48] Chandrasekaran S., Nunziante L., Serino G., Carannante F., Curvature Ductility of RC Sections Based on Eurocode: Analytical Procedure. *KSCE Journal of Civil Engineering* 15(1), 131–144, 2011.
- [49] Daniell J.E., Oehlers D.J., Griffith M.C., Mohamed Ali M.S., Ozbakkaloglu T., The softening rotation of reinforced concrete members. *Engineering Structures* 30(11), 3159–3166, 2008.
- [50] Haskett M., Oehlers D.J., Mohamed Ali M.S., Wu C., Rigid body moment-rotation mechanism for reinforced concrete beam hinges. *Engineering Structures* 31(5), 1032–1041, 2009.
- [51] EN 1992-1-1, *Eurocode 2: Design of concrete structures - Part 1-1: General rules and rules for buildings*, 2004.
- [52] International Federation for Structural Concrete (*fib*), *Constitutive modelling of high strength/high performance concrete*. State-of-art report. *fib Bulletin* 42, 2008.
- [53] International Federation for Structural Concrete (*fib*), *Practitioners' guide to finite element modelling of reinforced concrete structures*. State-of-art report. *fib Bulletin* 45, 2008.
- [54] Binici B., An analytical model for stress-strain behavior of confined concrete. *Engineering Structures* 27, 1040–1051, 2005.

## References

---

- [55] Carpinteri A., Corrado M., Mancini G., Paggi M., A numerical approach to modelling size effects on the flexural ductility of RC beams. *Materials and structures* 42(10), 1353–1367, 2009.
- [56] Weerheijm J., Van Doormaal J.C.A.M., Tensile failure of concrete at high strain rates: new test data on strength and fracture energy from instrumented spalling tests. *International Journal of Impact Engineering* 34, 609–626, 2007.
- [57] Schuler H., Mayrhofer C., Thoma K., Spall experiments for the measurement of the tensile strength and fracture energy of concrete at high strain rates. *International Journal of Impact Engineering* 32, 1635–1650, 2006.
- [58] Lambert D.E., Ross C.A., Strain rate effects on dynamic fracture and strength. *International Journal of Impact Engineering* 24, 985–998, 2000.
- [59] Brara A., Klepaczko J.R., Fracture energy of concrete at high loading rates in tension. *International Journal of Impact Engineering* 34, 424–435, 2007.
- [60] Abbas H., Gupta N.K., Alam M., Nonlinear response of concrete beams and plates under impact loading. *International Journal of Impact Engineering* 30, 1039–1053, 2004.
- [61] Zhang X.X., Ruiz G., Yu R.C., Tarifa M., Fracture behaviour of high-strength concrete at a wide range of loading rates. *International Journal of Impact Engineering* 36, 1204–1209, 2009.
- [62] Leppänen J., Concrete subjected to projectile and fragment impacts: Modelling of crack softening and strain rate dependency in tension. *International Journal of Impact Engineering* 32, 1828–1841, 2006.
- [63] He W., Wu Y.-F., Liew K.M., Wu Z., A 2D total strain based constitutive model for predicting the behaviors of concrete structures. *International Journal of Engineering Science* 44(18–19), 1280–1303, 2006.
- [64] Jirásek M., Bazant Z.P., Models for Localization of Softening and Size Effect. In: *Inelastic Analysis of Structures*, 517–539. John Wiley and Sons, Chichester, 2002.
- [65] Challamel N., Hjjaj M., Non-local behaviour of plastic softening beams. *Acta Mechanica* 178(3–4), 125–46, 2005.

- 
- [66] Vujovic M., *Studie van robuustheid en vervormingscapaciteit van balken in gewapend beton ter verhoging van de weerstand tegen voortschrijdende instorting*, Master Thesis. Vrije Universiteit Brussel, 2009.
- [67] G eradin M., Rixen D., *Mechanical vibrations: theory and application to structural dynamics*. Masson, Paris, 1994.
- [68] Engelen R.A.B., Geers M.G.D., Baaijens F.P.T., Nonlocal implicit gradient-enhanced elasto-plasticity for the modelling of softening behaviour. *International Journal of Plasticity* 19, 403–433, 2003.
- [69] Loret B., Prevost J.H., Dynamic strain localization in elasto-(visco-) plastic solids, Part 1. General formulation and one-dimensional examples. *Computer Methods in Applied Mechanics and Engineering* 83, 247–273, 1990.
- [70] EN 1991-1-1, *Eurocode 1 : Actions on structures - Part 1-1: General actions - Densities, self-weight, imposed loads for buildings*, 2002.
- [71] EN 1990, *Eurocode: Basis of structural design*, 2002.
- [72] Park J.Y., Krauthammer T., Development of an LEFM dynamic crack criterion for correlated size and rate effects in concrete beams. *International Journal of Impact Engineering* 36(1), 92–97, 2009.
- [73] Mechtcherine V., Fracture mechanical behavior of concrete and the condition of its fracture surface. *Cement and Concrete Research* 39(7), 620–628, 2009.
- [74] Kwak H.G., Kim S.P., Nonlinear analysis of RC beams based on moment-curvature relation. *Computers and Structures* 80(7–8), 615–628, 2002.
- [75] Rabczuk T., Akkermann J., Eibl J., A numerical model for reinforced concrete structures. *International Journal of Solids and Structures* 42, 1327–1354, 2005.
- [76] Inel M., Ozmen H.B., Effects of plastic hinge properties in nonlinear analysis of reinforced concrete buildings. *Engineering Structures* 28, 1494–1502, 2006.
- [77] Diamonds 2010 r.01. Buildsoft NV; <http://www.buildsoft.eu>.
- [78] Smith P.D., Hetherington J.G., *Blast and ballistic loading of structures*. Butterworth Heinemann, London, 1994.

## References

---

- [79] Priestley M.J.N., Seible F., Design of seismic retrofit measures for concrete and masonry structures. *Construction and Building Materials* 9(6), 365–77, 1995.
- [80] Pankaj P., Lin E., Material modelling in the seismic response analysis for the design of RC framed structures. *Engineering Structures* 27(7), 1014–1023, 2005.
- [81] Bischoff P.H., Perry S.H., Compressive Behaviour of Concrete at High Strain Rates. *Materials and Structures* 24, 425–50, 1991.
- [82] Malvar L.J., Crawford J.E., Dynamic increase factors for concrete. 28th DDESB seminar. Orlando, FL, USA, 1998.
- [83] Grote D.L., Park S.W., Zhou M., Dynamic behaviour of concrete at high strain rates and pressures: I. experimental characterization. *International Journal of Impact Engineering* 25, 869–886, 2001.
- [84] Li Q.M., Meng H., About the dynamic strength enhancement of concrete-like materials in a split Hopkinson pressure bar test. *International Journal of Solids and Structures* 40, 343–360, 2003.
- [85] Malvar L.J., Crawford J.E., Dynamic increase factors for steel reinforcing bars. 28th DDESB seminar. Orlando, FL, USA, 1998.
- [86] Tsang H.-H., Lam N.T.K., Collapse of Reinforced Concrete Column by Vehicle Impact. *Computer-Aided Civil and Infrastructure Engineering* 23, 427–436, 2008.
- [87] Itoh Y., Liu C., Kusama R., Dynamic simulation of collisions of heavy high-speed trucks with concrete barriers. *Chaos, Solitons and Fractals* 34, 1239–1244, 2007.
- [88] El-Tawil S., Severino E., Fonseca P., Vehicle Collision with Bridge Piers. *Journal of Bridge Engineering ASCE* 10(3), 345–353, 2005.
- [89] Pedersen R.R., Simone A., Sluys L.J., An analysis of dynamic fracture in concrete with a continuum visco-elastic visco-plastic damage model. *Engineering Fracture Mechanics* 75, 3782–3805, 2008.
- [90] Georgin J.F., Reynouard J.M., Modeling of structures subjected to impact: concrete behaviour under high strain rate. *Cement and Concrete Composites* 25, 131–43, 2003.

- 
- [91] Loreface R., Etse G., Carol I., Viscoplastic approach for rate-dependent failure analysis of concrete joints and interfaces. *International Journal of Solids and Structures* 45, 2686–2705, 2008.
- [92] Ragueneau F., Gatuingt F., Inelastic behavior modelling of concrete in low and high strain rate dynamics. *Computers and Structures* 81, 1287–1299, 2003.
- [93] Pandey A.K., Kumar R., Paul D.K., Trikha D.N., Strain Rate Model for Dynamic Analysis of Reinforced Concrete Structures. *Journal of Structural Engineering* 132(9), 1393–1401, 2006.
- [94] de Borst R., Sluys L.J., Geers M.G.D., *Computational methods for material nonlinearities*. Graduate School on Engineering Mechanics. Delft University of Technology. Delft, The Netherlands, 1998.
- [95] Heeres O.M., Suiker A.S.J., de Borst R., A comparison between the Perzyna viscoplastic model and the Consistency viscoplastic model. *European Journal of Mechanics and Solids* 21, 1–12, 2002.
- [96] Wang Z.-L., Stress-strain relationship of steel fiber-reinforced concrete under dynamic compression. *Construction and Building Materials* 22, 811–819, 2008.



# Appendix

Maximum values of the compressive strain rates obtained in the reference case of study (Section 4.2)

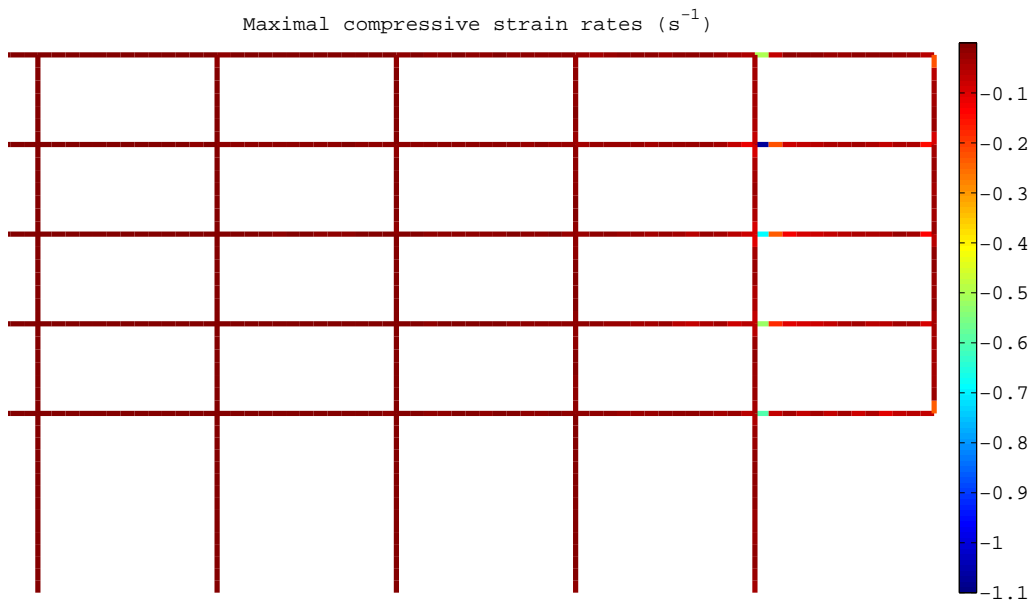


Figure A.1: Maximum compressive strain rate  $\dot{\epsilon}$ .

**Analytical expressions for the material parameters of the rate dependent model (Section 5.3)**

**Table A.1:** Young's modulus of concrete in tension  $E_t$ .

$$\begin{array}{l} \mathbf{E}_t(\dot{\epsilon}) \\ \hline 32; \quad \dot{\epsilon} \in [0, 3e-6] \\ \\ 32 \left( \frac{\dot{\epsilon}}{3e-6} \right)^{0.026}; \quad \dot{\epsilon} \in (3e-6, 300] \end{array}$$

**Table A.2:** Viscoplastic parameter of concrete in tension  $\eta_t$ .

$$\begin{array}{l} \mathbf{\eta}_t(\kappa_t) \\ \hline 0.05; \quad \kappa_t \in [0, 2.5e-4] \\ \\ 0.05 \exp[-3e4(\kappa_t - 2.5e-4)]; \quad \kappa_t \in (2.5e-4, +\infty] \end{array}$$

**Table A.3:** Young's modulus of concrete in compression  $E_c$ .

$$\begin{array}{l} \mathbf{E}_c(\dot{\epsilon}) \\ \hline 17; \quad \dot{\epsilon} \in [0, 3e-5] \\ \\ 17 \left[ 0.10 \log \left( \frac{\dot{\epsilon}}{3e-5} \right) + 1.00 \right]; \quad \dot{\epsilon} \in (3e-5, 30] \\ \\ 17 \left[ 1.34 \log \left( \frac{\dot{\epsilon}}{3e-5} \right) - 6.44 \right]; \quad \dot{\epsilon} \in (30, 300] \end{array}$$

**Table A.4:** Viscoplastic parameter of concrete in compression  $\eta_c$ .

$\eta_c(\dot{\epsilon})$	
0;	$\dot{\epsilon} \in [0, 3e-5]$
$373.33 \log^3 \left( \frac{\dot{\epsilon}}{3e-5} \right) - 1280.00 \log^2 \left( \frac{\dot{\epsilon}}{3e-5} \right) + 1146.66 \log \left( \frac{\dot{\epsilon}}{3e-5} \right);$	$\dot{\epsilon} \in (3e-5, 3e-4]$
$-77.06 \log^3 \left( \frac{\dot{\epsilon}}{3e-5} \right) + 516.80 \log^2 \left( \frac{\dot{\epsilon}}{3e-5} \right) - 1205.93 \log \left( \frac{\dot{\epsilon}}{3e-5} \right) + 1006.20;$	$\dot{\epsilon} \in (3e-4, 3e-3]$
$-8.00 \log^3 \left( \frac{\dot{\epsilon}}{3e-5} \right) + 91.20 \log^2 \left( \frac{\dot{\epsilon}}{3e-5} \right) - 344.00 \log \left( \frac{\dot{\epsilon}}{3e-5} \right) + 432.20;$	$\dot{\epsilon} \in (3e-3, 3e-2]$
$-0.23 \log^3 \left( \frac{\dot{\epsilon}}{3e-5} \right) + 4.65 \log^2 \left( \frac{\dot{\epsilon}}{3e-5} \right) - 28.02 \log \left( \frac{\dot{\epsilon}}{3e-5} \right) + 53.50;$	$\dot{\epsilon} \in (3e-2, 3e-1]$
$-0.31 \log^3 \left( \frac{\dot{\epsilon}}{3e-5} \right) + 4.87 \log^2 \left( \frac{\dot{\epsilon}}{3e-5} \right) - 25.91 \log \left( \frac{\dot{\epsilon}}{3e-5} \right) + 46.24;$	$\dot{\epsilon} \in (3e-1, 3]$
$-0.06 \log^3 \left( \frac{\dot{\epsilon}}{3e-5} \right) + 1.12 \log^2 \left( \frac{\dot{\epsilon}}{3e-5} \right) - 6.79 \log \left( \frac{\dot{\epsilon}}{3e-5} \right) + 13.80;$	$\dot{\epsilon} \in (3, 3e1]$
$0.01 \log^4 \left( \frac{\dot{\epsilon}}{3e-5} \right) - 0.28 \log^3 \left( \frac{\dot{\epsilon}}{3e-5} \right) + 2.63 \log^2 \left( \frac{\dot{\epsilon}}{3e-5} \right) - 10.96 \log \left( \frac{\dot{\epsilon}}{3e-5} \right) + 17.07;$	$\dot{\epsilon} \in (3e1, 3e2]$

**Table A.5:** Viscoplastic parameter of steel  $\eta_s$ .

$\eta_s(\dot{\epsilon})$	
0;	$\dot{\epsilon} \in [0, 1e-4]$
$-151.28 \log^3\left(\frac{\dot{\epsilon}}{1e-4}\right) - 136.97 \log^2\left(\frac{\dot{\epsilon}}{1e-4}\right) + 187.82 \log\left(\frac{\dot{\epsilon}}{1e-4}\right);$	$\dot{\epsilon} \in (1e-4, 3e-4]$
$4.39 \log^3\left(\frac{\dot{\epsilon}}{1e-4}\right) - 8.57 \log^2\left(\frac{\dot{\epsilon}}{1e-4}\right) - 25.42 \log\left(\frac{\dot{\epsilon}}{1e-4}\right) + 55.60;$	$\dot{\epsilon} \in (3e-4, 3e-3]$
$-2.65 \log^3\left(\frac{\dot{\epsilon}}{1e-4}\right) + 24.02 \log^2\left(\frac{\dot{\epsilon}}{1e-4}\right) - 74.34 \log\left(\frac{\dot{\epsilon}}{1e-4}\right) + 79.47;$	$\dot{\epsilon} \in (3e-3, 1e-1]$
$-0.28 \log^3\left(\frac{\dot{\epsilon}}{1e-4}\right) + 3.64 \log^2\left(\frac{\dot{\epsilon}}{1e-4}\right) - 15.7 \log\left(\frac{\dot{\epsilon}}{1e-4}\right) + 23.02;$	$\dot{\epsilon} \in (1e-1, 1]$
$-0.04 \log^3\left(\frac{\dot{\epsilon}}{1e-4}\right) + 0.65 \log^2\left(\frac{\dot{\epsilon}}{1e-4}\right) - 3.44 \log\left(\frac{\dot{\epsilon}}{1e-4}\right) + 6.11;$	$\dot{\epsilon} \in (1, 1e1]$
$0.01 \log^2\left(\frac{\dot{\epsilon}}{1e-4}\right) - 0.14 \log\left(\frac{\dot{\epsilon}}{1e-4}\right) + 0.44;$	$\dot{\epsilon} \in (1e1, 1e2]$

# List of Publications

## Journal paper

Santafé B., Berke P., Bouillard Ph., Vantomme J., Massart T.J., **Investigation of the influence of design and material parameters in the progressive collapse analysis of RC structures.** *Engineering Structures*, accepted manuscript, 2011.

## International conference papers

Santafé B., Massart T.J., Vantomme J., Bouillard Ph., **Rate-dependent moment-curvature relations for the progressive collapse of RC structures.** In Proc. COMPDYN 2009, Eccomas Thematic Conference on Computational Methods in Structural Dynamics and Earthquake Engineering, Papadrakakis M., Lagros N.D., Fragiadakis M. (Eds.), Rhodes, Greece, 2009.

Santafé B., Berke P., Massart T.J., Bouillard Ph., Vantomme J., **Effect of concrete rate dependent behaviour on structural progressive collapse**, 8th International Conference on Structural Dynamics (EURODYN 2011), Leuven, Belgium, 2011.

## International conference abstract

Santafé B., Massart T.J., Bouillard Ph., Vantomme J., **Rate dependent effects in the simulation of progressive collapse of RC structures**, 8th World Congress on Computational Mechanics (WCCM8), Venice, Italy, 2008.

## Book chapter

Bouillard Ph., Menchel K., Santafé B., Massart T.J., **Progressive collapse simulation techniques for RC structures.** In *Structural Design of Con-*

## List of Publications

---

*structions subjected to exceptional or accidental actions*, Bouillard Ph., Rammer Y., Vantomme J. (Eds.), Presses Universitaires de Bruxelles, Brussels, 92–114, 2008.

# Acknowledgements

I would like to express my gratitude to Professor John Vantomme for offering me the possibility of working at the Civil and Materials Engineering Department of the Royal Military Academy. I would also like to thank Professors Philippe Bouillard and Thierry J. Massart for making possible this joint supervision thesis with the Université Libre de Bruxelles.

Thanks as well to Professors Bernard Espion (ULB), Mohammed Hjiiaj (INSA Rennes), Luc Rabet (RMA), and to David Lecompte (RMA) for accepting to make part of my PhD committee.

The accomplishment of this work would have not been conceivable without the invaluable guidance and dedication of Professor Thierry J. Massart. My deepest thanks for his infinite patience and generous involvement in this project.

I am most grateful to the people who helped me in the composition of this manuscript, in particular Professor Thierry J. Massart, ‘Herr Doktor’ Péter Berke and Professor Philippe Bouillard. Thanks to Kfir Menchel for being my guide during the first steps of this research work.

It would be impossible to individually acknowledge all those who have helped me at one time or another during these last years, so I would like to thank all my present and past colleagues at both institutions, the Royal Military Academy and the Université Libre de Bruxelles. Again, thanks to the crew at the Structural and Material Computational Mechanics branch of the BATir department, for ensuring such an excellent work-atmosphere, livened-up by the frequent ‘work meetings’ in the common room. ‘Gracias’ Guy Paulus for attempting (and most often succeeding) to figure out the many mysteries of my laptop.

I could not forget to mention my friend Jean-Marie Ndambi, for his cheerfulness and his permanent help in my computer-related (and -unrelated) trou-

## Acknowledgements

---

bles: thanks for being the best colleague one could have. Another big thanks goes to the ‘Spanish Mafia’ (including the Greek branch) for the good times passed during my stay in Brussels.

I finally would like to thank in a very special way my parents, siblings, relatives and friends, near and far, for the support they provided me during these years. In particular, I want to acknowledge Antoine for his kind encouragement and for always putting a smile on my face.

Berta Santafé Iribarren  
Brussels, May 2011.